NASA CR-167861
Report ME-TSPC-TR-82-11
May 1982

The Design and Instrumentation of the Purdue Annular Cascade Facility with Initial Data Acquisition and Analysis

R. Charles Stauter and Sanford Fleeter

Thermal Science and Propulsion Center
School of Mechanical Engineering
Purdue University
West Lafayette, Indiana 47907

Prepared for
National Aeronautics and Space Administration
NASA-Lewis Research Center
Grant NSG-3285

NASA CR-167861
Report ME-TSPC-TR-82-11

THE DESIGN AND INSTRUMENTATION OF THE PURDUE ANNULAR CASCADE FACILITY WITH INITIAL DATA ACQUISITION AND ANALYSIS

BY

R. Charles Stauter
Sanford Fleeter

May 1982

Thermal Sciences and Propulsion Center
School of Mechanical Engineering
Purdue University
West Lafayette, Indiana 47907

Prepared for
NATIONAL AERONAUTICS AND SPACE ADMINISTRATION
NASA-LEWIS RESEARCH CENTER
Grant NSG-3285

1. Report No.	2. Government Accession No.	3. Recipient's Catalog No.
NASA CR-167861		

4. Title and Subtitle	5. Report Date
The Design and Instrumentation of the Purdue Annular Cascade Facility with Initial Data Acquisition and Analysis	May, 1982
	6. Performing Organization Code
7. Author(s)	8. Performing Organization Report No.
R. C. Stauter and S. Fleeter	ME-TSPC-TR-82-11
	10. Work Unit No.
9. Performing Organization Name and Address	11. Contract or Grant No.
Purdue University West Lafayette, Indiana 47907	NSG-3285
	13. Type of Report and Period Covered
12. Sponsoring Agency Name and Address	Contractor Report
National Aeronautics and Space Administration Washington, DC 20546	14. Sponsoring Agency Code

15. Supplementary Notes

Project Manager, Donald R. Boldman, NASA Lewis Research Center, Cleveland, Ohio 44135

16. Abstract

The Purdue Annular Cascade Facility has been designed for the express purpose of acquiring benchmark three-dimensional aerodynamic data required to validate and/or indicate necessary refinements to inviscid and viscous analyses of the flow through turbomachine blade rows. The facility has been extensively instrumented and provides state-of-the-art capabilities for pressure measurement, probe insertion and traversing, and flow visualization. It also has the flexibility to utilize advanced measurement techniques including Laser Doppler Anemometry.

A computer-controlled data acquisition system has been utilized to permit automated acquisition and online data reduction and examination. Statistical techniques have been incorporated into the data-processing software.

Several experiments have been performed with an instrumented, classical airfoil cascade at zero incidence angle. Predictions obtained from the inviscid numerical flow analyses MERIDL and TSONIC utilizing the cascade geometry and the experimentally-determined upstream inlet annulus velocity profile as input, have been correlated with the experimental data. In addition, a flow visualization technique using helium-filled soap bubbles has been demonstrated.

17. Key Words (Suggested by Author(s))	18. Distribution Statement
Cascade Flow Turbomachinery Annular Cascade	Unclassified-unlimited STAR Category 02

19. Security Classif. (of this report)	20. Security Classif. (of this page)	21. No. of Pages	22. Price*
Unclassified	Unclassified		

* For sale by the National Technical Information Service, Springfield, Virginia 22161

ACKNOWLEDGEMENTS

The work reported herein was sponsored by the Fluid Mechanics and Acoustics Division, NASA-Lewis Research Center, Cleveland, Ohio, under Grant NSG-3285.

SUMMARY

The Purdue Annular Cascade Facility has been designed and fabricated for the express purpose of acquiring benchmark quality, three-dimensional aerodynamic data required to validate and/or indicate the necessary refinements to inviscid and viscous analyses of the flow through turbomachine blade rows. The facility has been extensively instrumented and provides the conventional state-of-the-art capabilities of pressure measurement, probe insertion and traversing, and flow visualization. It has also been designed with the fexibility necessary to utilize advanced measurement techniques including Laser Doppler Anemometry.

A computer-controlled data acquisition system is utilized to permit automated data acquisition and online data reduction and examination. Statistical techniques have been incorporated into the data-processing software such that confidence intervals can be placed on the data.

Several experiments have been performed with an instrumented, classical airfoil cascade at zero incidence to obtain the data necessary to determine the airfoil surface pressure coefficients. Predictions obtained from the inviscid numerical flow analyses MERIDL and TSONIC utilizing the cascade geometry and the experimentally-determined upstream

inlet annulus velocity profile as input, have been correlated with the experimental data. In addition, a flow visualization technique using helium-filled soap bubbles has been demonstrated.

TABLE OF CONTENTS

LIST OF TABLES

LIST OF FIGURES

Appendix Figure

LIST OF SYMBOLS

A	Area
C_p	Pressure Coefficient
E	Error
dA	Differential Area
$\dot{m}$	Mass Flow
n	Number of Samp'ings
P	Pressure
R_{air}	Gas Constant for Air
s	Standard Deviation Estimate
T	Temperature
t	Student's t-Distribution Factor
U	Velocity
$\bar{U}$	Mass-Averaged Velocity
V	Voltage
$\bar{V}$	Mean Voltage Estimate

Greek Symbols

ρ	Density
μ	True Mean
σ	True Standard Deviation
γ	Ratio of Specific Heats
Γ	Function $\frac{\gamma-1}{\gamma}$

Superscripts

'	Interval Quantity

Subscripts

af	Airfoil Surface
c	Calibration
i	Summing Index
o	Ambient
r	Reference
s	Static
t	Total

Unit Symbols

cm	Centimeters
cms	Cubic Meters Per Second
kW	Kilowatt
m	Meters
mm	Millimeters
s	Seconds
cfm	Cubic Feet Per Minute
Hp	Horsepower
in	Inches
kPa	Kilopascals
psi	Pounds Per Square Inch
psid	Pounds Per Square Inch Difference

CHAPTER 1

INTRODUCTION

Continual demands for increased efficiency and thrust-to-weight ratio of gas turbine engines have necessitated an ever-improving knowledge of the flow field through-out the engine. Of particular importance are the compressor and turbine components of such an engine, where the mechanical energy transfer between the engine and the fluid takes place. For design and analysis purposes, it has long been assumed that the flow field in an axial-flow turbomachine is two-dimensional. However with the continuing requirements for increased efficiency and thrust-to-weight ratio, it is becoming necessary to replace the assumption of two-dimensional flow with a predictive model, verified by concise data, which accurately describes the three-dimensionality of the flow field.

The flow field in an axial-flow turbomachine, schematically depicted in Figure 1, consists of many elements which interact with one another in a complex manner. Complicating the through-flow are endwall boundary layers, tip flows and vortices, hub vortices, secondary flows, and blade wakes. These are in addition to the boundary layers

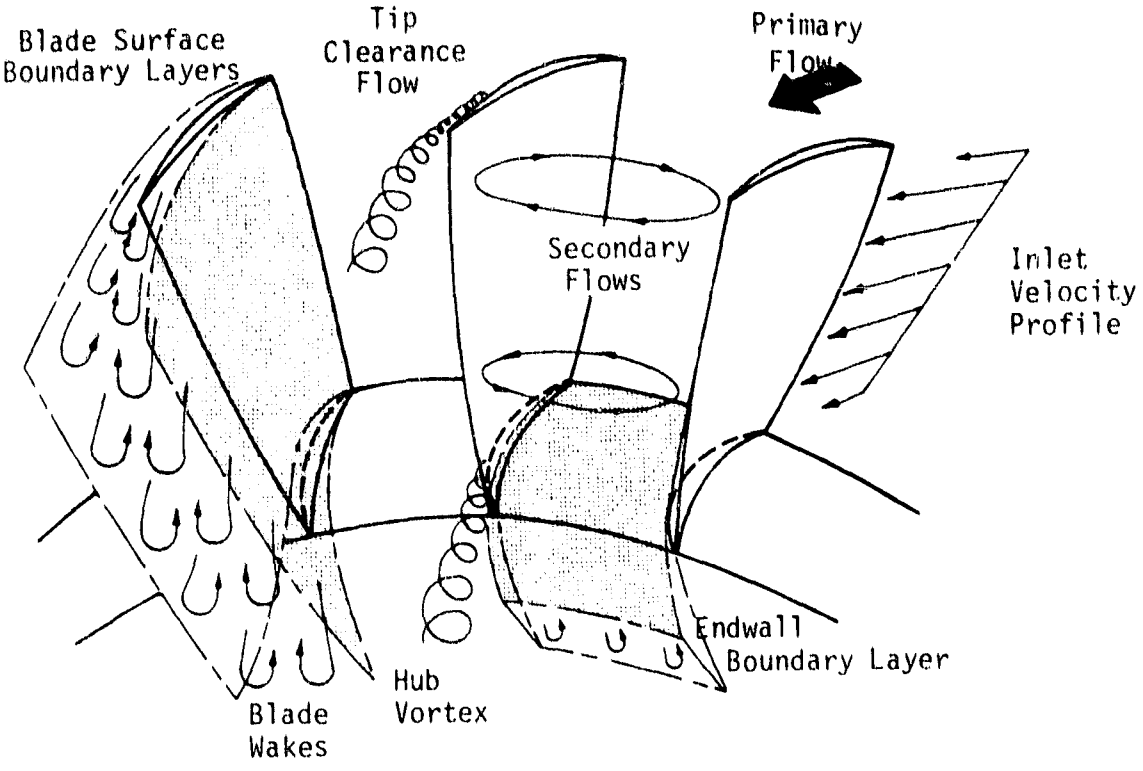

Figure 1. Schematic Representation of the Flow Field in a Turbomachine Blade Row.

and sharp pressure gradients which exist on the blade surfaces. Significantly complicating the situation further is the fact that the flow field entering a blade row is neither uniform nor steady.

Ideally, the solution to the equations describing the flow field (the continuity equation, the Navier-Stokes equations, and the thermodynamic equations) would be utilized to predict the flow field for any specified turbomachine or blade-row geometry. However, the solutions to these equations are not readily determined except for certain specific, generally relatively simplistic situations. Numerical solutions for the complete flow-field equations are currently being developed, but at present they tend to have severe drawbacks such as being limited to low Reynolds number and requiring exceedingly large amounts of computer time, making them impractical for design and analysis applications.

Numerical solutions are currently being developed by NASA and others to describe and predict the three-dimensional flow fields in turbomachine blade rows. To overcome the above-noted general limitations as well as the difficulties associated with the internal flow geometries, these numerical solutions involve many significant numerical and physical assumptions. For example, to simplify the Navier-Stokes equations, the flow is assumed to be inviscid. If accounted for, viscous effects are generally

limited to boundary layer theory. An example of an important numerical assumption in such numerical solutions is the generation of a computational grid which is assumed to be suitable for the computations involved in solving the simplified flow-field equations. The effect of such assumptions on the accuracy of the numerical solutions for the flow field is not well known. Therefore, to be truly useful to the turbomachine designer and analyst, the accuracy of the numerical solutions being developed for application to turbomachine components must be validated by correlating their predictions with appropriate benchmark experimental data.

The lack of such benchmark data prompted the initiation of the Purdue Annular Cascade Experimental Research Program, directed at the acquisition of such data. This report concerns the design and instrumentation of the Purdue Annular Cascade Facility, shown in Figure 2, and the analysis of the initial data from this facility.

Figure 2. Purdue Annular Cascade Facility

CHAPTER 2

DESIGN OF THE PURDUE ANNULAR CASCADE FACILITY

One of the primary design considerations for the Purdue Annular Cascade Facility was to make the flow passages large so as to amplify the fundamental flow phenomena as well as to preclude the need for miniaturizing instrumentation. Another important design consideration was to provide flexibility for future instrumentation such as Laser-Doppler Anemometry. Other design considerations will be discussed as specific features of the facility are described in this chapter.

The facility, schematically shown in Figure 3, is comprised of honeycomb fiberglass sections supported and connected by aluminum rings. The front section consists of a bellmouth-shaped entrance to facilitate orderly boundary layer development and minimize the entrance pressure losses. The centerbody and the outer shroud converge in the bellmouth to form an annulus 15.24 cm (6.0 in) high. The outer shroud diameter is 1.27 m (50.0 in). After the bellmouth, the flow passes through Section A where its velocity profile undergoes further development before reaching the airfoil row which is installed in Section B. There are 36

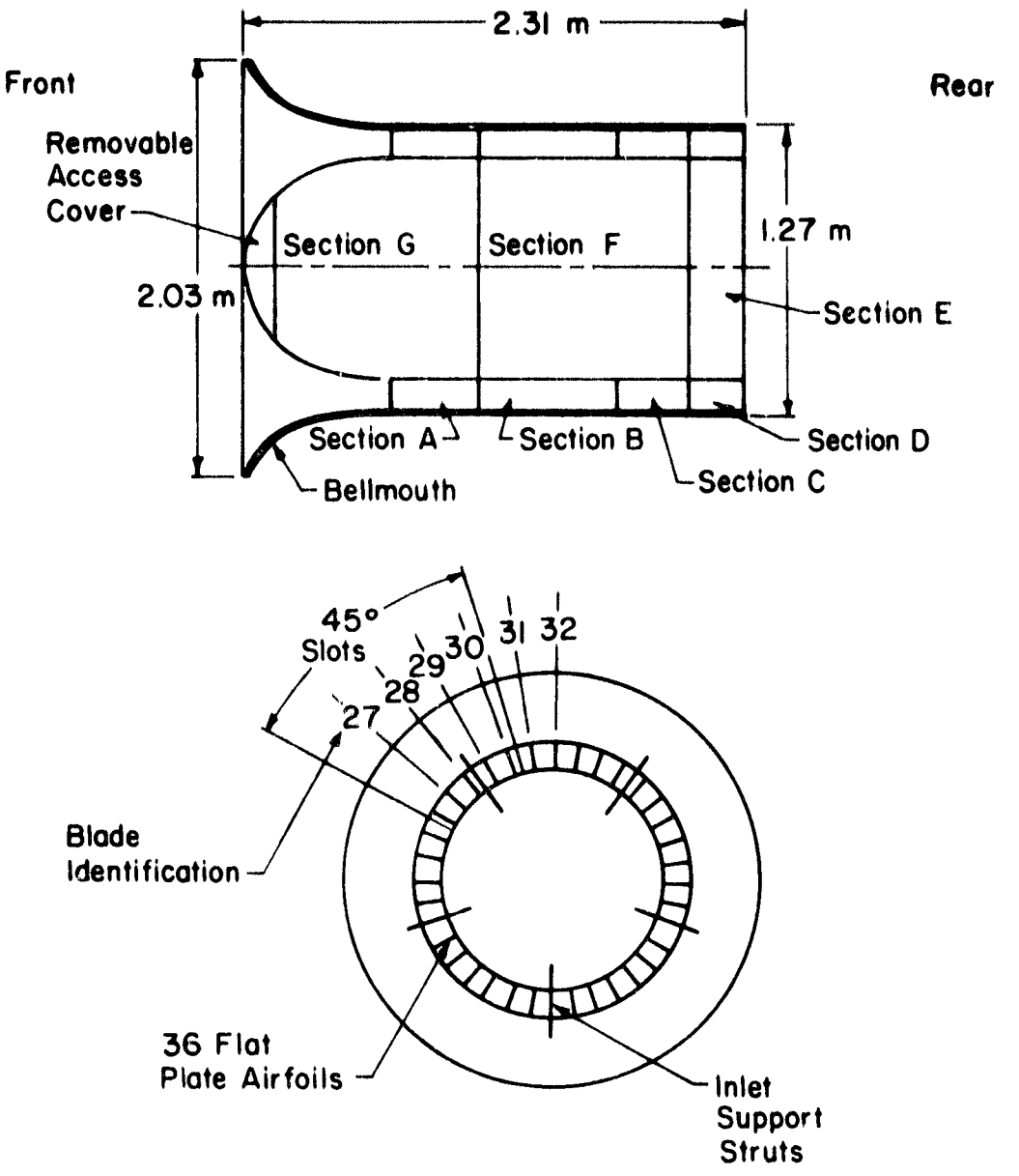

Figure 3. Schematic of the Purdue Annular Cascade Facility

airfoil trunnion holes machined into Section B which was designed for airfoils with chords of up to 30.48 cm (12.0 in). Section D permits the analysis of the airfoil exit wakes.

The Annular Cascade Facility exhausts into a 24 cubic meter plenum chamber, shown in Figure 4, which decelerates the flow and provides for an even back pressure to the airfoil cascade. From the plenum, the flow is drawn through ducting 1.47 m (57.0 in) in diameter to a large-capacity centrifugal compressor which functions as the facility exhauster. This facility exhauster, shown in Figure 5, has a capacity of 354 cms (150,000 cfm) at 46 cm (18 in) of water and is powered by an Allis-Chalmers 224 kW (300 Hp) three-phase induction motor. Controls to the exhauster system include the on-off switch to the motor and variable inlet-guide vanes at the inlet to the exhauster.

For the demonstration and validation phase, the facility was equipped and instrumented with a flat-plate airfoil cascade. The airfoils have a chord of 15.24 cm (6.0 in) and a thickness of 0.48 cm (0.19 in) with rounded leading and trailing edges. A typical airfoil is depicted in Figure 6. The airfoils were mounted with 0 stagger angle (hence, 0 incidence) for the initial experiments described herein.

BLACK AND WHITE PHOTOGRAPH

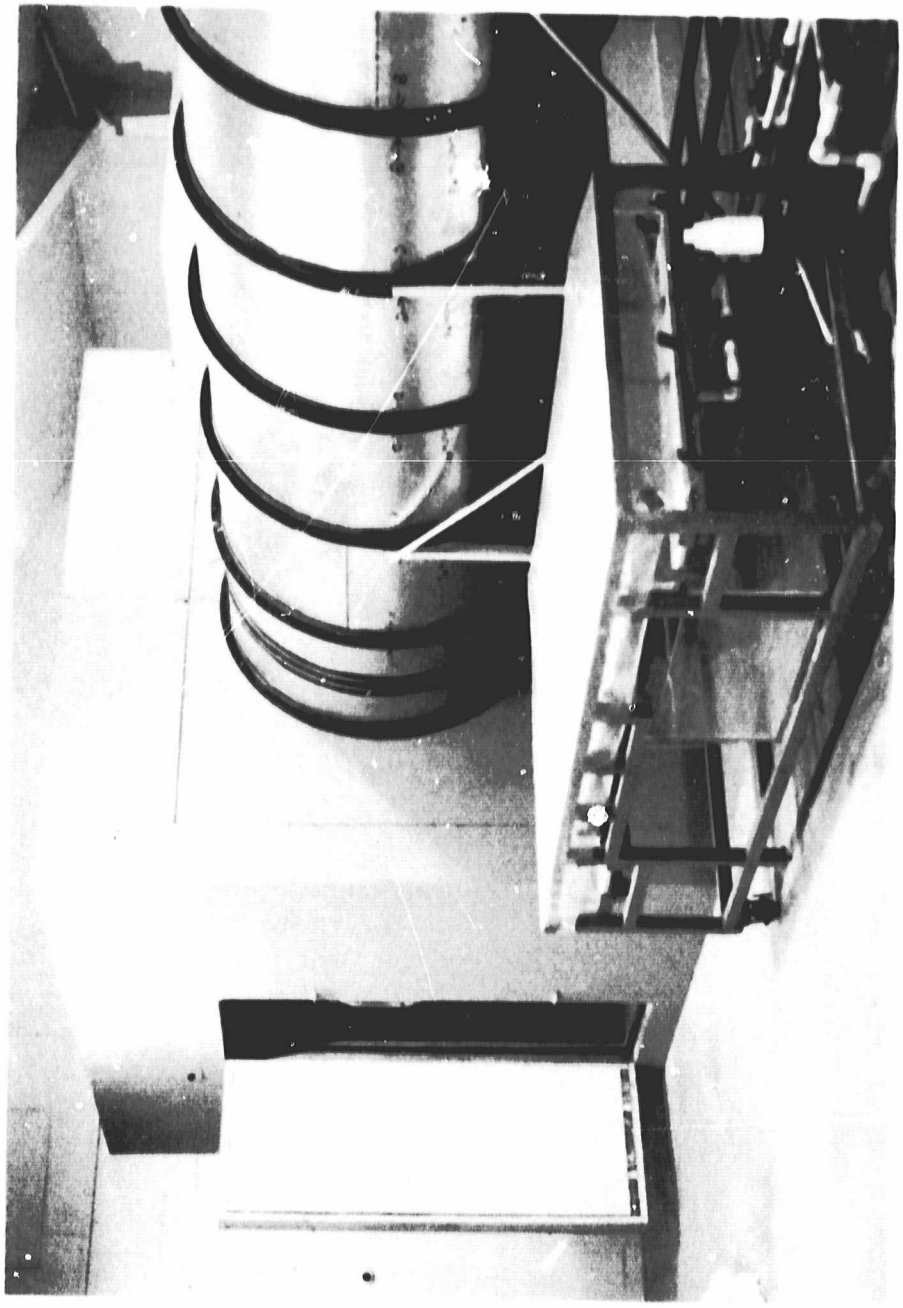

Figure 4. Exterior View of Plenum Chamber and Ducting.

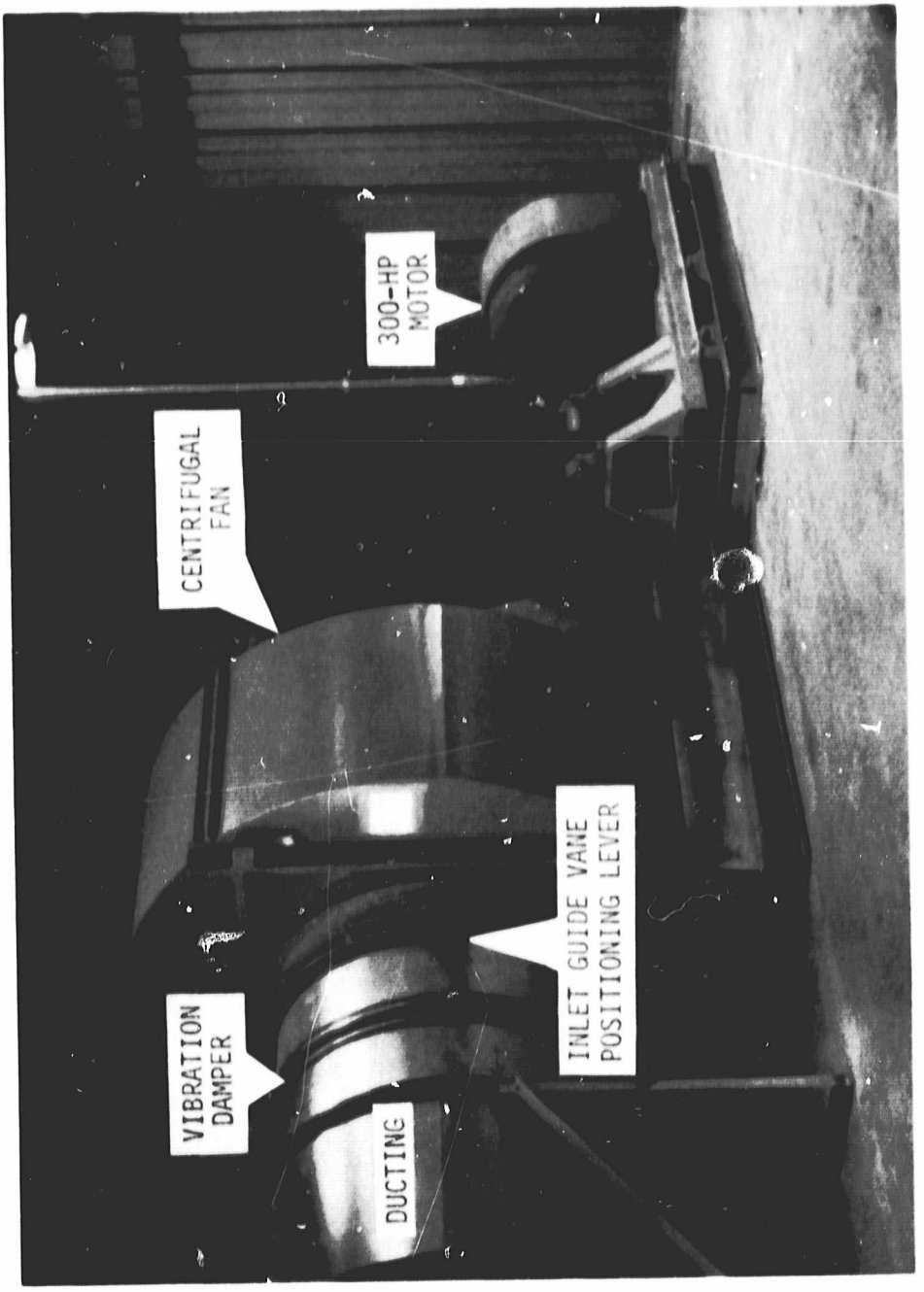

Figure 5. Facility Exhauster System.

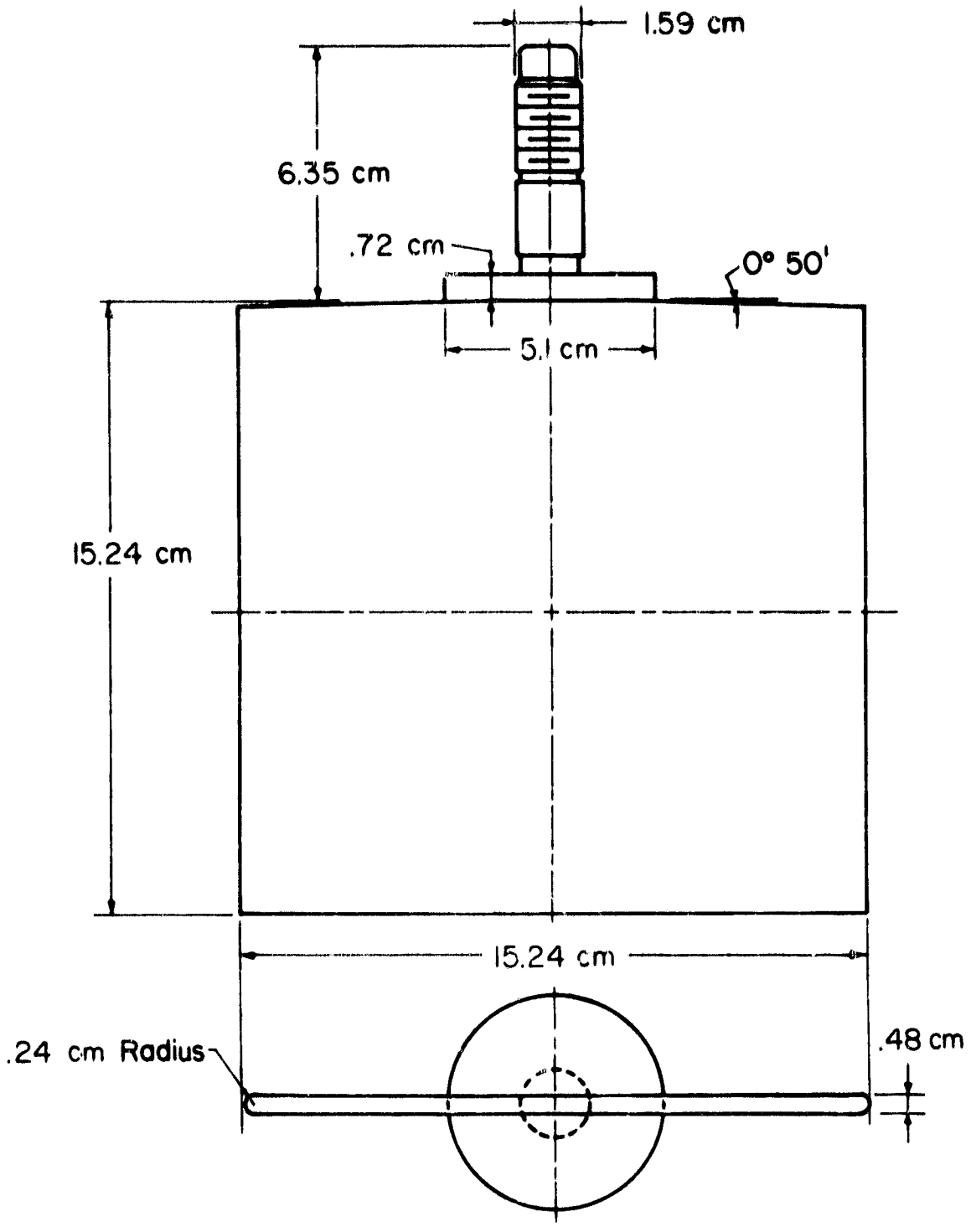

Figure 6. Flat Plate Airfoil Design

Provisions for instrumentation were designed into the facility to anticipate future measurement needs. In addition to a large number of pressure taps, there are provisions for probe insertion and for the application of flow visualization and Laser Doppler Anemometry techniques.

To determine the velocity profiles in the Annular Cascade Facility, a set of total pressure rakes were designed and fabricated. There are six rakes mounted upstream of the airfoil cascade, in Section A, and three downstream of the airfoil cascade, in Section C. The nine locations are shown schematically in Figure 7. Each rake has a total of ten total pressure taps. The taps are radially distributed such that each tap is located at the center of a concentric, equal-area annulus such that the mass flow integral

$$\dot{m} = \int \rho U \, dA \qquad (1)$$

converts to the simple sum

$$\dot{m} = \rho A \, \Sigma U_i \qquad (2)$$

A typical rake is depicted in Figure 8 and pictured mounted in the facility in Figure 9.

Each rake was designed to minimize the effects of misalignment, viscosity, and proximity to the annulus wall. The rake tubes were designed with an inner to outer

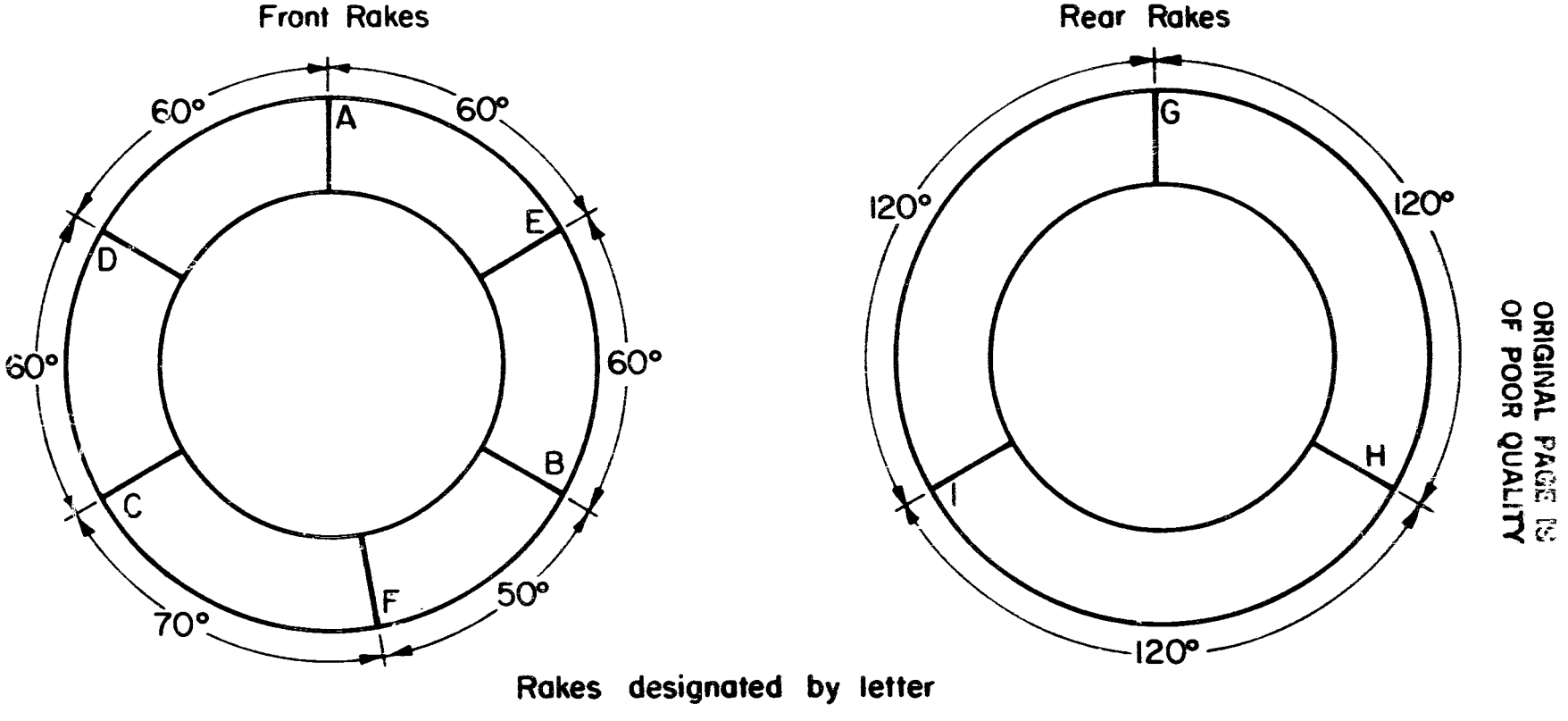

Figure 7. Pressure Rake Circumferential Locations.

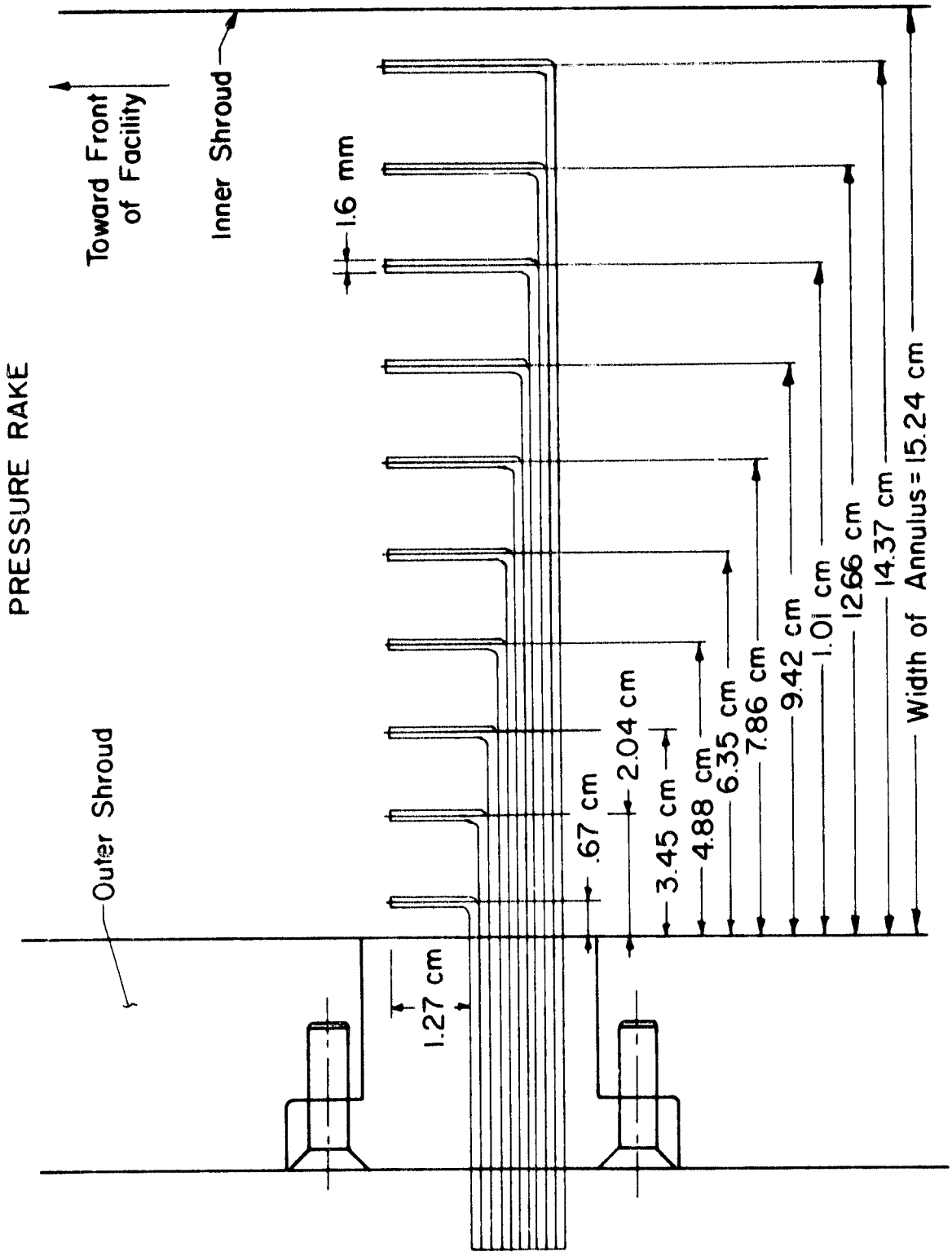

Figure 8. Schematic of Total Pressure Rake

Figure 9. Total Pressure Rake Mounted in Facility.

diameter ratio greater than 0.663. This allows for a misalignment of the total-pressure tube of up to ±11 degrees without significantly affecting the measurement. To minimize interference due to wall proximity, the maximum outer tube diameter was determined to be 0.318 cm (0.125 in) for this configuration. The outer tube diameter of 0.16 cm (0.063 in) was selected so as to be compatible with the pressure measurement system to be described later. With this rake configuration and the facility design flow speeds, viscous effects on the rake measurements are negligible [1].*

The Purdue Annular Cascade Facility is also extensively instrumented with static pressure taps, one of which is depicted in Figure 10. There are four distinct sets of static taps. One set of static pressure taps is located adjacent to the total pressure rakes. The static pressure data from this set of taps is used with the corresponding total pressure rake data to determine the velocity profile in the annulus flow field. These static pressure taps are located in the same axial plane as the rake inlets, and are offset circumferentially from the rakes by five degrees so as to preclude interference from the rake bodies. There are two static taps associated with each rake; one on the outer shroud wall and one on the inner shroud wall.

* Numbers in brackets refer to the list of references.

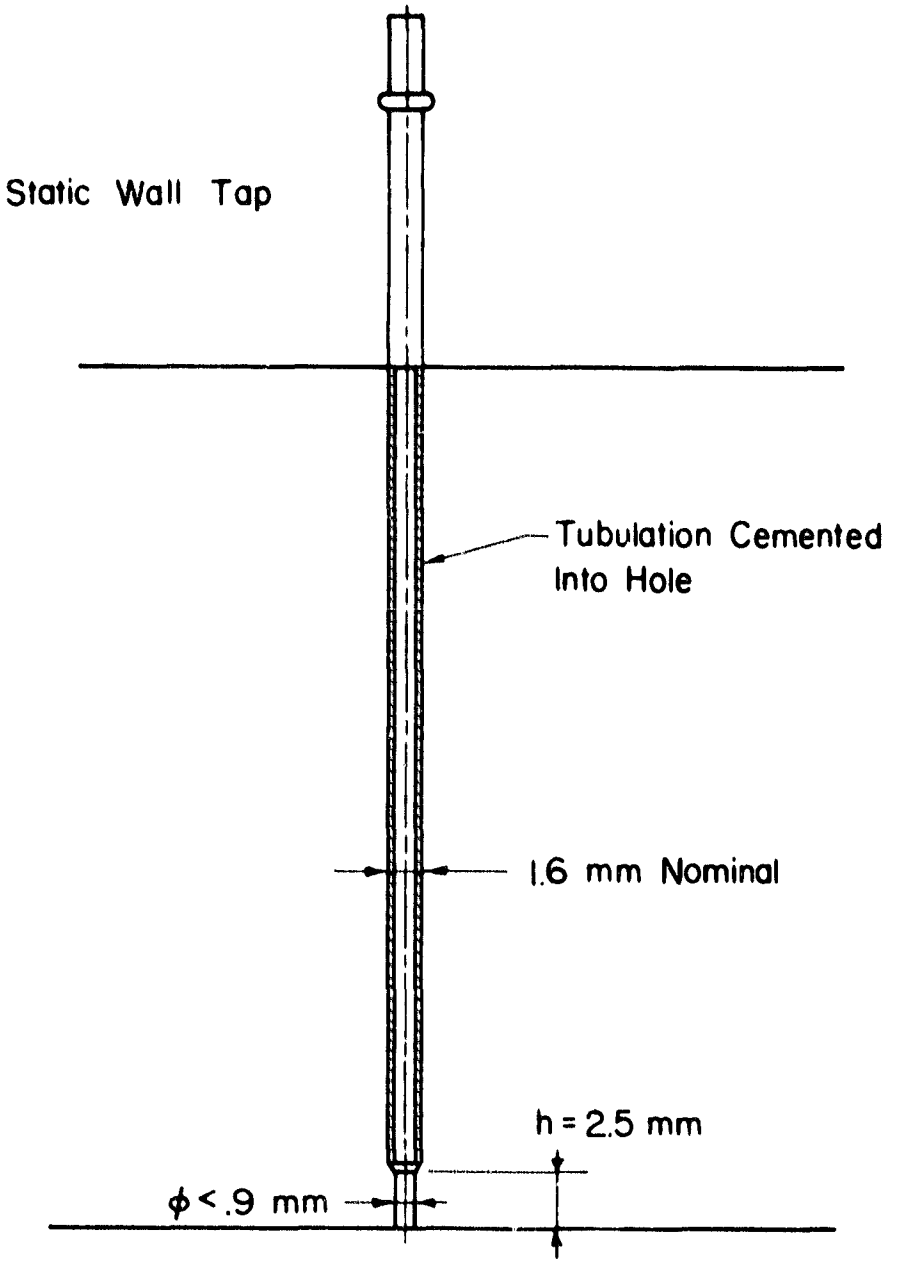

Figure 10. Facility Wall Static Pressure Tap Design.

A second set of static pressure taps is located at points in the inner and outer shroud walls of the facility. Their locations are indicated in Figure 11 by the intersection of the "static tap lines". There are 32 such static taps and they permit monitoring and verification of the flow field.

A third set of static pressure taps is located in a high-density array in the outer shroud wall covering the endwalls of two airfoil passages as depicted in Figure 12. They allow the acquisition of data describing the behavior of the flow in the endwall region and are unequally spaced so as to provide adequate coverage for blades of varying chord lengths.

Four airfoils were also instrumented with surface static taps, the fourth set of static pressure taps. Two types of instrumented blades were designed and fabricated. One type has 15 static pressure taps along a chord line at mid-span. The other type of instrumented airfoil has 30 static taps: 15 along a chord line at 10% span and 15 along a chord line at 90% span. These two types of blades are depicted in Figure 13. Two blades of each type were fabricated, and hence, airfoil surface chordwise pressure distribution data can be acquired at 10%, 50% and, 90% of the airfoil span on both the airfoil pressure and suction surfaces. These four airfoils were installed immediately in front of the probe traversing slots (to be described

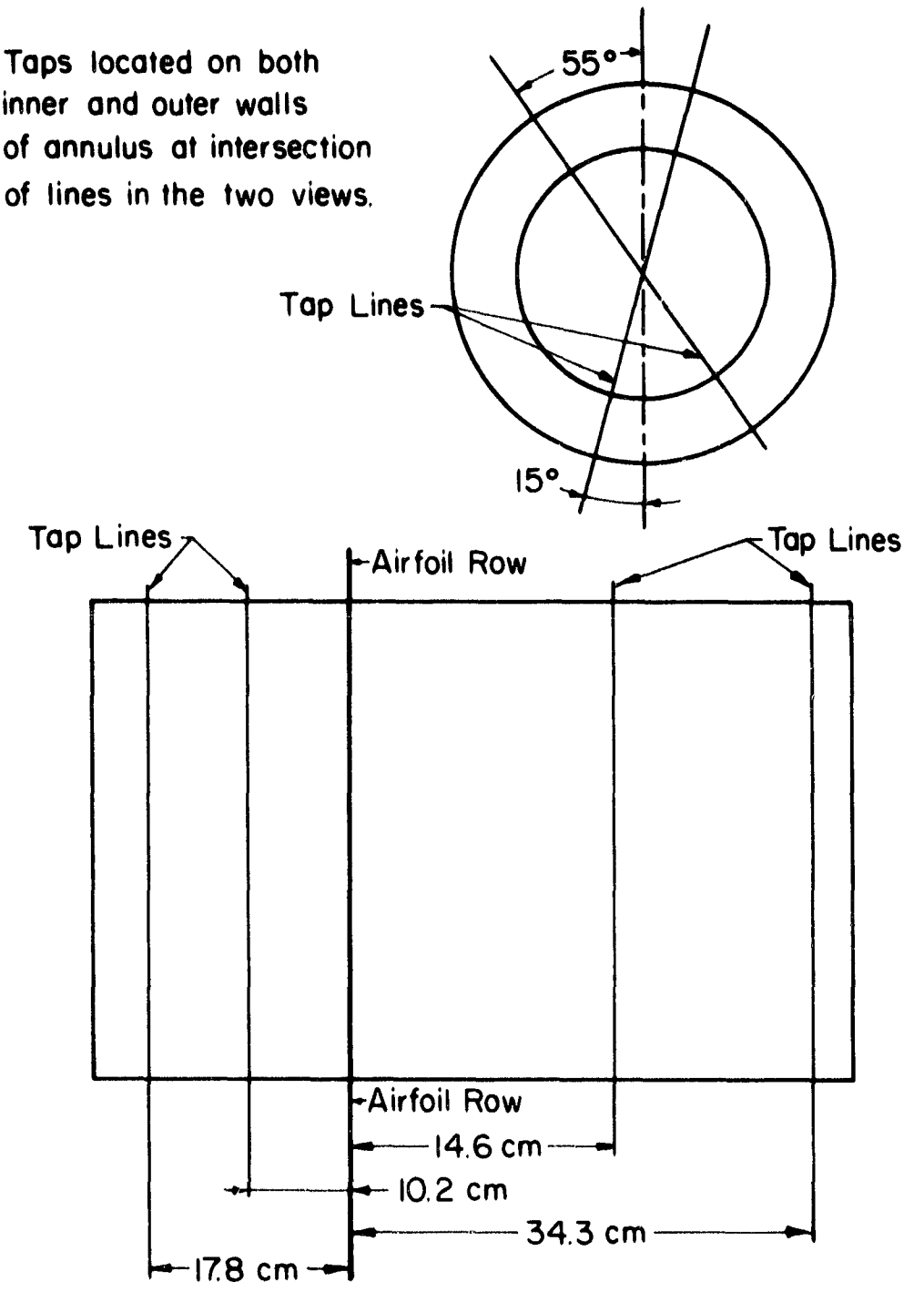

Figure 11. Location of Inner and Outer Shroud Wall Static Pressure Taps.

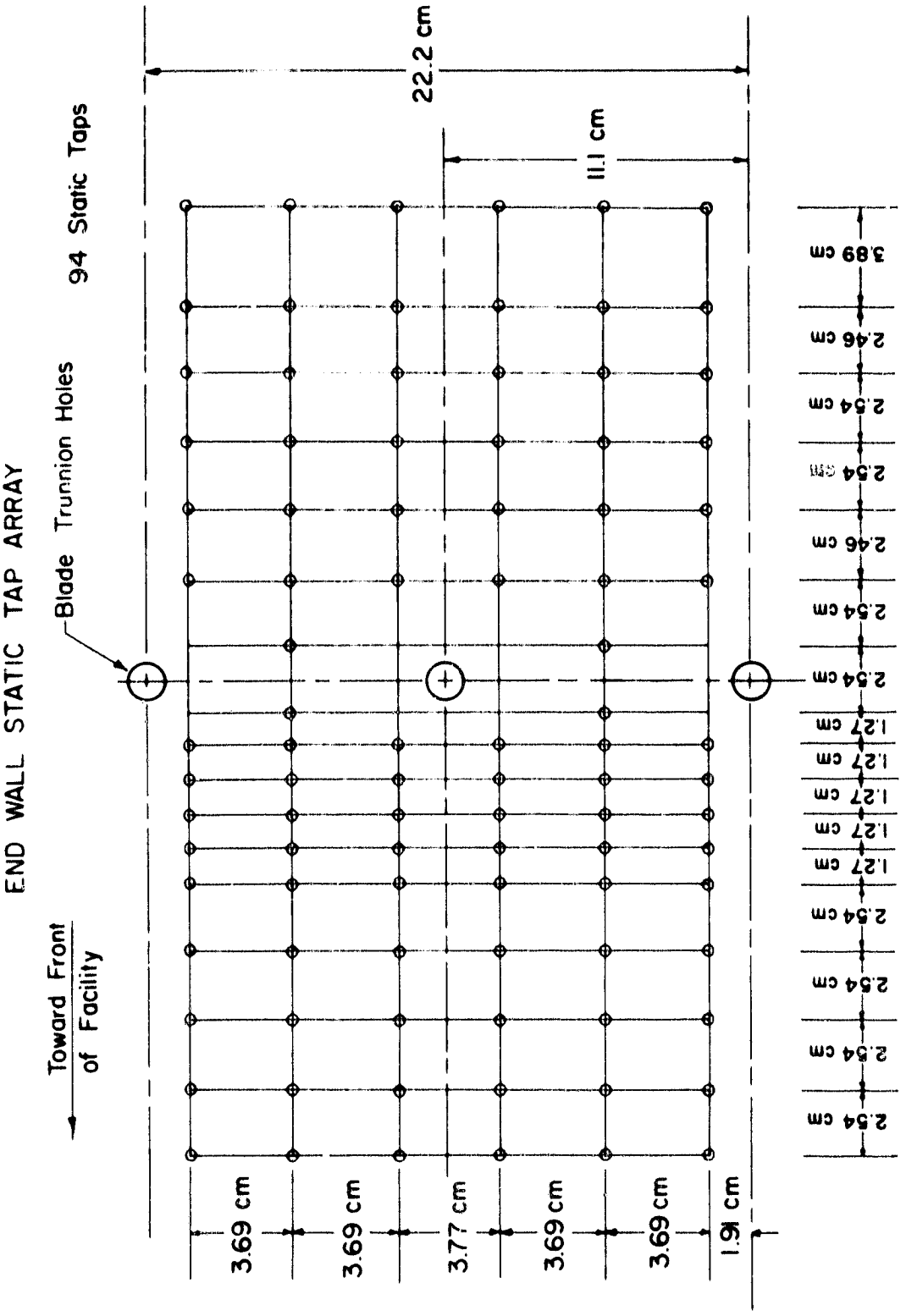

Figure 12. Endwall Array of Static Pressure Taps.

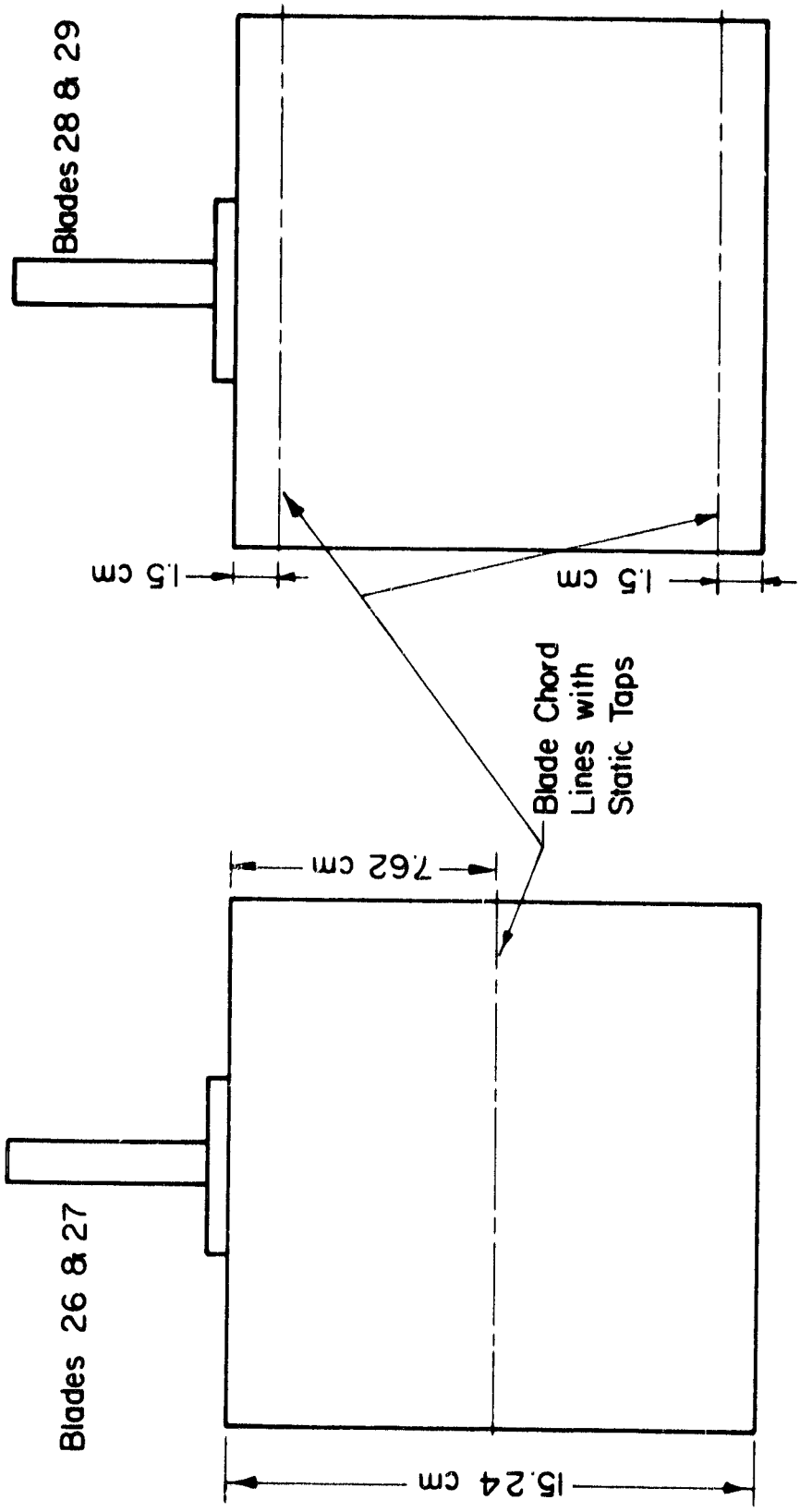

Figure 13. Airfoil Surface Static Pressure Tap Spanwise Locations.

below) so as to permit the investigation of the entire flow field by pressure tap and probe methods.

The airfoil surface static pressure taps are distributed in a Gauss-Legendre chordwise array [2], illustrated in Figure 14. The Gauss-Legendre distribution was selected partially in expectation of using the associated quadrature, but more as a means of rationally distributing the airfoil surface static pressure taps such that there would be a higher density near the leading and trailing edges of the airfoils, where the more interesting and important flow phenomena are expected.

To facilitate the application of flow visualization techniques and Laser Doppler Anemometry (LDA), the facility test section was fabricated with transparent sections as an integral part of the inner and outer shroud walls. The window in the outer shroud wall extends circumferentially for approximately 90 degrees, covering eight complete airfoil passages. A window was also placed on the inner shroud wall in direct alignment with the outer shroud window so as to allow the possibility of a light source on one side of the flow passage and a receiving device on the other side.

To further facilitate the application of optical measurement techniques, five airfoils, circumferentially centered on the test section window were designed to be

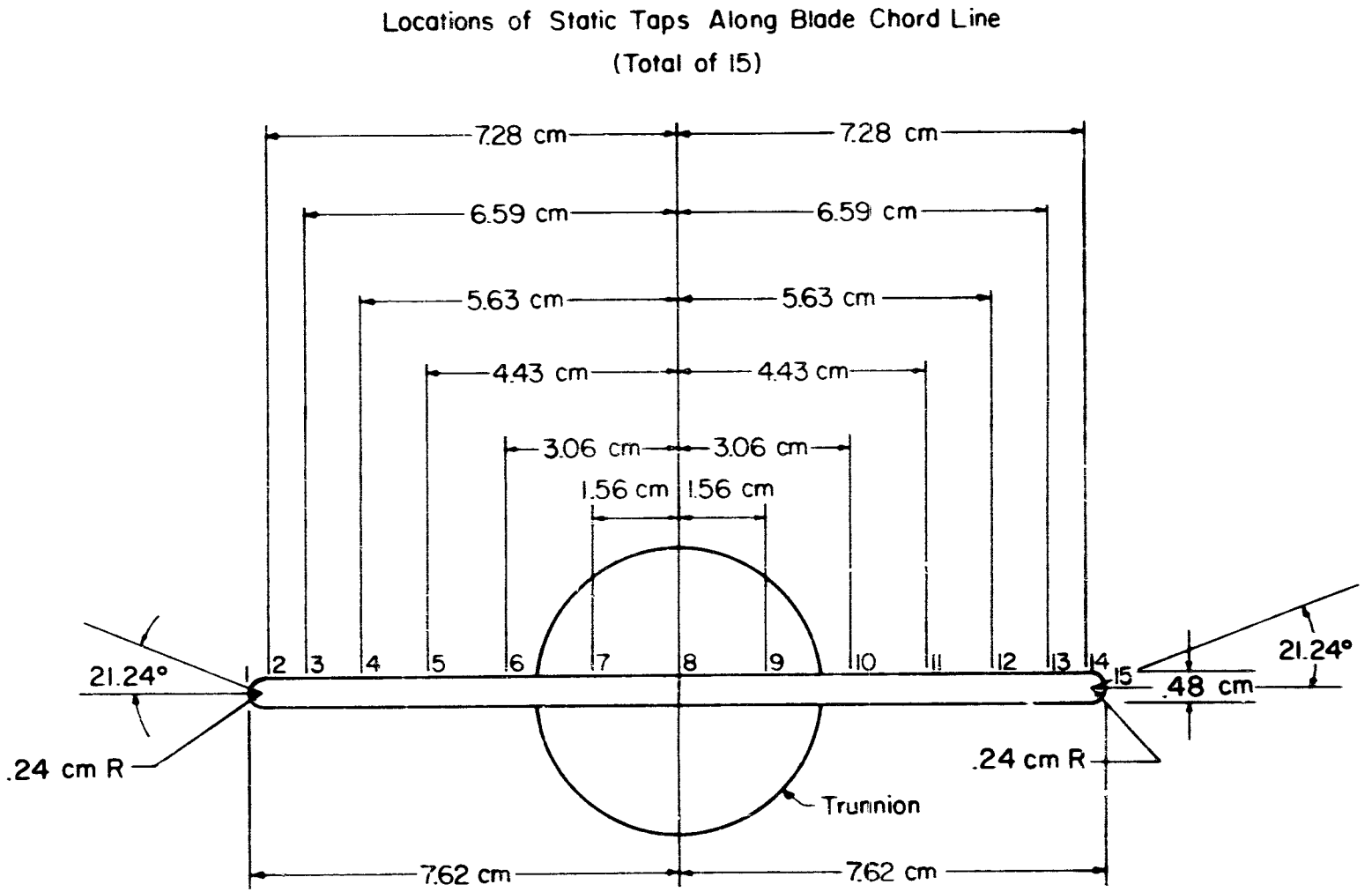

Figure 14. Chordwise Distribution of Airfoil Surface Static Pressure Taps.

cantilevered from the inner shroud wall so that the airfoil-mounting trunnions do not interfere with the airfoil passage flow visualization or Laser Doppler Anemometry data acquisition. This permits the entire airfoil passage and exit flow regions, as seen in Figure 15, to be investigated with various optical techniques.

The facility was fabricated with two slots in the airfoil cascade exit region to permit the insertion of various types of probes into the flow stream. The slots permit full radial traverses and 45-degree circumferential traverses of the annulus. Each exit-region slot has provisions for mounting a circumferential and radial traversing mechanism as is shown in Figure 16.

The flow entering the facility must be steady and uniform. In particular, it must be free from flow structures, such as vortices, which would be drawn into the inlet, causing the flow to be unsteady.

Air being drawn into the inlet of the facility causes radial sink flow to occur on inlet-adjacent surfaces perpendicular to the facility through-flow. Such surfaces include walls, ceilings, and floors. Radial sink flow streamlines converge toward a stagnation point on the surface at which point they curve away from the surface and into the inlet. If such a stagnation point is permitted to occur on this surface, a free vortex forms [3]. The

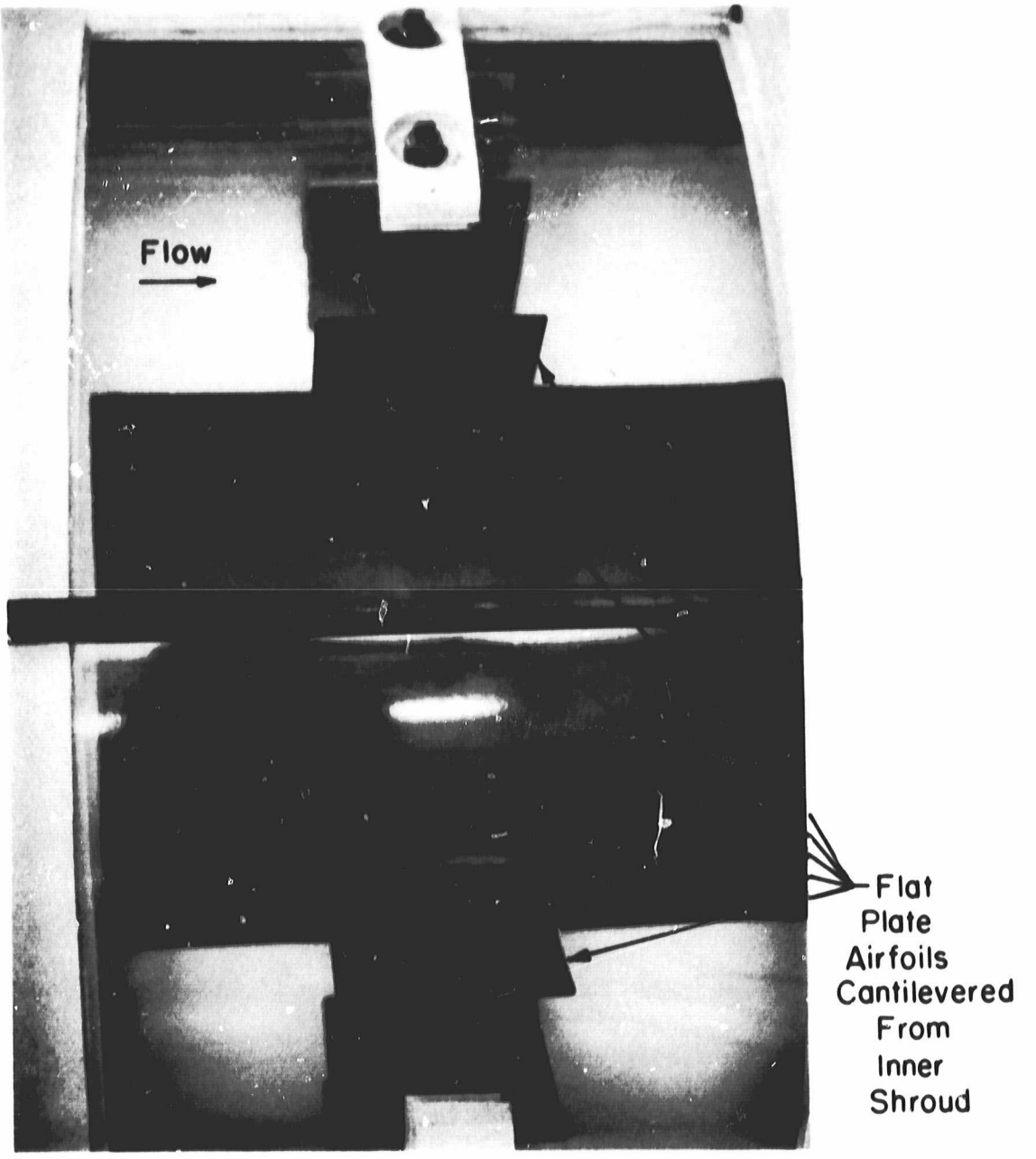

Figure 15. View of Airfoil Cascade Mounted in Test Section Through Transparent Outer Section.

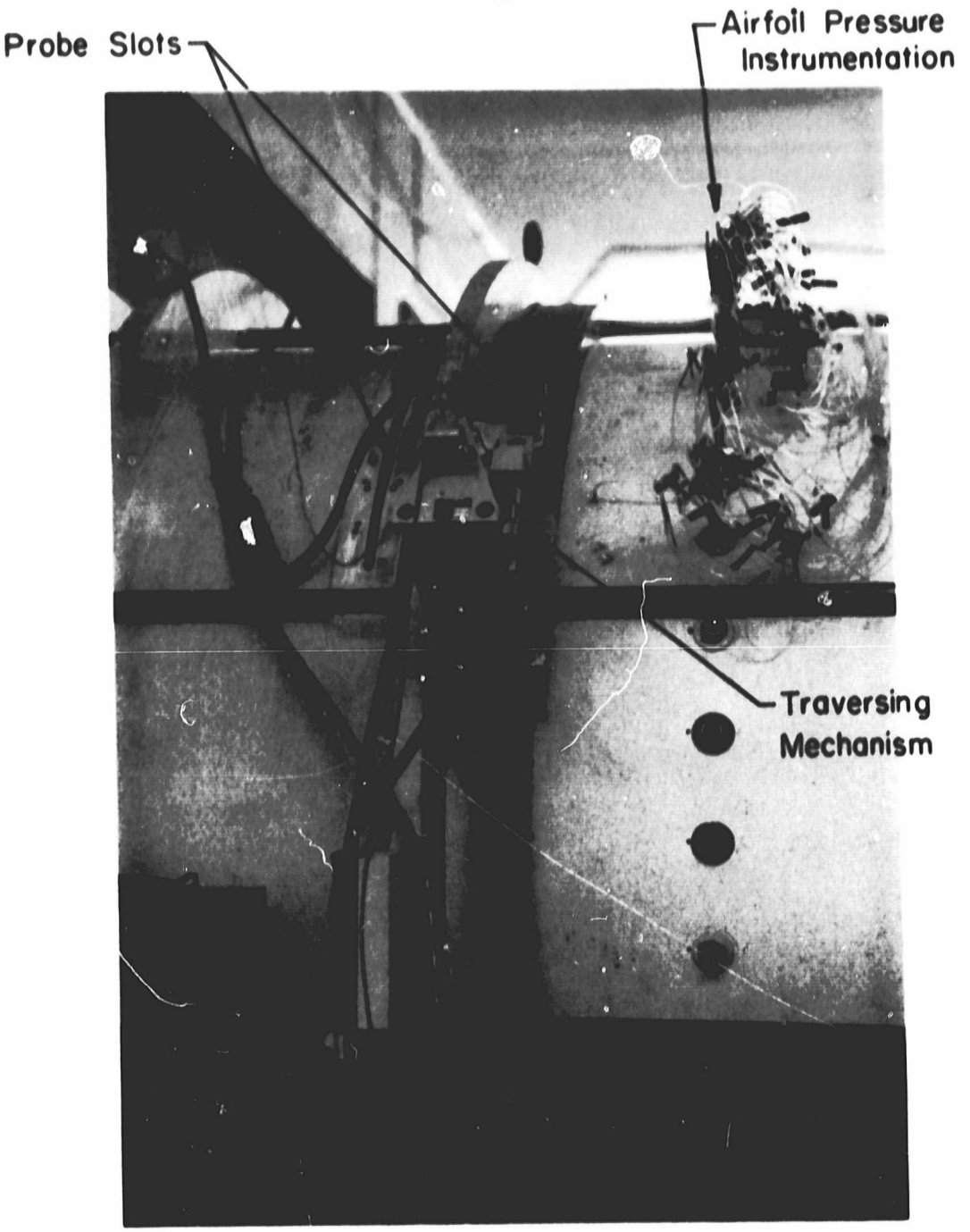

Figure 16. Cascade Exit Region Wall Slots With Traversing Mechanism for Probe Insertion.

resulting vorticity enters the inlet causing unsteadiness in the flow, which is easily seen using flow visualization techniques. The inlet vortices themselves can be easily visualized by placing styrofoam packing material on the floor near the inlet.

Several schemes were tried to suppress the formation of these inlet vortices. Because there is a large stagnant region behind the bellmouth inlet, a wall, shown in Figure 17, was built immediately behind the bellmouth to prevent the stagnant region from feeding the sink flows from behind. This was only partially successful in suppressing the vortex formation.

A second scheme, based on the experience of Colehour and Farquhar of the Boeing Company [3], was the construction of six asterisk-shaped fences to impede circular flows. Shown in Figure 18, three of the fences were mounted on the floor while the other three were mounted on the ceiling. Even though the "vortex splitters" considerably weakened the inlet vortices, there was still some vorticity at the inlet and accompanying unsteadiness in the facility.

To further condition the flow ertering the facility, a porous inlet section comprised of a series of screens was constructed to break up any flow structures. Shown in Figures 19 and 20, the screen assembly consists of two

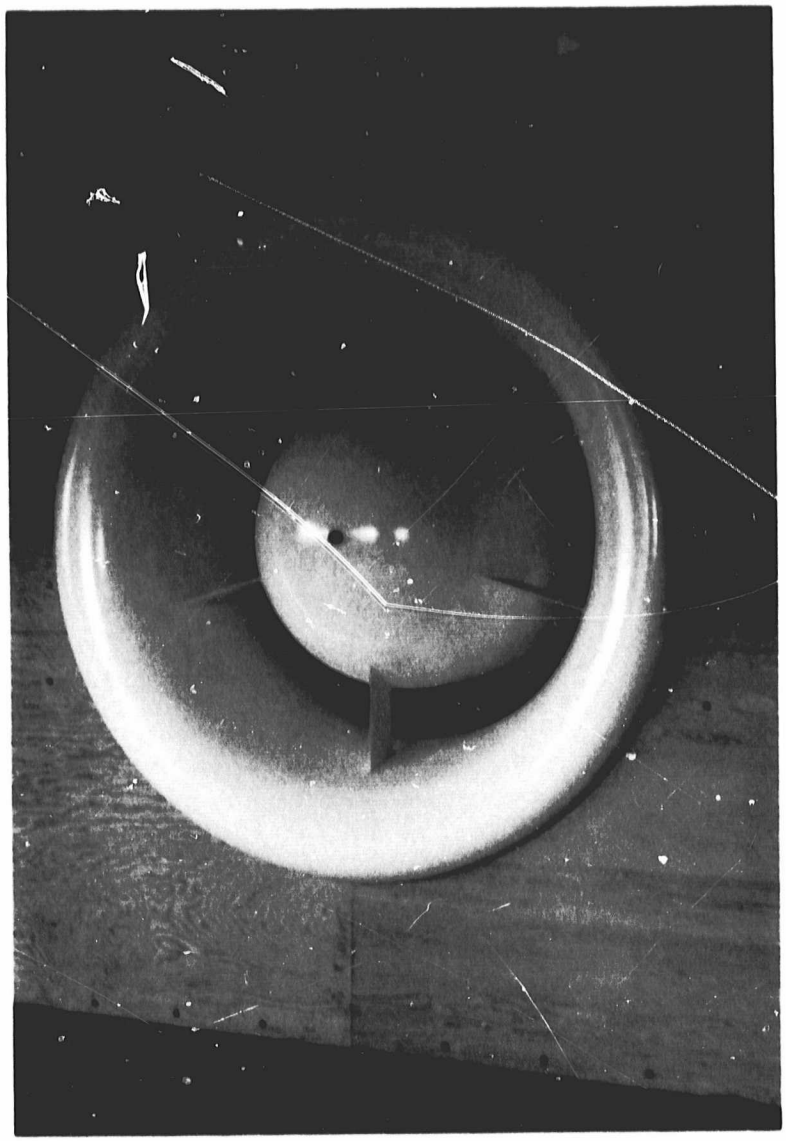

Figure 17. Inlet Bellmouth and Extension Sidewall.

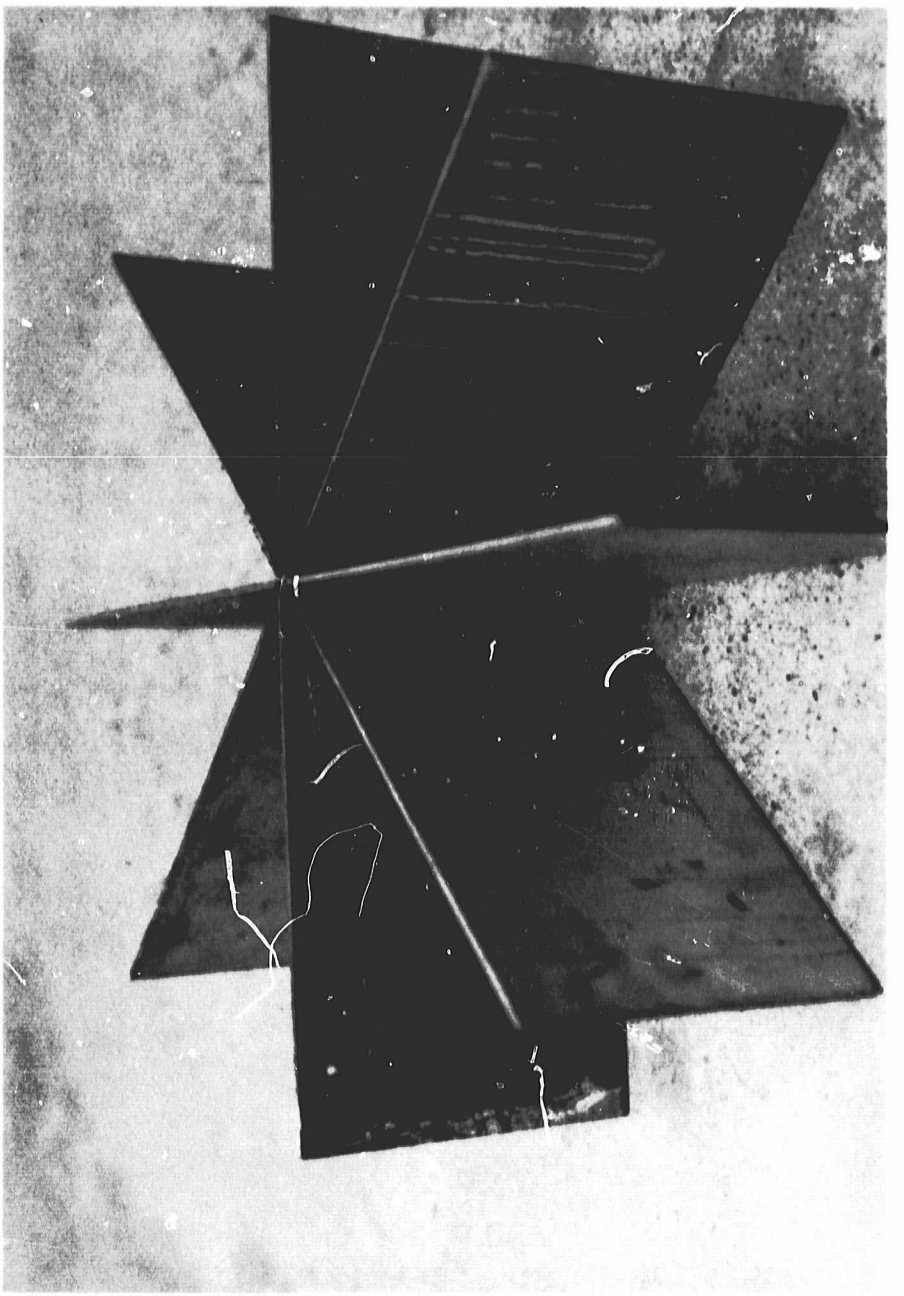

Figure 18. Vortex Splitter.

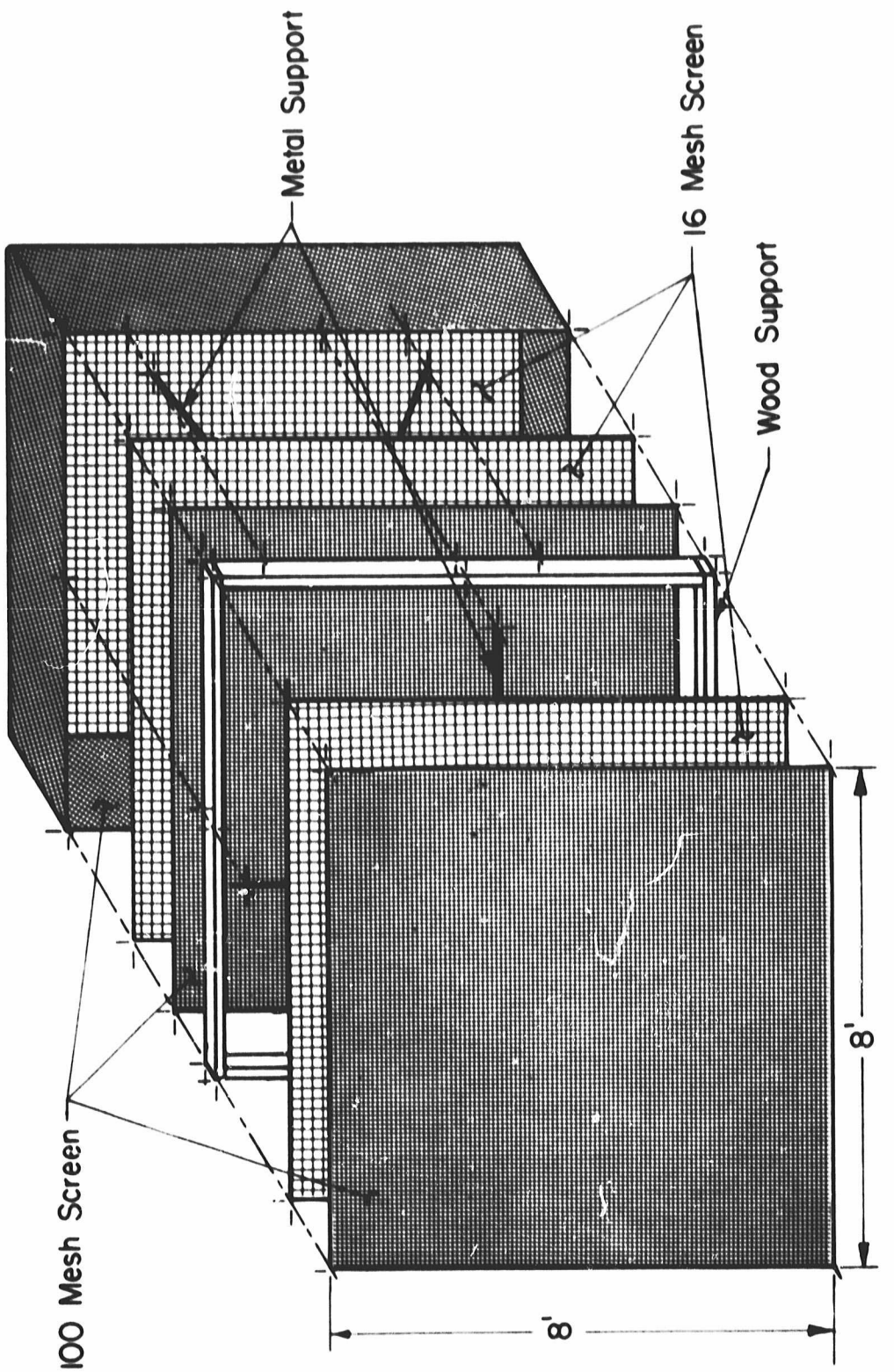

Figure 19. Exploded View of Inlet Screen Assembly.

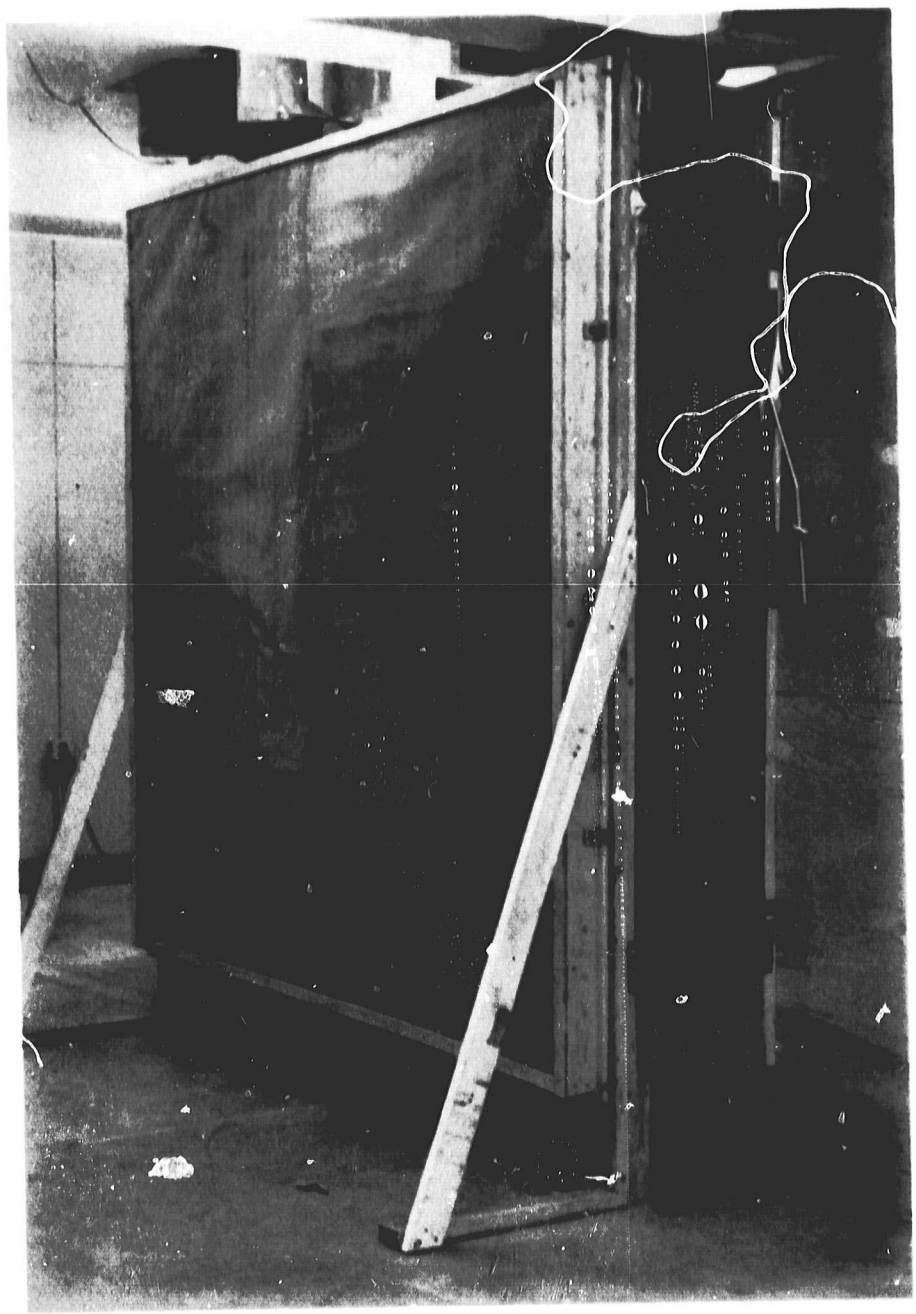

Figure 20. Inlet Screen Assembly.

series of 100-mesh screen, each structurally supported by a layer of ordinary window screen (16-mesh), with a spacing of 9.5 cm (3.75 in) between the two series. This makes for a "relaxation zone" for the flow between these two series of screen. The side walls of the screen assembly are 30.5 cm (12.0 in) wide and porous, also consisting of 100-mesh screen. A third layer of window screen was placed directly over the bellmouth to provide a support structure for future additional screen and mesh combinations to be utilized to generate a variety of inlet velocity profiles. With this inlet screen assembly in place, together with the devices described above, the flow through the facility was found to be steady, indicating that the screen assembly had suppressed the inlet vortices.

CHAPTER 3

INSTRUMENTATION OF THE FACILITY

Because the measuring instruments interact so intimately with the data which they produce, the selection of instrumentation is of prime importance. This chapter describes in detail several instrumentation areas of the Purdue Annular Cascade Facility, with emphasis on the design philosophy of the instrumentation systems.

As described in Chapter 2, designed into the facility are provisions for substantial quantities of pressure instrumentation, with many pressure taps of various types. Including the total pressure rakes, airfoil surface static pressure taps, and the other facility static pressure taps, there are a total of 324 pressure measurement locations.

There are, of course, several methods for measuring an essentially steady pressure. Two common devices are the water manometer and the electrical pressure transducer. However, providing one pressure transducer for each pressure tap would most certainly be prohibitively expensive (e.g. a typical transducer with amplifier costs approximately $800). Manually recording the readings from banks of water manometers would be an exercise in tedium.

To surmount such difficulties, a pressure measurement system was designed based on the "Scanivalve" method. In particular, the Scanivalve Corporation manufactures a valve-switching device which enables a single transducer to sequentially be exposed to and measure 48 different pressure inputs. In addition to minimizing the cost of transducers and associated support equipment, it removes the necessity of calibrating a large number of transducers.

There are six major units in the basic Scanivalve system. There is the valve switching module, the solenoid advance, the position indicator, the transducer, its signal conditioner, and the controller. A picture of a typical Scanivalve system is shown in Figure 21 [4]; this is a multiple unit which has four valve-switching modules in tandem. The system selected for the facility has three such modules; however, it is capable of being expanded to include additional modules.

The key to the Scanivalve system is the valve-switching module. The pressure transducer is installed in this unit. The inner mechanisms of the unit are driven by the solenoid advance and rotate in such a way that the the transducer is exposed to only one of the 48 pressures to which the unit is connected. The position-indicator is driven in tandem with the valve-switching modules and electrically indicates which of the 48 pressure ports is being exposed to the transducer. The 48 pressures are

Figure 21. Typical Scanivalve Multiple-Module Unit.

connected to the system by means of pneumatic tubing attached to the stainless steel tubulations at the top of the valve-switching modules.

A plexiglass case was fabricated to house the Scanivalve system. This protective case makes it possible to virtually eliminate direct contact with the Scanivalve units themselves by using the case as the primary interface between the facility and the pressure measurement system. This was accomplished by creating a 12 X 24 array of stainless steel tubulations drilled and cemented through the front of the case. These tubulations are connected with pneumatic tubing to the Scanivalve units within the case. On the exterior of the case, the tubulations are connected to the facility pressure taps also with pneumatic tubing. Pressure tap to port connections are changed with relative ease on the exterior face of the case. The transducer signal conditioners are fastened to the rear face of the case with all of the necessary electrical cables running through ports in the rear face of the box. An exterior view of the resulting system is shown in Figure 22.

To further expand the number of pressure measurements which can be made without significantly increasing the cost, two quick-disconnect couplings were installed within the protective case. These couplings permit relatively quick changes in specifying which pressure lines enter a

Figure 22. Scanivalve Pressure Measurement System.

module. Each coupling carries 48 pressure lines--the number and configuration exactly corresponding to that of the valve-switching modules. Changing the disconnects is the only time that it is necessary to enter the case.

Inasmuch as there are currently more than 250 pressure lines originating at the facility and connected into the Scanivalve case, it was necessary to devise a labeling and bookkeeping system for the pressure lines. Mnemonic labels were devised for each pressure tap and attached to each pneumatic tube. A diagramatic representation of the front face of the Scanivalve case was utilized to show at a glance how the facility pressure taps interfaced with the Scanivalve system. Such a scheme is invaluable in making impromptu changes and in trouble-shooting.

The pressure transducers chosen for this system are 6.9 kPa (1.0 psid) bi-directional, differential transducers. Thus, the output is proportional to the difference of two pressures, one on either side of the diaphragm.

The ambient pressure is by nature steady, hence it is used as the reference pressure for all the pressure measurements. The ambient pressure is also the highest pressure possible anywhere in the system. This means that all pressures are measured as vacuum pressures. Absolute pressures are easily obtained as the ambient pressure can

easily be determined with a barometer.

The transducer input-output calibration curves were verified to be at least piece-wise linear, as demonstrated in Appendix B. A typical piece-wise calibration curve is shown in Figure 23. The variation in the curve at 0 pressure difference is a result of the strain gage in the transducer being mounted on one side of the transducer diaphragm; hence, it reacts differently to positive and negative deflections.

Because the ambient pressure was chosen as the reference pressure, all pressure measurements involve the negative leg of the calibration curve. To determine this negative leg, a known negative pressure is needed to set the span point in addition to the reference pressure which determines the zero point. Once determined, the calibration curves for the pressure transducers and their signal conditioners are not invariant. Both the zero output and the span output may drift due to changes in temperature, for example. Therefore, to obtain a very high degree of accuracy, it is necessary to either recalibrate the transducers prior to each use, or to determine the necessary correction factors and subsequently use them to correct the data.

To determine the calibration curve, and to deal with the problem of drift, a system was designed and built to

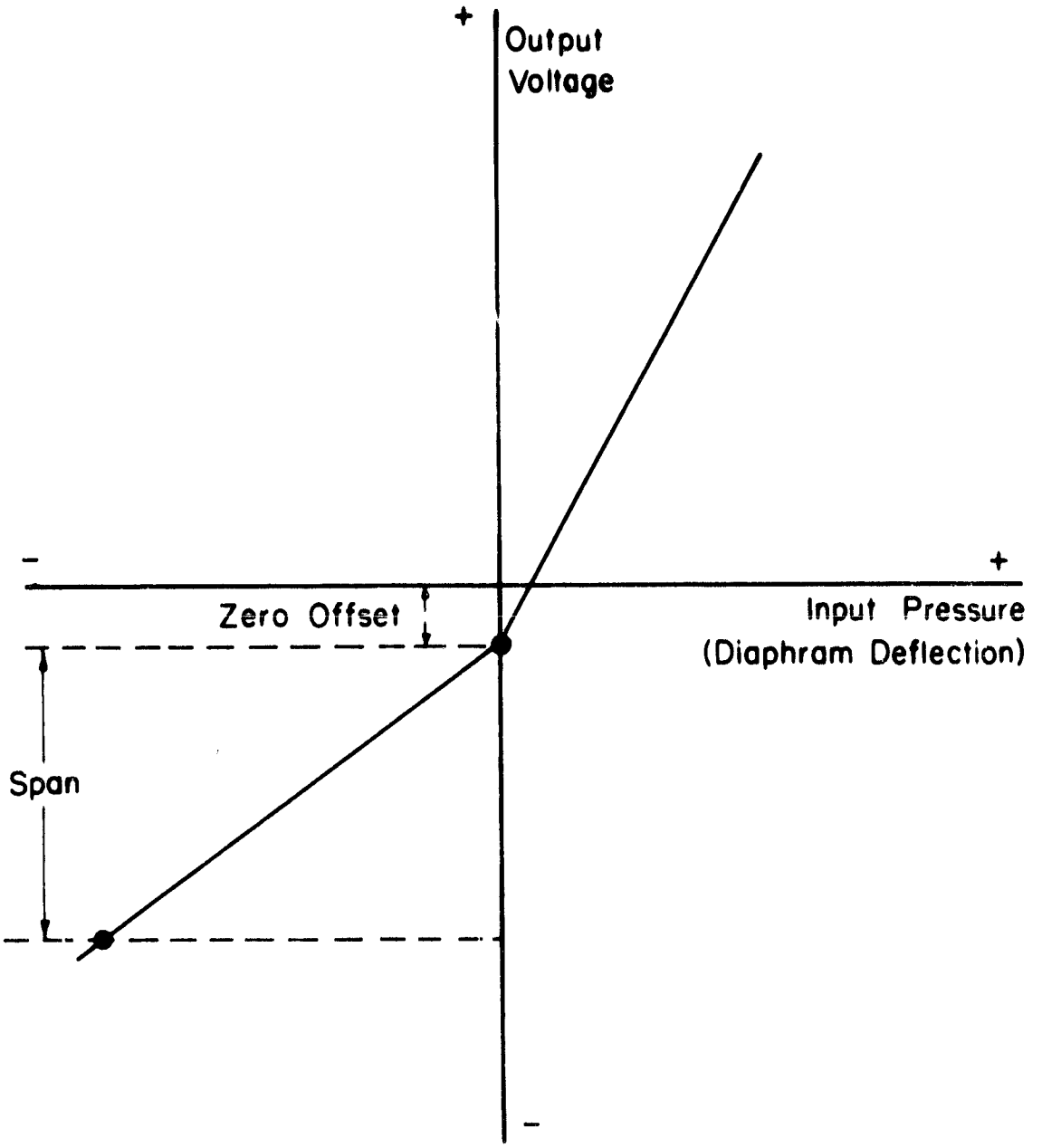

Figure 23. Typical Transducer Calibration Curve.

provide a calibration pressure of one psi vacuum. This system consists of a suction pump (maximum suction is 35.6 cm of mercury), a vacuum pressure regulator, a plexiglass plenum chamber to damp out any pump pulsations, and a 200 cm U-tube water manometer. The exact amount of vacuum is set by adjusting the regulator and is measured by the manometer. The complete system is shown in Figure 24. It is relatively difficult to set the calibration system to exactly reproduce a specified vacuum level. This is circumvented by making an approximate setting and then noting the manometer level. The vacuum level so obtained and the corresponding transducer output yield the span point of the calibration curve.

The vacuum side of the pressure calibration system is connected to Port #1 of each of the three valve-switching modules of the pressure measurement system. Port #2 of each module is connected to the ambient pressure. In this way, the transducers are recalibrated each time a pressure scan is executed as this arrangement yields the transducer outputs for the span pressure and for the zero pressure. This completely determines the necessary leg of the calibration curve and eliminates the drift problem as the pressure scan time (the time necessary to measure the pressures at all 48 ports) is extremely short as compared to the drift time of the transducer input-output curve.

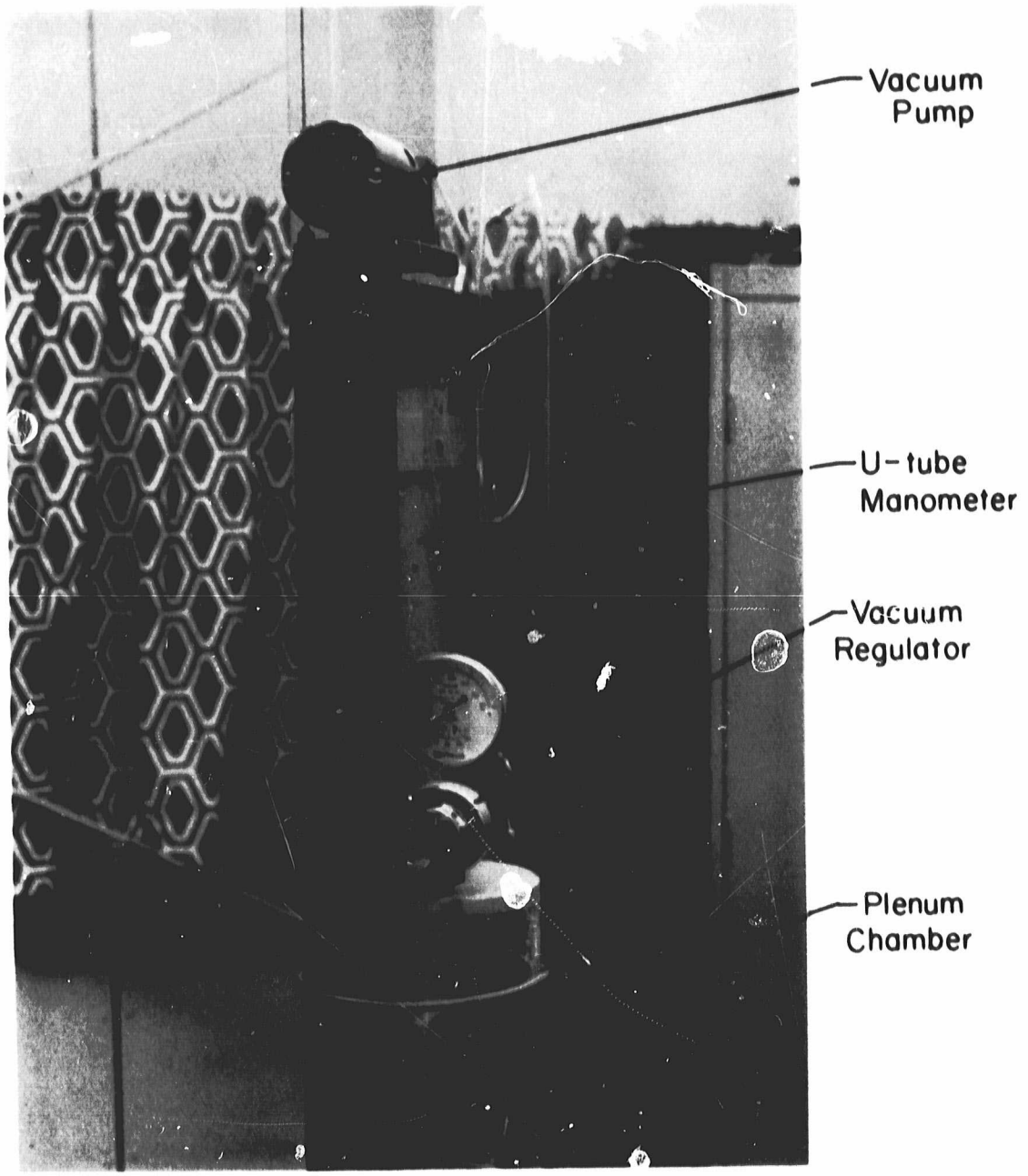

Figure 24. Calibration Pressure System.

To automate the pressure data acquisition, a Hewlett-Packard 3497 data acquisition system and a Hewlett-Packard 85 desktop computer, shown together in Figure 25, are utilized. The data acquisition unit has five slots into which various function-performing circuit boards are inserted. The boards chosen for this system include a 20 channel analog input board which controls the input channel seen by the built-in voltmeter, a 16 channel actuator board for switching peripheral devices, and a 16 bit digital input board. In the pressure measurement system, the actuator board is used to advance the Scanivalve port position, the digital input board reads the port position, and the analog input board and the voltmeter sequentially measure the three transducer outputs at each port position.

The data acquisition unit is controlled by the HP-85 computer. This computer is programmed in the Basic language, has graphics capability, and both a CRT screen and a 10.5 cm wide printer. Commands to operate certain channels, read registers, etc., are sent to the acquisition unit over a hardware bus via the Basic OUTPUT command. Quantities resulting from their execution are placed in a buffer in the data acquisition unit until they are transferred over the bus to the computer memory upon receipt of an ENTER command from the computer.

In writing the software to control the pressure measurement system, several objectives were taken into

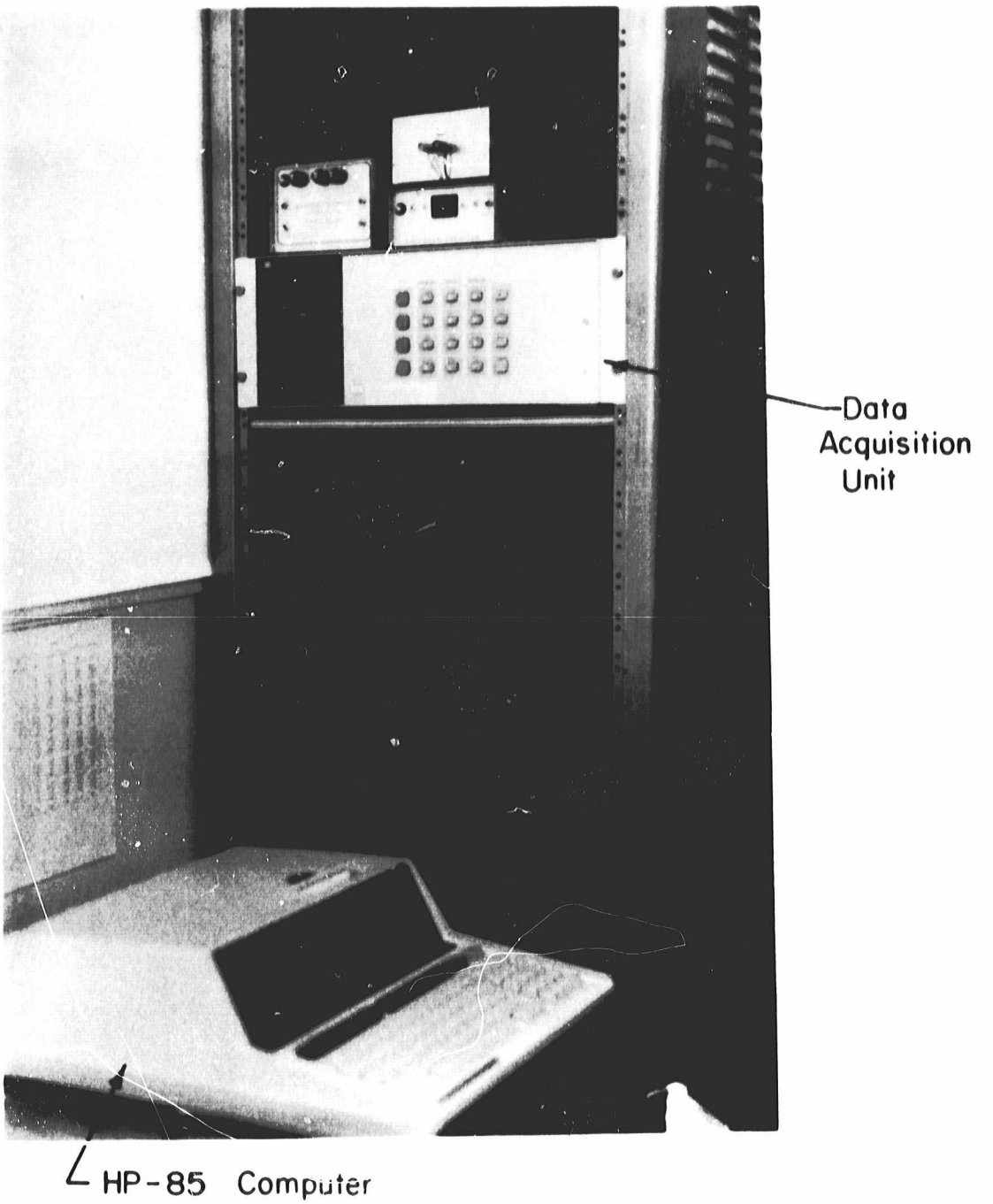

Figure 25. Data Acquisition System.

consideration. One of the objectives was to write an operator-efficient code. By this it is meant that there be a maximum number of options with a minimum amount of operator input. Among the options desired were the abilities to inspect the data online in both graphical form and in numerical form immediately after a pressure measurement scan had been completed. In this way the integrity of the data can be verified in the course of an experiment. It is important that it be easy for the operator to crosscheck between various representations of the data so that an equipment or instrument problem area can be bounded and corrected in a timely mannner. The software is further described in Appendix A.

Another objective considered in developing the controlling software was the temporal efficiency of the pressure scanning portion of the code. Flow conditions in the facility may drift slowly over an extended time period. This is mostly due to a very slowly increasing temperature resulting from the work input to the air by the facility exhauster system when the facility is operated in a re-circulating mode. Another factor resulting in some drift is variations in the electrical power supplied to the exhauster motor. Because of these factors, it is important that the Scanivalve system scan time be very short as compared to the time it takes for the flow conditions to drift.

Still another consideration in writing the software was to insure data security. Basically, this involves writing into the code the ability to recover from all possible errors--both resulting from processing bad data and from spurious input. Without proper error recovery, the computer would abort the program resulting in all of the data being unrecoverable. This is important because even bad data is often invaluable in determining its cause.

Before using the pressure measurement system to collect data, it was necessary to validate the system. This consisted of two different tasks: leak testing and transducer linearity testing.

To insure that the over 500 lengths of pneumatic tubing and associated fittings were free from leaks, a short computer program was written to carry out a scheme whereby alternate Scanivalve ports were exposed to a vacuum pressure and the ambient pressure respectively (e.g. ports 1,3,5...=vacuum pressure and ports 2,4,6...=ambient pressure). The alternating scheme was to prevent compensating leaks in adjacent ports. After the odd numbered ports had been verified to be free from leaks, the vacuum and ambient pressure lines were reversed in order to test the even-numbered ports. In this leak testing process, it was discovered that small amounts of water in the pressure lines are more detrimental than leaks because the presence of water is very subtle. Leaks cause gross

deviations from the expected readings which are easily noticed, but water in the lines affects the transducer outputs by just a few percent, an amount that could easily go unnoticed during the course of an experiment. Water in the pressure lines is the result of condensation caused by very humid air being used to purge the lines. Hence, it is easily prevented by taking appropriate precautions when the lines are purged. Any water can easily be purged with the compressed air supply as verified by experience.

The linearity of the transducers and their signal conditioners was verified by exposing them to the calibration pressure system. The calibration pressure system was set to various vacuum pressures which were recorded and plotted against the corresponding transducer outputs. The input-output response of all three transducers was verified to be very linear. The input-output curves are presented in Appendix B.

Flow visualization is an important tool for gaining an intuitive and visual understanding of the complex phenomena occurring in the flow field. It provides an aid to interpreting data produced by other experimental techniques.

The essential part of any flow visualization scheme is the presence of elements in the flow field which follow the flow pathlines and, with appropriate lighting, can be seen

and photographed. Smoke inserted into air flows and hydrogen bubbles produced by electrolysis in water flows have long been standard techniques.

The scheme chosen for flow visualization in the Purdue Annular Cascade Facility involves helium-filled soap bubbles. This technique [5] consists of inserting uniformly-sized, neutrally-buoyant, helium-filled soap bubbles into the upstream region of the flow. Because of their neutral buoyancy and their relatively small diameter (0.32 cm or 0.13 in), they follow the flow pathlines. With adequate lighting, the pathlines can be photographed.

The elements necessary to create the soap bubbles are helium, a soap solution, and compressed air. These three elements are regulated by metering valves in the bubble generator console and combine to form bubbles in the bubble head, shown together in Figure 26. The bubble head consists of three concentric tubes as shown in Figure 27. The helium flows out of the innermost tube and mixes with the soap solution flowing through the annulus around the helium tube to form helium-filled soap bubbles. The air flowing through the outer annulus causes the bubbles to detach and enter the flowstream when they reach the correct size for neutral buoyancy. This produces a durable bubble which is capable of traversing the entire flow circuit (including the exhauster). The bubble head is shown in position in the facility inlet in Figure 28.

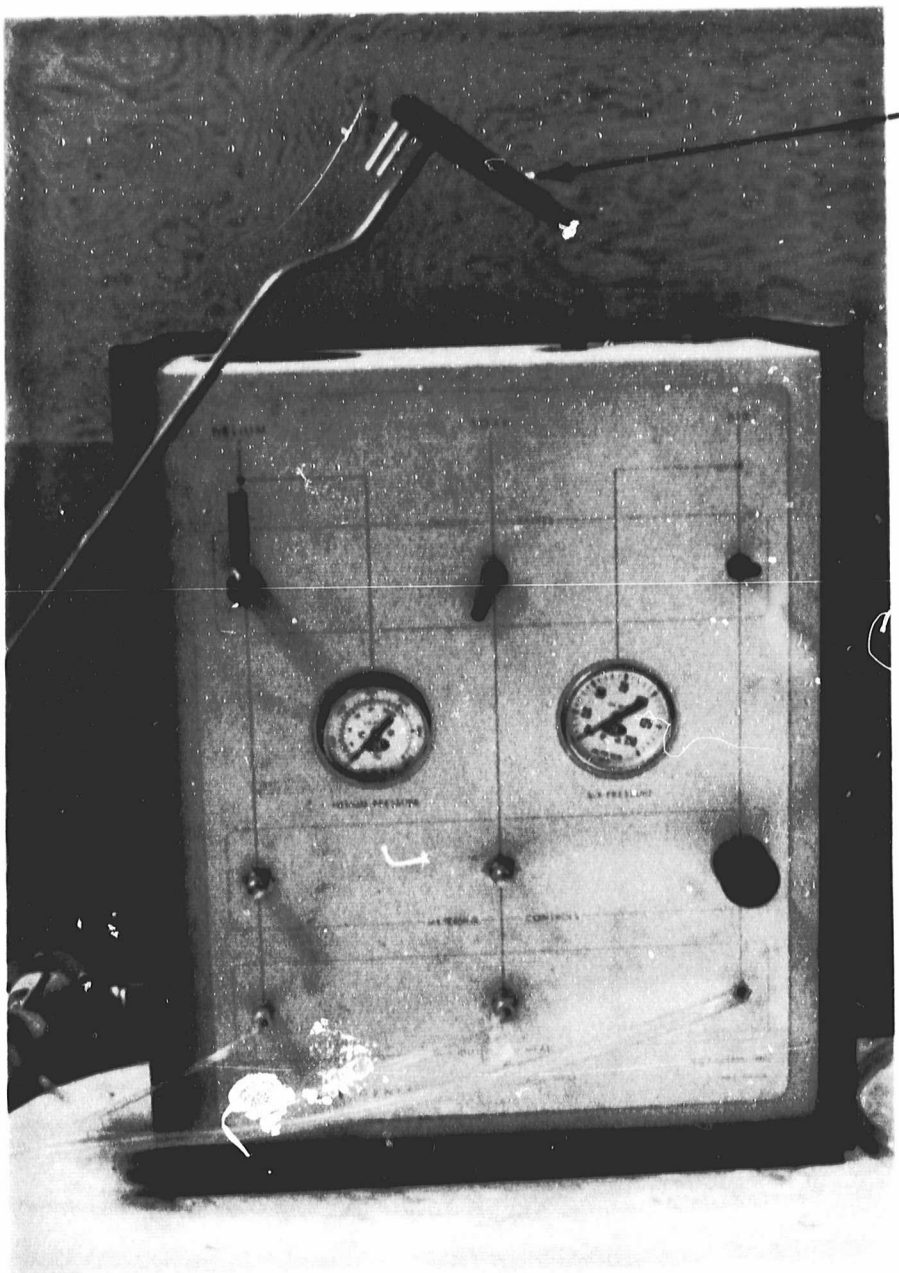

Figure 26. Bubble Generator Head and Console.

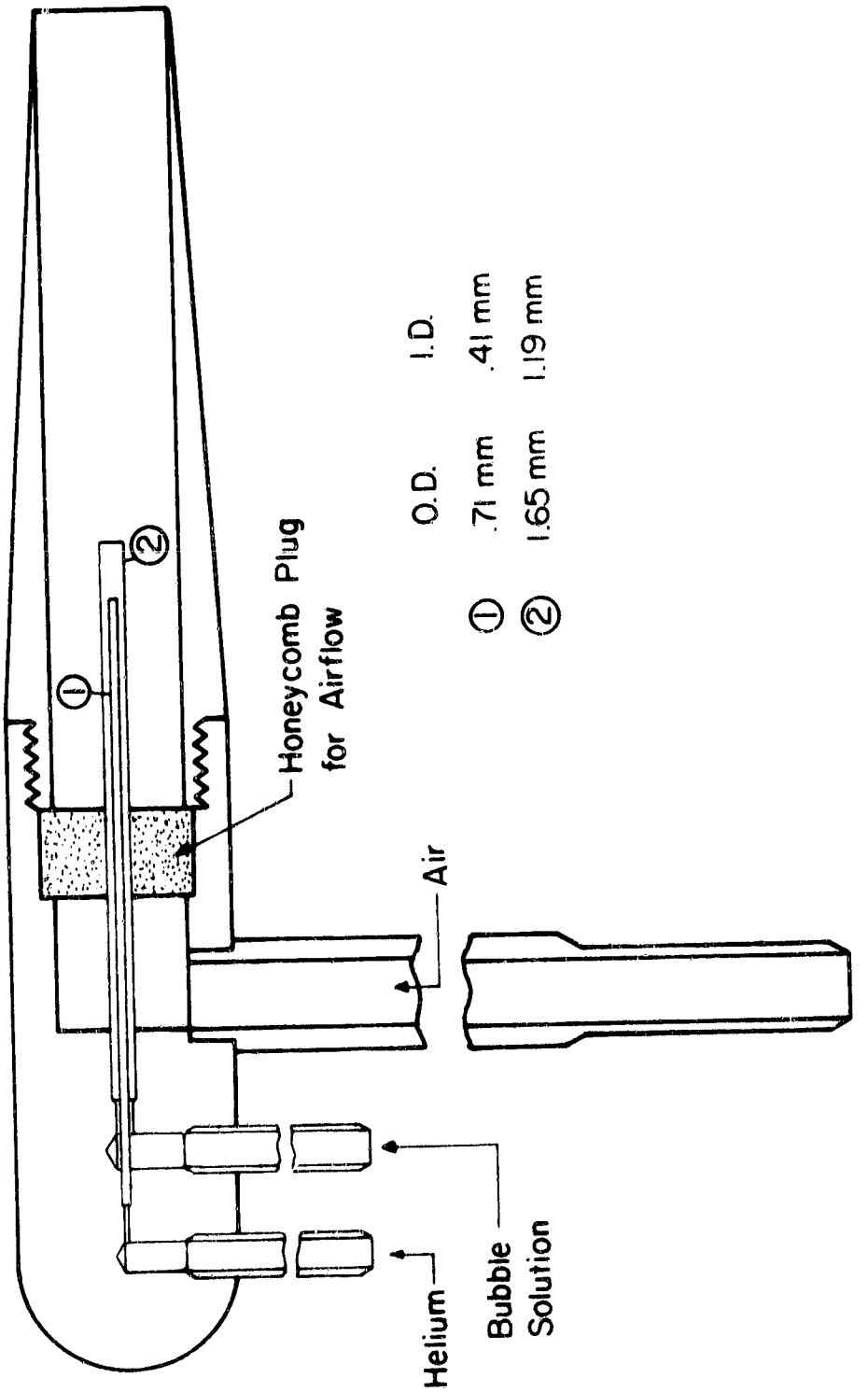

Figure 27. Schematic of Bubble Generator Head.

Figure 28. Bubble Generator Head in Position.

CHAPTER 4

DATA ACQUISITION AND REDUCTION

The acquisition and analysis of benchmark quality data from the Purdue Annular Cascade Facility is in part dependent on the data acquisition and reduction procedures. This chapter describes the acquisition and reduction procedures for the pressure data including an analysis of the experimental error. Also included is a description of the flow visualization experimental technique.

The pressure data is collected automatically using the previously described data acquisition unit with the desktop computer as its controller. After soliciting various ambient and calibration data from the operator, the computer initiates the pressure scan by advancing the Scanivalve system to the first port. The pressure transducers now see a step change in their inputs. Since each transducer is a second order input-output device [6], it is necessary that the computer delay a sufficient length of time for the output signal of each transducer to settle to within a desired tolerance of its final value. Time response tests conducted on the transducers indicated that the outputs were within approximately 0.02% of their final

values after 160 milliseconds. The exact time response characteristics were difficult to determine because of random signal noise which will be discussed below.

During the 160 milliseconds that the computer is programmed to delay before reading the transducer outputs, it reads the digital output from the Scanivalve position indicator and verifies that the system is in its expected position. After the settling time has passed, the computer directs the voltmeter in the data acquisition unit to sequentially read the outputs from the three transducers a specified number of times determined by the operator. The voltage readings are summed in three respective registers as are the squares of the voltage readings. After the specified number of readings have been taken, the system is advanced to the next port where the entire procedure is repeated until all data from all 48 positions of the Scanivalve system have been collected.

At this point the two following statistical quantities are calculated:

(1) an estimate for the standard deviation s

$$s = \left[\frac{n\Sigma V^2 - \left[\Sigma V\right]^2}{n\left[n-1\right]}\right]^{1/2} \qquad (3)$$

(2) an estimate for the mean $\bar{V}$

$$\bar{V} = \frac{\Sigma V}{n} \qquad (4)$$

There are now 144 (3x48) mean voltage readings and 144 associated standard deviations stored in the computer memory. These data are scanned for anomalies and the operator is flagged if any are found.

As previously noted, signal noise causes random scatter in the individual voltage readings. Any single reading of the transducer output is merely a sampling of an infinite population of potential readings. The infinite population has an unknown true mean μ, and an unknown standard deviation σ. The calculated $\bar{V}$ and s are only estimates of these quantities. If it is assumed that the populations from which each of the samplings is drawn follows the normal distribution, then a confidence interval can be established using Student's t distribution [7]. The most critical element of the normal distribution assumption is that there exists no bias in the population.

Using Student's t distribution, the true mean can be bounded with a specified confidence level as follows:

$$\bar{V} - \frac{s}{\sqrt{n}}t < \mu < \bar{V} + \frac{s}{\sqrt{n}}t \qquad (5)$$

where t is Student's factor which is a function of the number of samplings taken and of the confidence level of

the interval so created. Using this technique upper and lower bounds can be placed on each raw datum (mean voltage). When each reduced datum (pressure, velocity, etc.) is computed, the worst case combinations of the raw data can be used to compute upper and lower bounds on the reduced datum. This will be discussed further.

Obviously, one of the most important reduced data to be computed from the voltage data is the pressure at each port in the scan. The first port in each module of the Scanivalve system is subjected to the calibration pressure while the ambient pressure is connected to the second port in each module. Denoting each quantity which has a high and a low bound by ', the calibration voltage V'_c and the ambient reference voltage V'_r can be combined with the calibration pressure P'_c (which is input from the operator)* and the voltage V' at each port to obtain the pressure P' at each port as follows:

$$P' = \frac{\left(V' - V'_r\right) \times P'_c}{V'_c - V'_r} \qquad (6)$$

To compute the upper bound on P', it is necessary that the numerator be as large as possible while the denominator be

* The quantities P'_c, T'_o, and P'_o are the vacuum calibration pressure, ambient temperature, and ambient pressure respectively. The bounds on these quantities are due to resolution limits on the instruments which the facility operator reads and inputs to the computer. They are not statistically calculated, and hence, they represent 100% (sic) confidence levels.

as small as possible. For the numerator to be a maximum, the largest magnitude of V' must be combined with the smallest magnitude of V'_r (V' and V'_r have the same sign).

Once all the pressures have been calculated by the computer, they are used to compute the velocities corresponding to the pressure rake data. The velocity U' is calculated from the total pressure P'_t and the static pressure P'_s using the Bernoulli Law for steady, compressible flow:

$$U' = \left\{ \frac{2 \times R_{air} T'_o}{\Gamma} \left[1 - \left(\frac{P'_s}{P'_t} \right)^{\Gamma} \right] \right\}^{1/2} \qquad (7)$$

where $\Gamma = \frac{\gamma - 1}{\gamma}$ and γ is the specific heat ratio.

Another datum of particular interest is the pressure coefficient C'_p which is defined as:

$$C'_p = \frac{\bar{P}'_{taf} - P'_{af}}{\frac{\bar{\rho}' \bar{U}'^2}{2}} \approx \left[\frac{U'_{af}}{\bar{U}'} \right]^2 \qquad (8)$$

where the subscript af denotes the surface of the airfoil and the bar indicates mass-averaged quantities through the facility. The approximation for the square of the velocity ratio is based on incompressible flow assumptions. In this flow situation where the Mach number is on the order of

0.1, this is a quite accurate assumption. The square of the velocity ratio is used to correlate the numerical predictions for the pressure coefficient.

Assuming that there is no total pressure loss in the freestream between the axial positions of the inlet total pressure rakes and the airfoil cascade, the pressure coefficient can be rewritten as follows:

$$C'_p = \frac{\bar{P}'_t - P'_{af}}{\frac{\bar{\rho}' \bar{U}'^2}{2}} \qquad (9)$$

where the variable density is computed with the isentropic relationship:

$$\bar{\rho}' = \bar{\rho}'_t \times \left[\frac{\bar{P}'_s}{\bar{P}'_t}\right]^{\frac{1}{\gamma}} \qquad (10)$$

When intervals are used in the above manner to calculate upper and lower bounds of reduced data, the problem of error accumulation arises. Even though the raw data (voltage readings) intervals are known with a confidence of X%, an error of E=(100-X)% exists which accumulates in the calculations of the reduced data. Suppose there are n pieces of raw data which are used in the calculation of a reduced datum. Each raw datum has a confidence interval

with an error of E%. Then the resulting reduced datum would have a confidence interval with error of n x E% resulting in a confidence level of (100 - nxE)%. However, this is the worst possible case. For it to actually occur, the raw data would have to assume the appropriate maximum and minimum values (as previously noted), which is in itself a rather improbable event. Therefore, the actual confidence level can be expected to be much higher.

Photographs of the helium-bubble flow visualization technique can also be taken during the data acquisition process. The bubble paths are illuminated with two light sources with light slits such that illumination occurs only in a "plane" of finite thickness (approximately 2.5 cm). This plane is located so that it perpendicularly intersects the span of the airfoil. This is accomplished by placing the light sources in the exit plenum chamber of the facility and directing the light upstream into the test section. A sharply defined, illuminated region at any desired airfoil span can thus be obtained.

All surfaces in the illumination zone are painted flat black to minimize reflection. It is necessary that there be no light in or around the facility other than that from the light sources to avoid washing out the bubble pathlines.

The bubble pathlines are photographed with a 35 mm SLR camera using a 55 mm, f1.8 lens. The camera is positioned on a tripod to view the airfoils through the outer-casing window in the test section, and is focused on the illuminated portion of the airfoil. Kodak 2475 Recording film, a high speed, black and white film is used with a shutter speed of 1 second and a wide open aperture. It is helpful to specially develop the film for high contrast following the instructions from Kodak.

CHAPTER 5

DATA PRESENTATION AND ANALYSIS

To demonstrate and verify the operation of the Purdue Annular Cascade Facility and its associated instrumentation systems, an initial set of experiments was performed on the instrumented flat-plate airfoil cascade. In particular, the cascade inlet flow field and airfoil surface pressure distributions were experimentally determined and correlated with appropriate numerical predictions. In addition, the helium-bubble flow visualization technique was demonstrated. The cascade physical and flow parameters for these initial verification experiments are presented in Table 1.

Table 1. Purdue Annular Cascade Experimental Conditions

Tip Diameter (cm)	127.0
Hub/Tip Radius Ratio	0.76
Airfoil Span (cm)	15.24
Cascade Solidity	1.38
Number of Airfoils	36
Airfoil Shape	Flat Plate
Airfoil Chord (cm)	15.24
Stagger Angle	0.0
Incidence Angle	0.0
Axial Velocity (m/s)	30.0
Flow Rate (m^3/s)	16.1
Chord Reynolds Number	430,000

The first data acquisition task performed was the determination of the number of transducer samplings to be taken at each port position. Obviously, taking more samplings improves the confidence intervals. However, more samplings also cause the data acquisition time to be longer, increasing the possibility that flow conditions within the facility might drift. Increasing the number of samplings from 5 to 20 generally decreased the width of a 99% confidence interval by 50-65% while increasing the data acquisition time from 1.5 minutes to 5.0 minutes. Because there was no drift in the facility flow conditions over a 5 minute time frame, 20 samplings per port were acquired.

The cascade inlet flow field, as measured with the facility inlet total pressre rakes, was circumferentially uniform and essentially flat in the spanwise direction, as shown in Figure 29 which shows this inlet profile for Experiment 1. As seen, the velocity measured by the total pressure tap adjacent to the outer shroud wall was consistently lower by about 2%, indicating a slightly thicker boundary layer on the outer shroud wall. All velocity profile data is tabulated in Appendix D. The mass-averaged velocity $\bar{U}$ (obtained as noted in Chapter 2) tended to be approximately 30 m/s for all four experiments. The exact values of $\bar{U}$ together with the corresponding airfoil surface pressure coefficients are also tabulated in Appendix D.

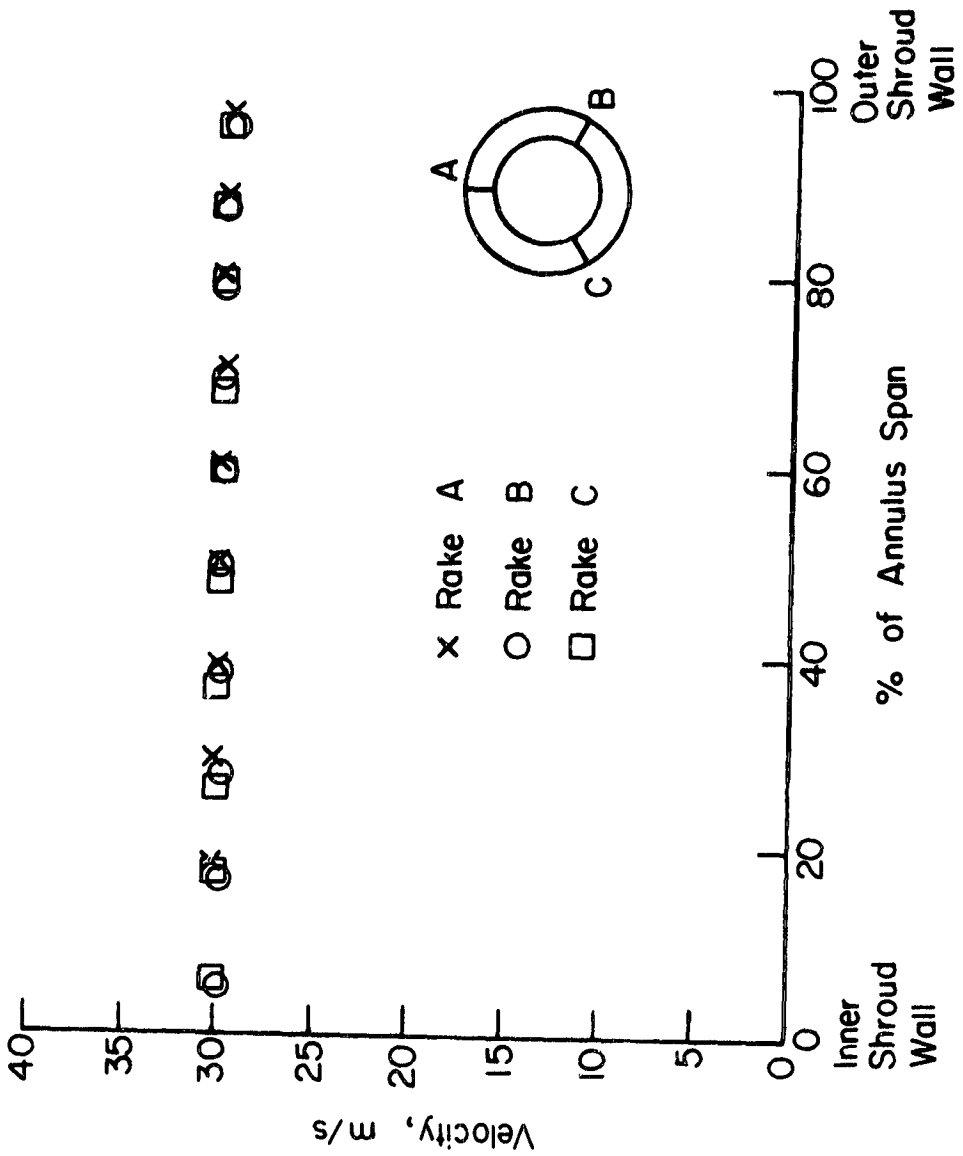

Figure 29. Inlet Velocity Profile - Experiment 1.

The inlet velocity profiles thus obtained were input into the NASA computer programs MERIDL [8] and TSONIC [9] which are described in Appendix E. Other input to these programs included the facility geometry, the airfoil shape, and the ambient conditions. The primary output from these computer codes of interest herein were the chordwise distributions of the airfoil surface pressure coefficient.

The chordwise distributions of the airfoil surface pressure coefficient data and the corresponding predictions are presented in Figures 30 through 35. The hub (10% span), midspan (50% span), and tip (90% span) spanwise locations of the airfoils are instrumented on both the pressure and the suction surfaces, as previously described. Thus, there are two sets of data, corresponding to the pressure and suction surfaces, at each of the three spanwise locations. However, these initial demonstration and verification experiments utilized a flat-plate airfoil cascade set at zero incidence angle. Hence, the pressure and suction surface data should be identical, and a comparison of the corresponding span location data will indicate the periodicity of the cascade flow phenomena. It should be noted that the confidence intervals which result from calculating the pressure coefficient data from raw data with 99% confidence intervals are also presented. The corresponding predictions are indicated by the solid lines.

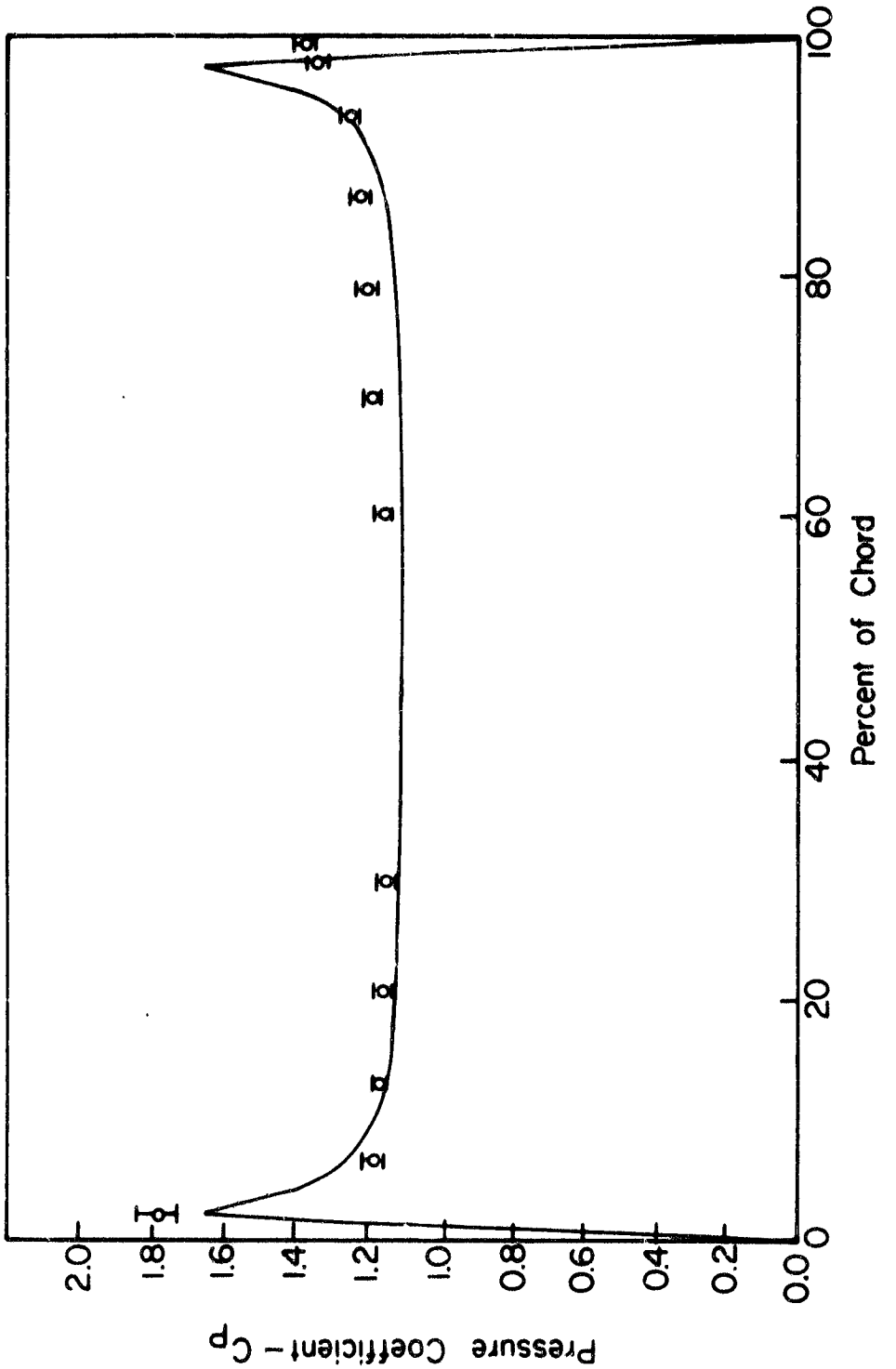

Figure 30. Pressure Coefficient Data, Experiment 1, Tip Data, Surface 1.

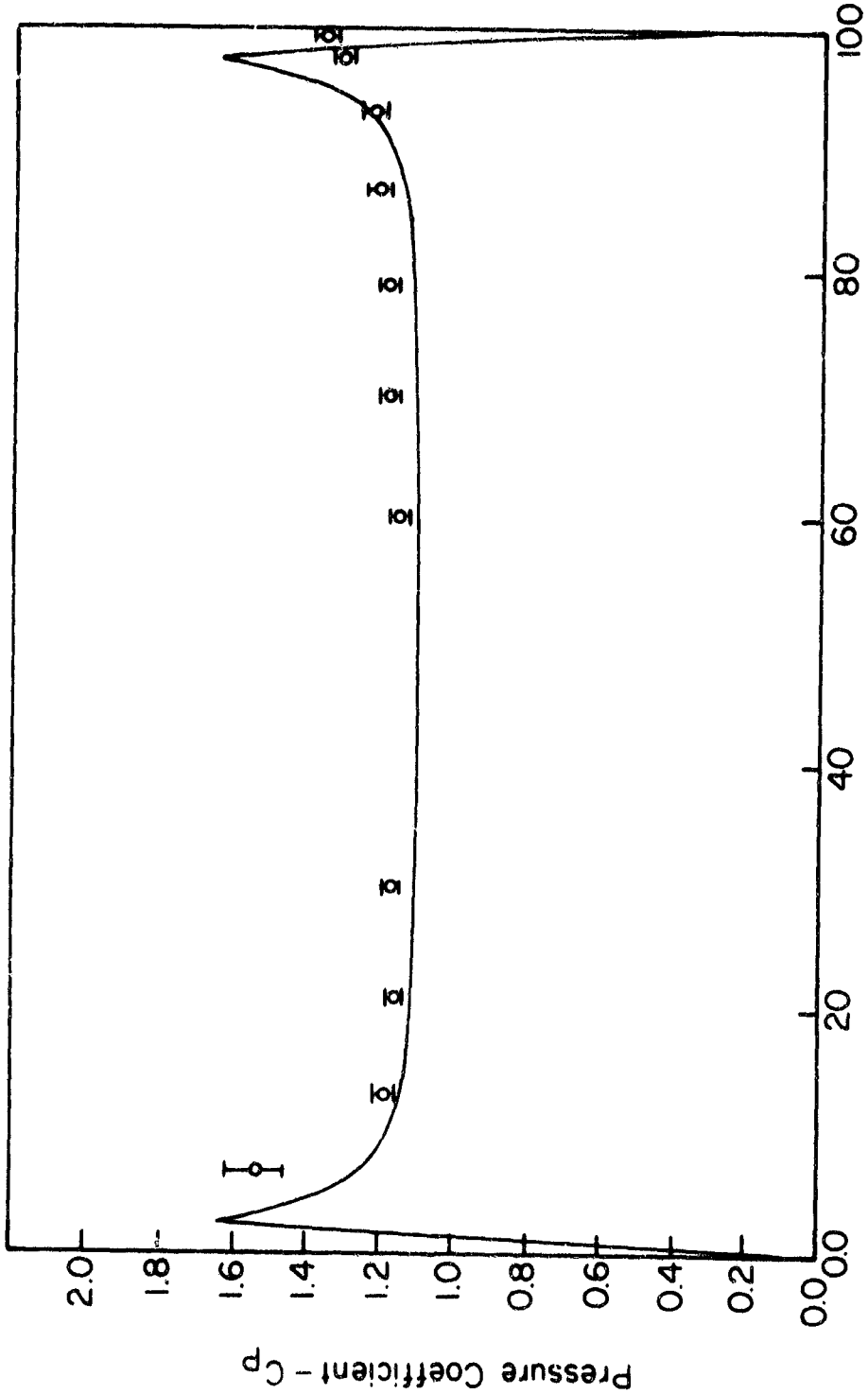

Figure 31. Pressure Coefficient Data, Experiment 1, Tip Data, Surface 2.

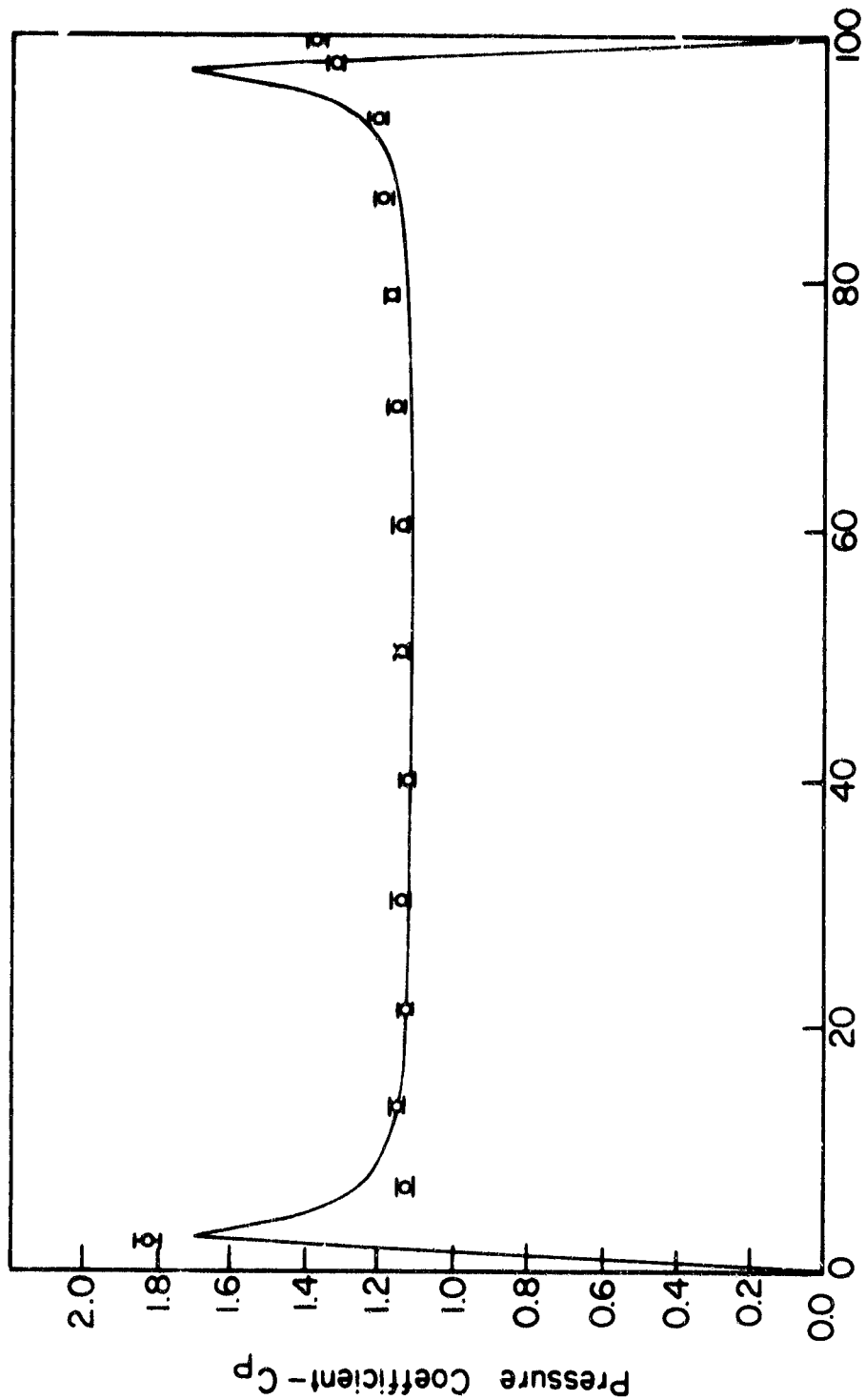

Figure 32. Pressure Coefficient Data, Experiment 1, Midspan Data, Surface 1.

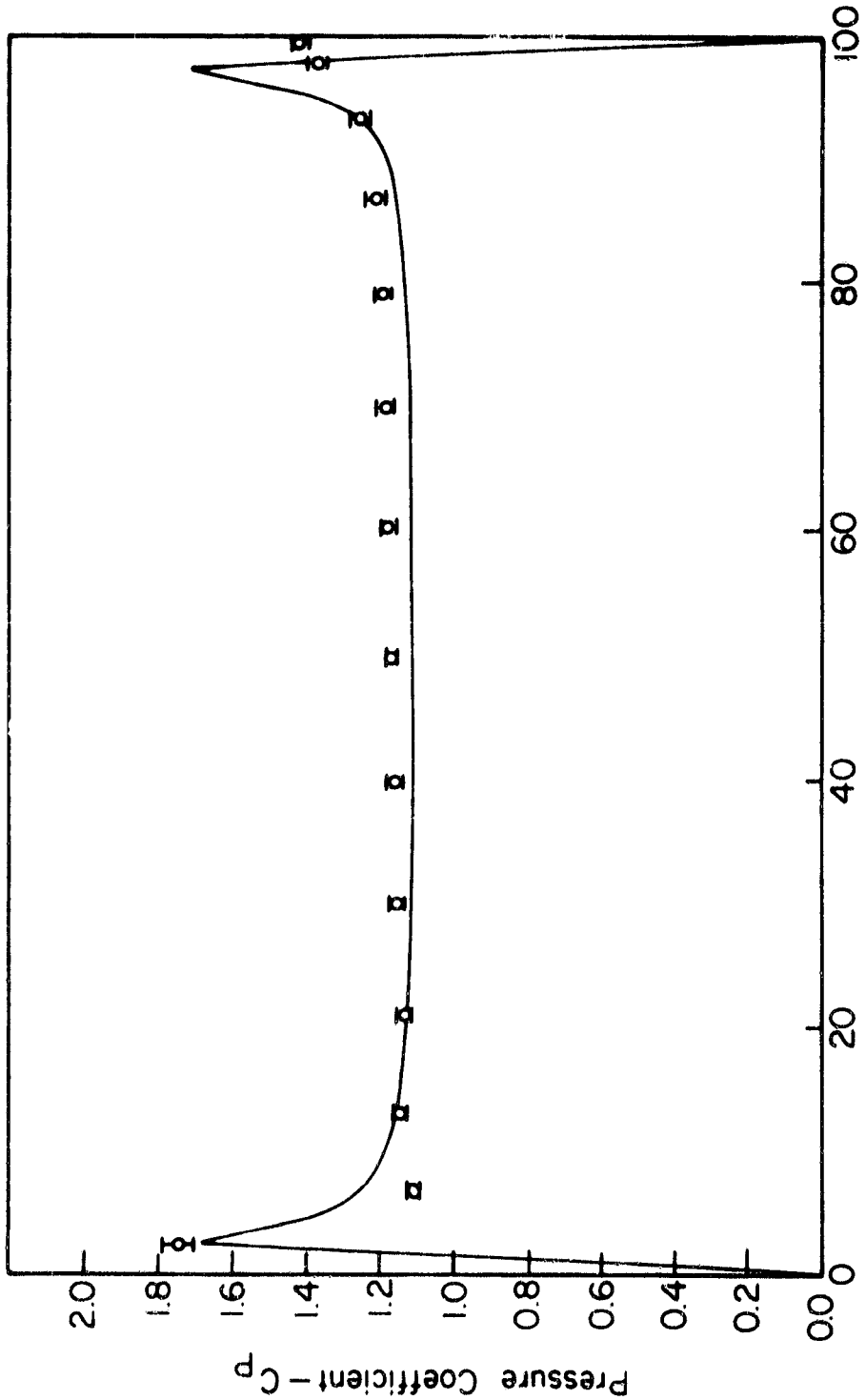

Figure 33. Pressure Coefficient Data, Experiment 1, Midspan Data, Surface 2.

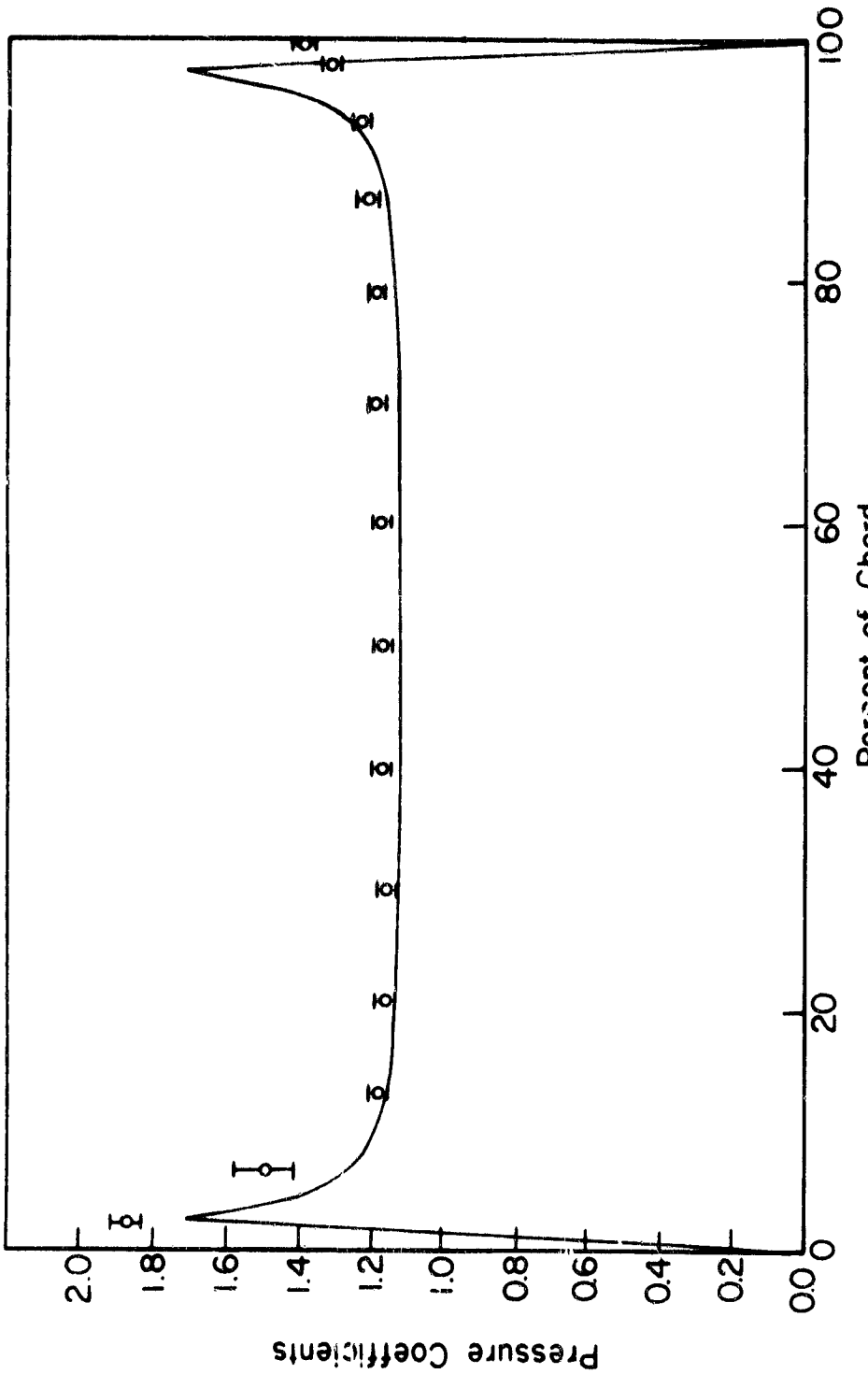

Figure 34. Pressure Coefficient Data, Experiment 1, Hub Data, Surface 1.

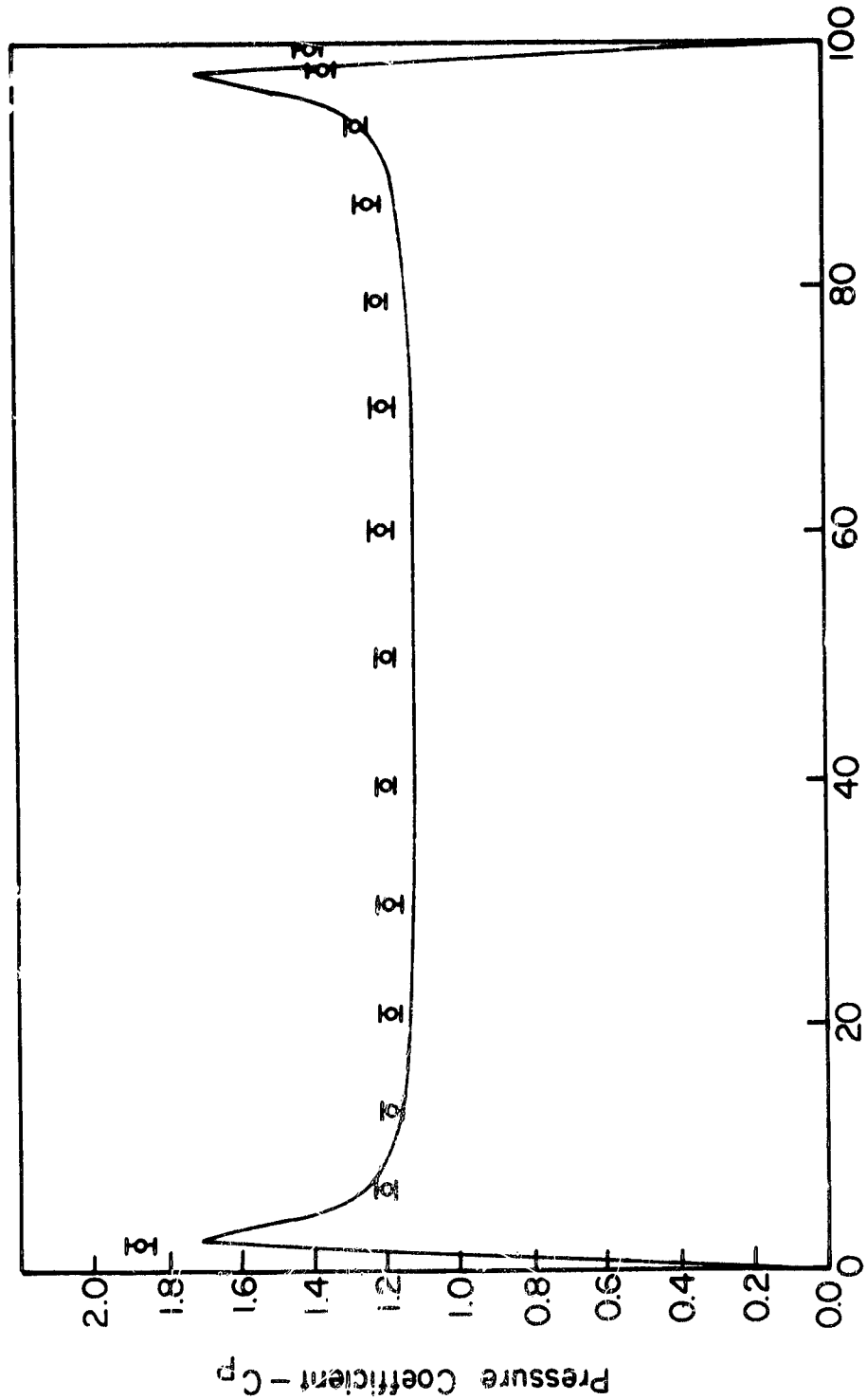

Figure 35. Pressure Coefficient Data, Experiment 1, Hub Data, Surface 2.

As can be seen from these figures, there is generally good correlation of the experimental and numerical results at all spanwise locations in the leading edge (0% Chord) region. The experimental data exhibit somewhat sharper gradients, but this is at least partially expected because the numerical methods used in the computer programs tend to smooth out sharp gradients. It should be noted that some of the data at 7% of the chord contradicts this trend. However, these particular data exhibit a larger confidence interval than the majority of the data, indicating a relatively larger degree of scatter in the pressure transducer voltage samplings for these points.

The pressure coefficient data are also seen to increase slightly in the chordwise direction as compared to the corresponding predictions at all spanwise locations. This is due to the increasing displacement effect of the growing boundary layer on the airfoil surface, a phenomenon not considered in the numerical analysis. The data in the trailing edge region is in relatively poor agreement with the predictions. The behavior of the experimental data in this region reflects the relatively thick boundary layer and the flow separation at the trailing edge. The boundary layer phenomena are not considered in the predictions as they are based on inviscid analyses, essentially generating potential flow solutions.

A comparison of the pressure and suction surface data at each spanwise location indicates the high degree of periodicity existing in the flow phenomena in the annular cascade, as expected.

A series of flow visualization photographs were also taken. There were two photographs taken at the airfoil leading edge, one on each side of the airfoil, Figures 36 and 37, and two sets at the trailing edge, again one on each side, Figures 38 and 39. The helium bubble paths are easily seen, and as the flow through the cascade is steady, the pathlines can be interpreted as streamlines. The streamline curvature can be clearly seen in the leading edge photographs while the airfoil wakes are highlights of the trailing edge photographs.

Figure 36. Flow Visualization at Airfoil Leading Edge, Surface 1.

Figure 37. Flow Visualization at Airfoil Leading Edge, Surface 2.

Figure 38. Flow Visualization at Airfoil Trailing Edge, Surface 1.

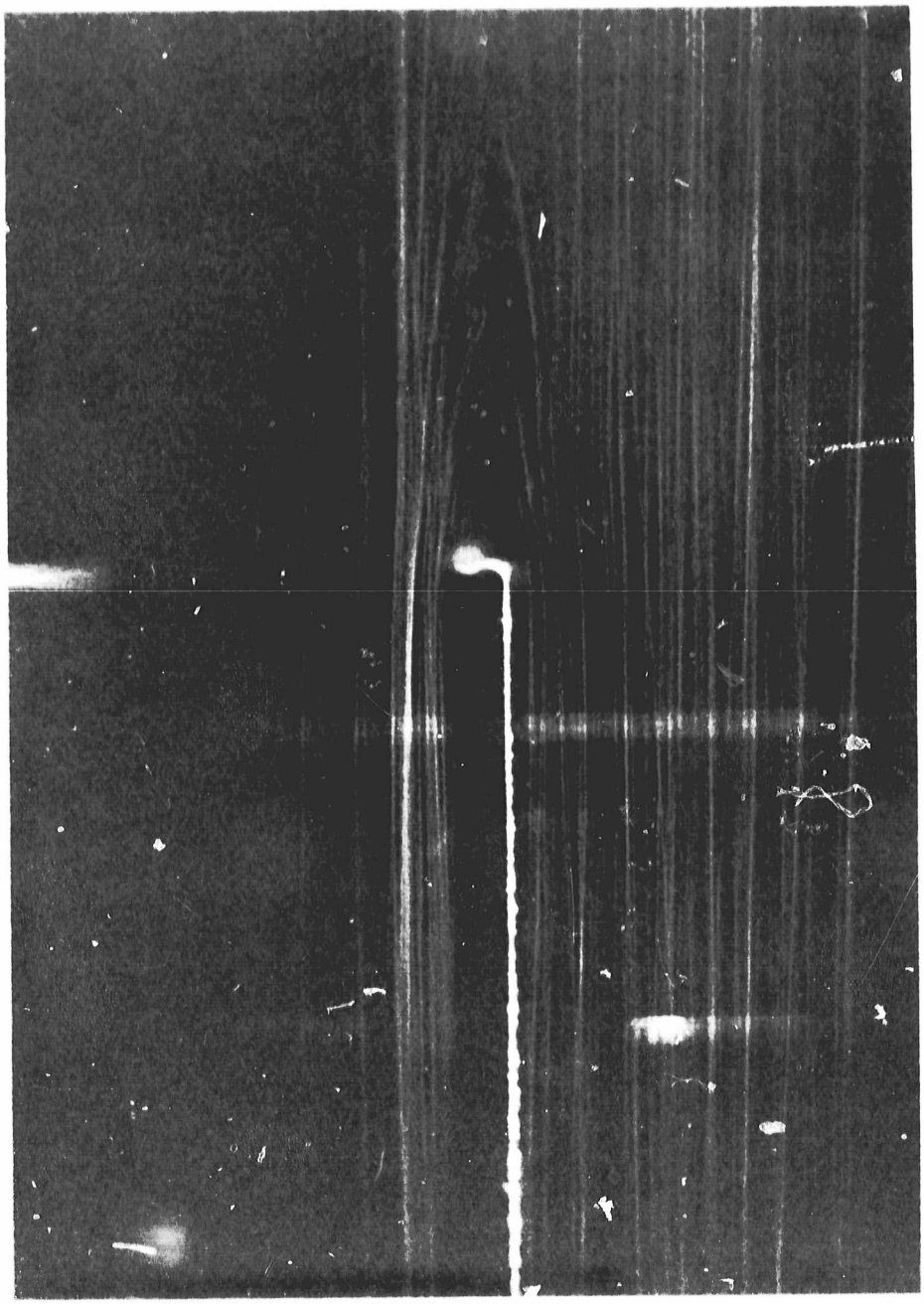

Figure 39. Flow Visualization at Airfoil Trailing Edge, Surface 2.

CHAPTER 6

CONCLUSIONS

The Purdue Annular Cascade Facility was designed and fabricated for the express purpose of acquiring the benchmark three-dimensional, internal aerodynamic data necessary to validate flow analyses being developed for application to advanced-design turbomachinary flow fields. The facility was instrumented with inlet total pressure rakes to obtain the cascade inlet velocity profile, and a high-density array of endwall pressure taps. Wall slots and provisions for a traversing mechanism in the exit region of the cascade test section permit the use of probe methods in the exit flow field. It was also designed with the flexibility necessary to utilize state of the art measurement techniques such as Laser Doppler Anemometry by including transparent sections in the airfoil test section. These transparent sections also permit the use of flow visualization techniques.

The data acquisition and analysis system for the facility is centered around a computer-controlled data acquisition unit which permits automated data acquisition and online data reduction and examination. The data

acquisition system controls the Scanivalve pressure measurement system which is utilized to collect the pressure data from the many pressure taps in the facility. A calibration pressure system was designed and fabricated to provide a vacuum calibration pressure to the three pressure transducers in the pressure measurement system. This allows the transducers to be recalibrated each time they are used as an integral part of the pressure scanning procedure. Statistical techniques were incorporated into the data-processing software such that confidence intervals can be placed on the data. The worst-case combinations of the raw data intervals are used when computing reduced data in order to retain upper and lower bounds on the data.

To demonstrate and verify the operation of the facility and its associated basic instrumentation system, experiments were performed utilizing an instrumented flat-plate airfoil cascade at zero incidence.

A helium-filled soap bubble flow visualization technique was successfully demonstrated using light sources located in the downstream in the plenum chamber to illuminate the helium bubbles. The photographs of the flow visualization technique clearly show the streamline curvature near the leading edge of the flat-plate airfoils and the wake region at the trailing edge.

The chordwise distribution of the airfoil surface pressure coefficient on the hub, midspan, and tip spanwise locations was also measured. Predictions obtained from the inviscid-flow computer codes MERIDL and TSONIC with the measured cascade-inlet velocity profile as input were correlated with the corresponding airfoil surface pressure coefficient data. At all three spanwise locations, the experiment-theory correlation was very good. In the leading edge region of the airfoil, the data exhibited steeper gradients than the predictions. Viscous effects at the trailing edge of the airfoil caused deviations between the data and prediction, as would be expected.

It is concluded that the Purdue Annular Cascade Facility is fully capable of generating benchmark-quality data with direct application to the complex flow fields in turbomachinary blade rows.

LIST OF REFERENCES

LIST OF REFERENCES

[1] Bryer, D.W. and Pankhurst, R.C. Pressure Probe Methods For Determining Wind Speed And Flow Direction. London: Her Majesty's Stationery Office, 1971.

[2] Kopal, Zdenek. Numerical Analysis. London: Chapman and Hall, 1955.

[3] Colehour, J.L. and Farquhar, B.W. "Inlet Vortex". Journal of Aircraft, Vol.8, No.1, January 1971, pp. 39-43.

[4] Scanivalve "J" Catalog. Scanivalve Corporation, San Diego, California.

[5] Hale, P.W., Ton, P., Stowell, R.C., and Ordway, D.E. "Development of an Integrated System for Flow Visualization in Air Using Neutrally-Bouyant Bubbles". Technical Report #2 (SAI-RR 7107), Office of Naval Research, 1971.

[6] Doebelin, Ernest O. Measurement Systems. New York: McGraw-Hill, Inc., 1975.

[7] Freund, John E. and Miller, Irwin. Probability and Statistics For Engineers. Englewood Cliffs, NJ: Prentice-Hall, Inc., 1965.

[8] Katsanis, Theodore and McNally, William D. "Revised Fortran Program for Calculating Velocities and Streamlines on the Hub-Shroud Midchannel Stream Surface of an Axial-, Radial-, or Mixed-Flow Turbomachine or Annular Duct", NASA TN D-8430 and TN D-8431, 1977.

[9] Katsanis, Theodore. "Fortran Program for Calculating Transonic Velocities on a Blade-to-Blade Stream Surface of a Turbomachine", NASA TN D-5427, 1969

APPENDICES

Appendix A

Data Acquisition Software

The computer software developed for the acquisition and reduction of data was designed to give maximum flexibility to the operator. Upon entering the program the operator has the option of either taking new data or reading data previously stored on tape. The operator can specify any desired confidence interval at the beginning of the data processing phase of the program. After data reduction has been completed (about 30 seconds), the operator can specify output in either tabular or graphical form, automatic or manual graph scaling, and specific pieces of data or bulk amounts of data. The raw data (mean voltages, standard deviations, and ambient conditions) can be stored on tape at any time for later processing. The flowchart presented in Figure A1 illustrates the software.

The software was designed to prevent the operator from destroying data by erroneous input. Bad input could cause the computer to abort the program making data in the computer memory either difficult or impossible to recover. This is accomplished by testing the validity of all input requested by the software. In addition to protecting

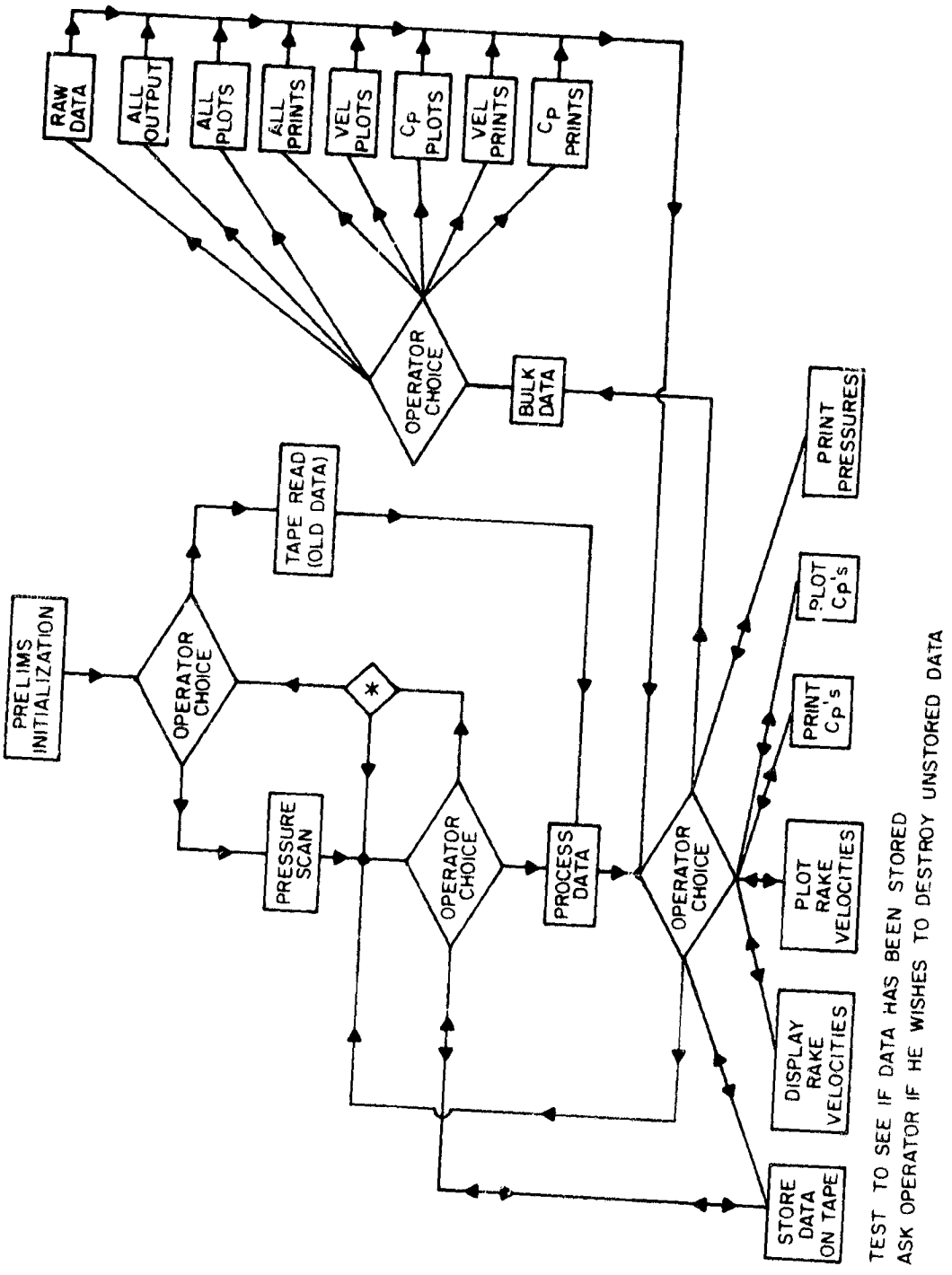

Figure A1. Data Acquisition Software Flowchart.

C - 2

itself from erroneous input, the software provides orderly recovery from arithmetic errors, e.g., attempting to compute the square root of a negative quantity or dividing by zero, which result from the processing of bad data.

Appendix B

Transducer Input-Output Curves

This appendix presents the pressure transducer input-output response in graphical form. The three graphs are presented in Figures B1, B2, and B3. They clearly demonstrate the linearity of the transducer response.

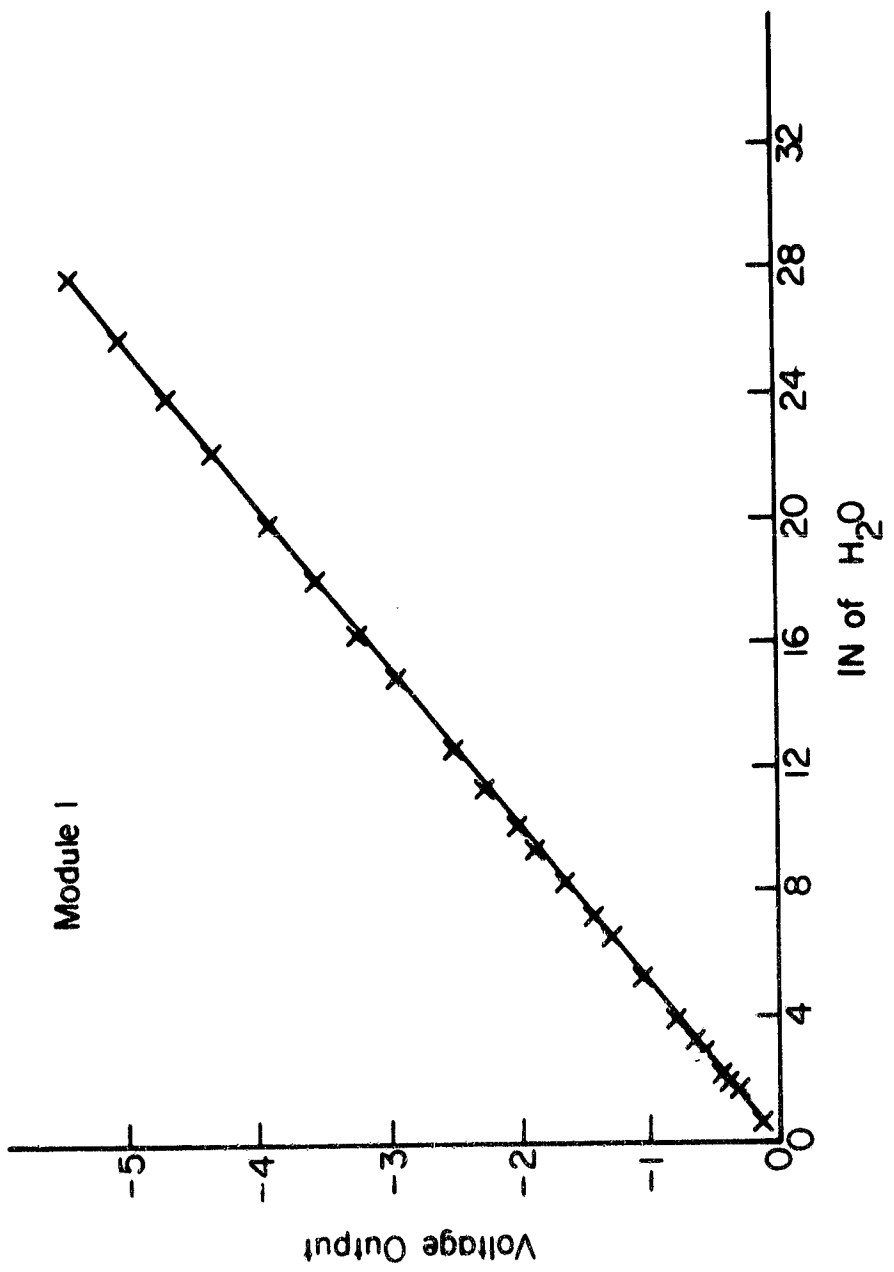

Figure B1. Module 1 Transducer Input-Output Curve.

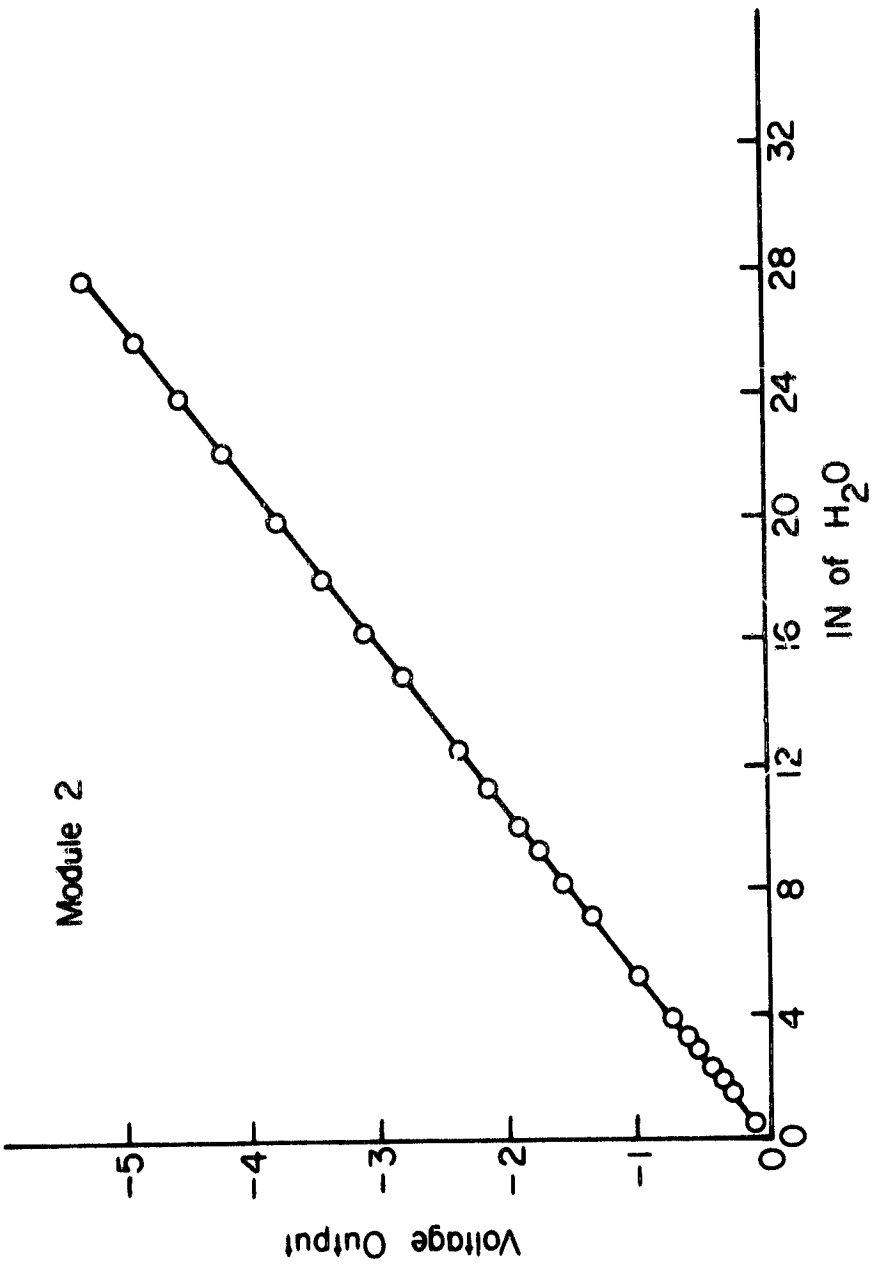

Figure B2. Module 2 Transducer Input-Output Curve.

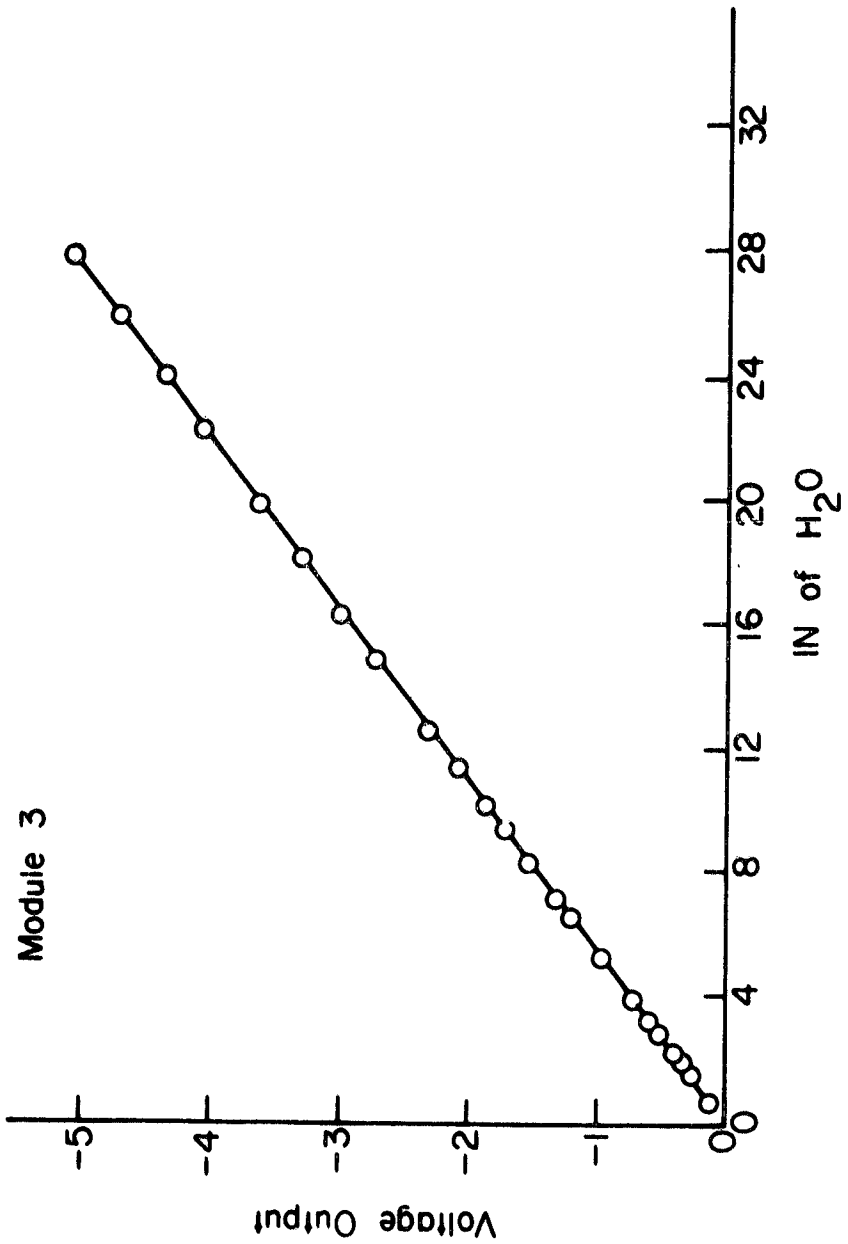

Figure B3. Module 3 Transducer Input-Output Curve.

Appendix C

Graphical Presentation of Repeatability Data

For completeness in this facility demonstration and verification series of experiments, and to demonstrate the repeatability of the data so acquired, three additional complete sets of airfoil surface data were obtained and correlated with predictions, analogous to the data described and presented in Chapter 5. As seen in the figures below, these data exhibit an extremely high degree of repeatability. All data is tabulated in Appendix D.

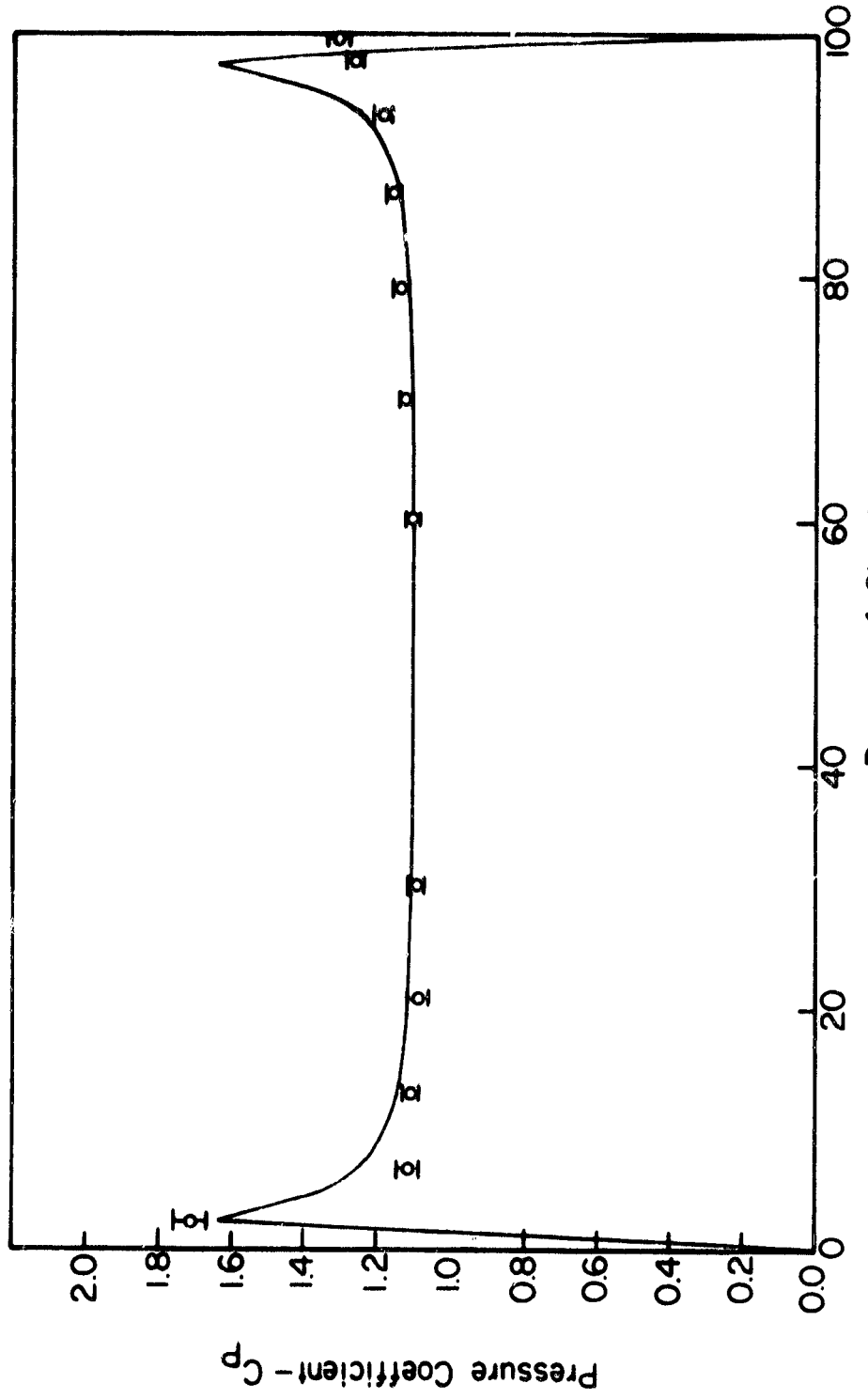

Figure C1. Pressure Coefficient Data, Experiment 2, Tip Data, Surface 1.

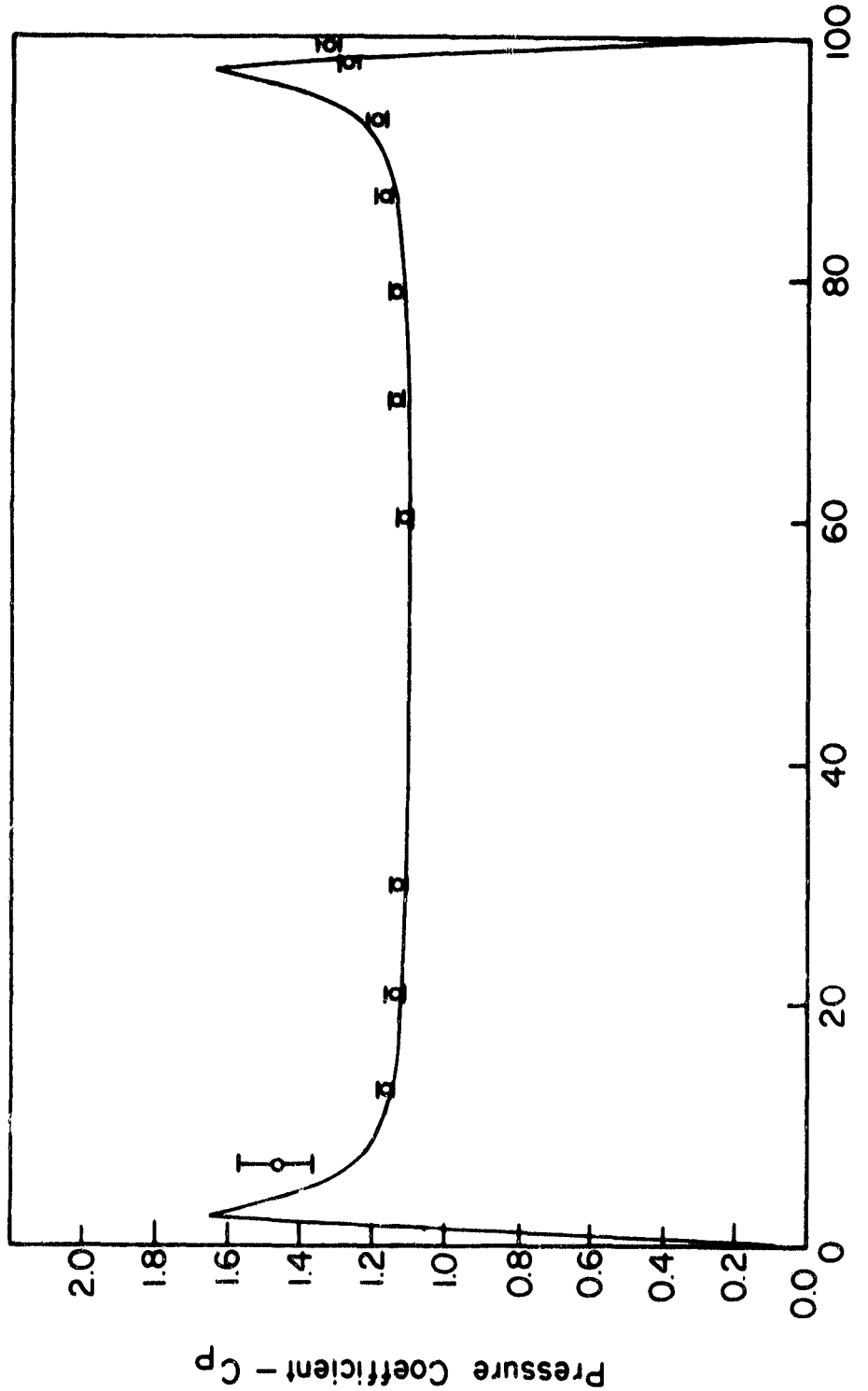

Figure C2. Pressure Coefficient Data, Experiment 2, Tip Data, Surface 2.

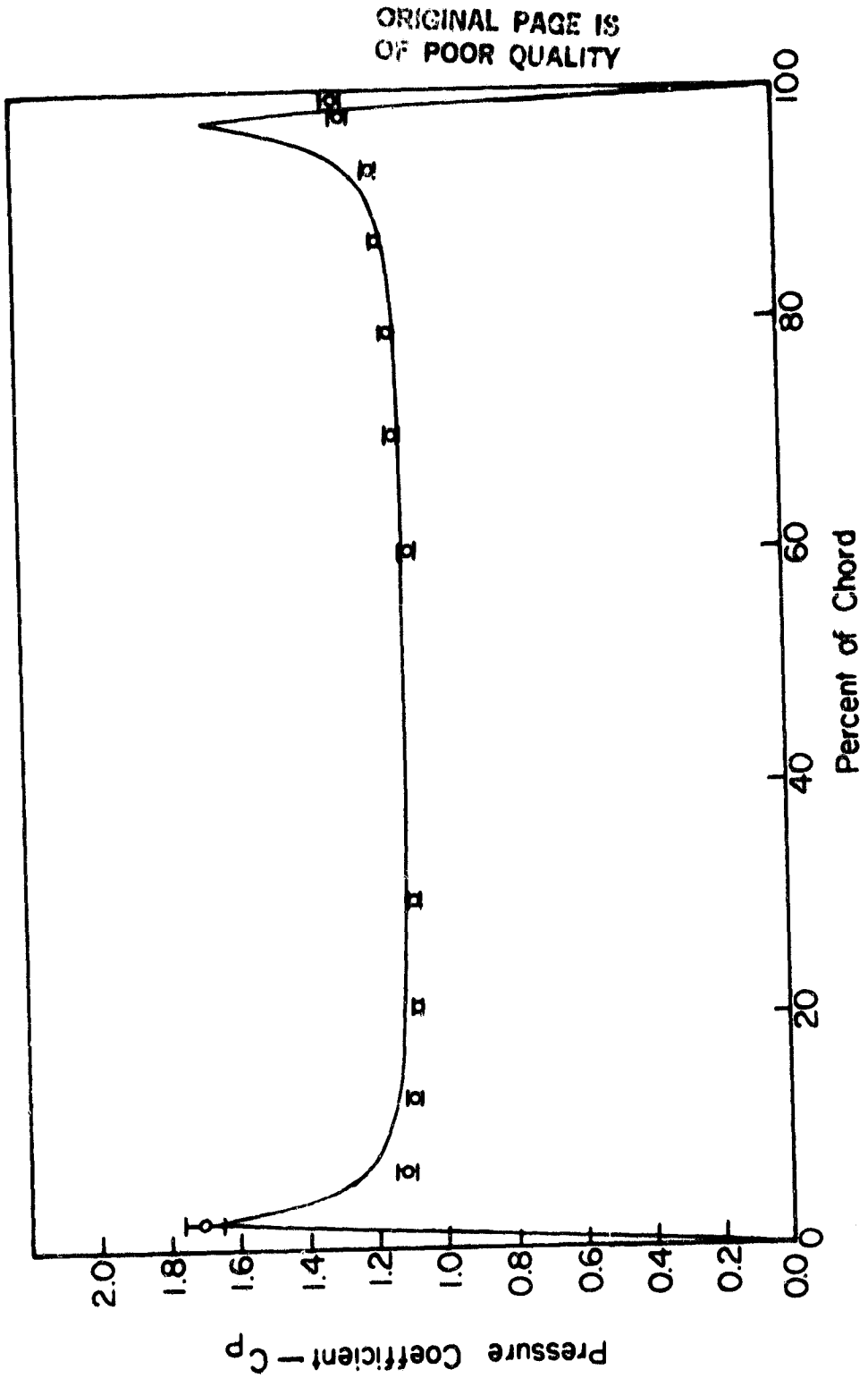

Figure C3. Pressure Coefficient Data, Experiment 3, Tip Data, Surface 1.

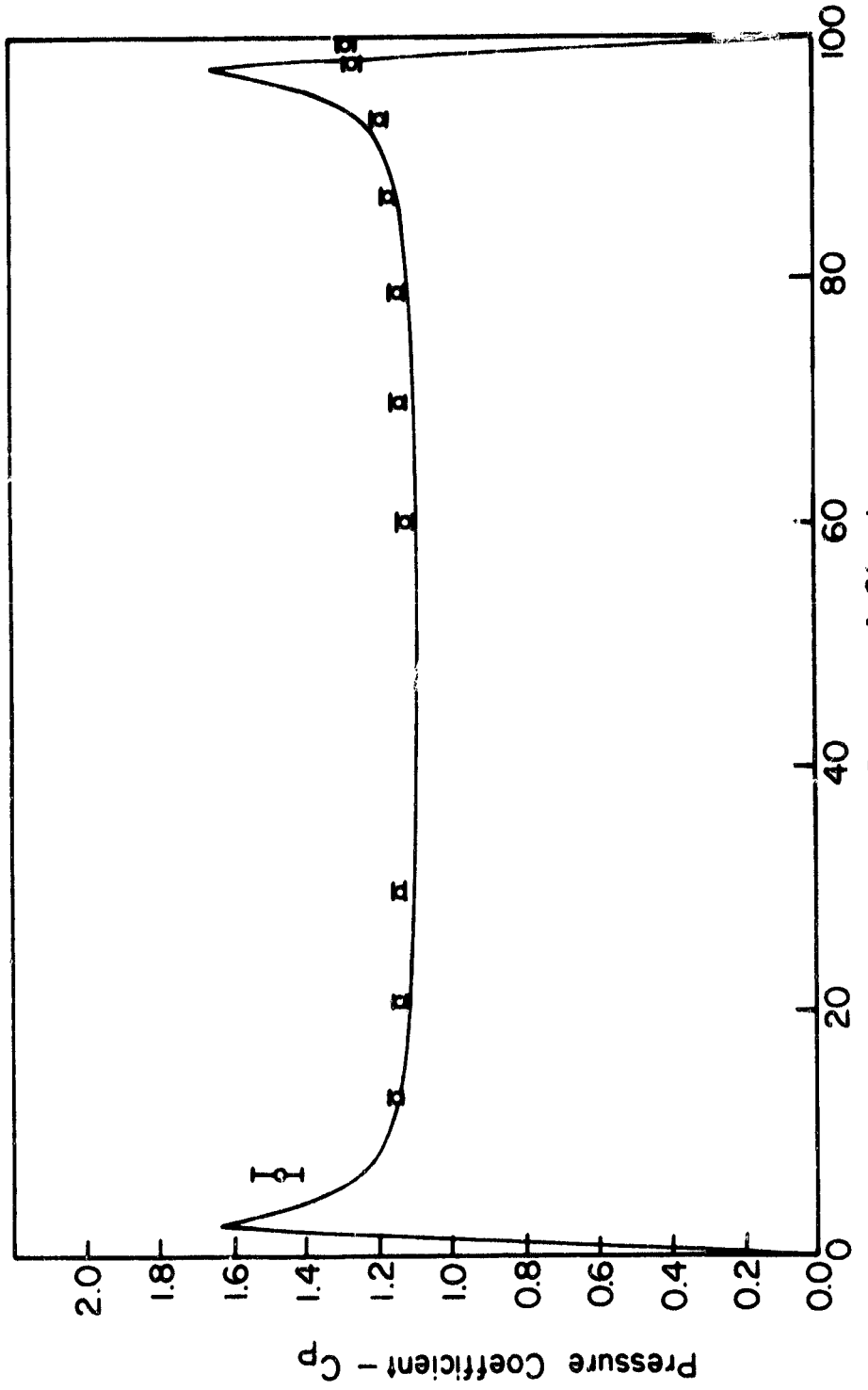

Figure C4. Pressure Coefficient Data, Experiment 3, Tip Data, Surface 2.

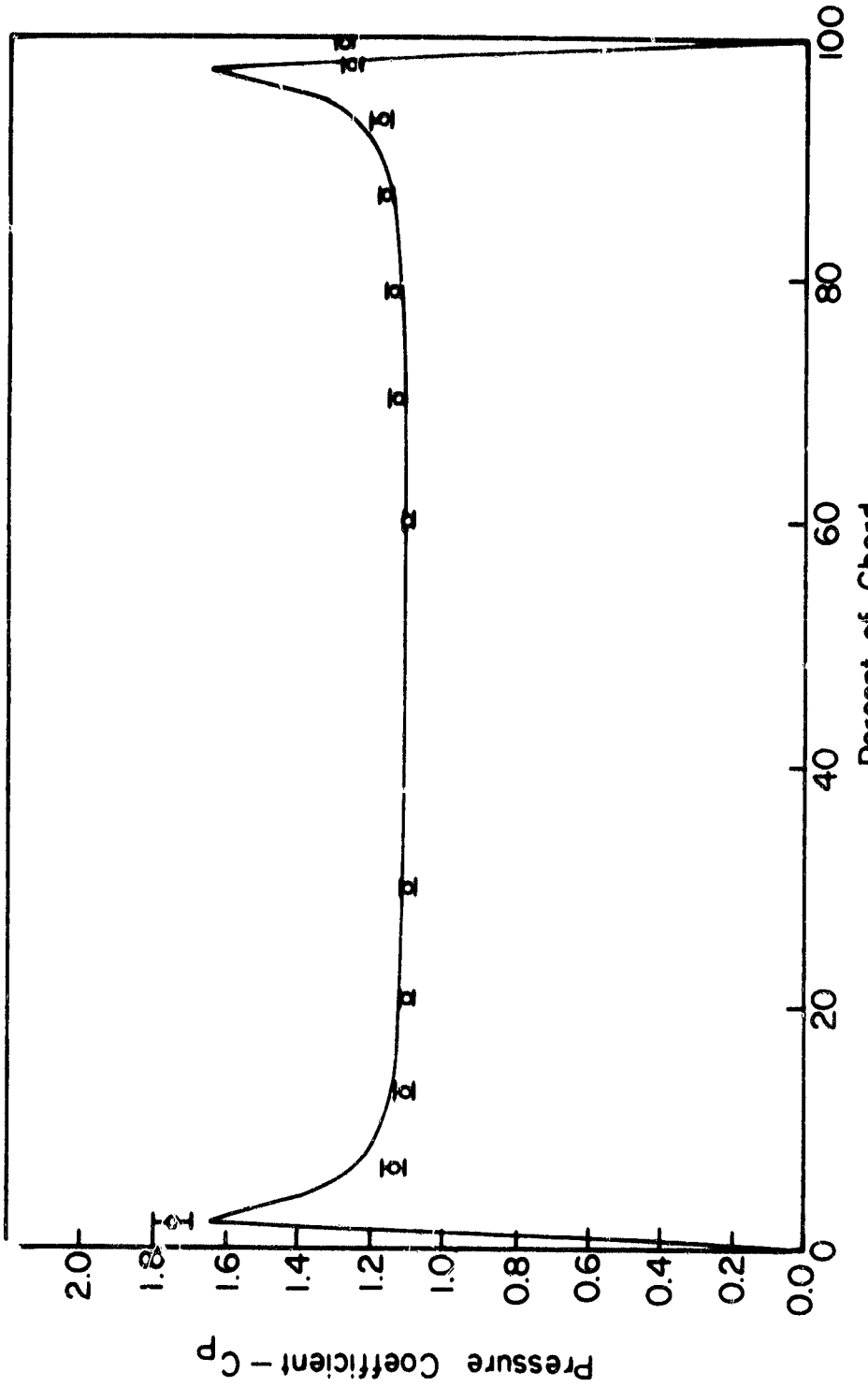

Figure C5. Pressure Coefficient Data, Experiment 4, Tip Data, Surface 1.

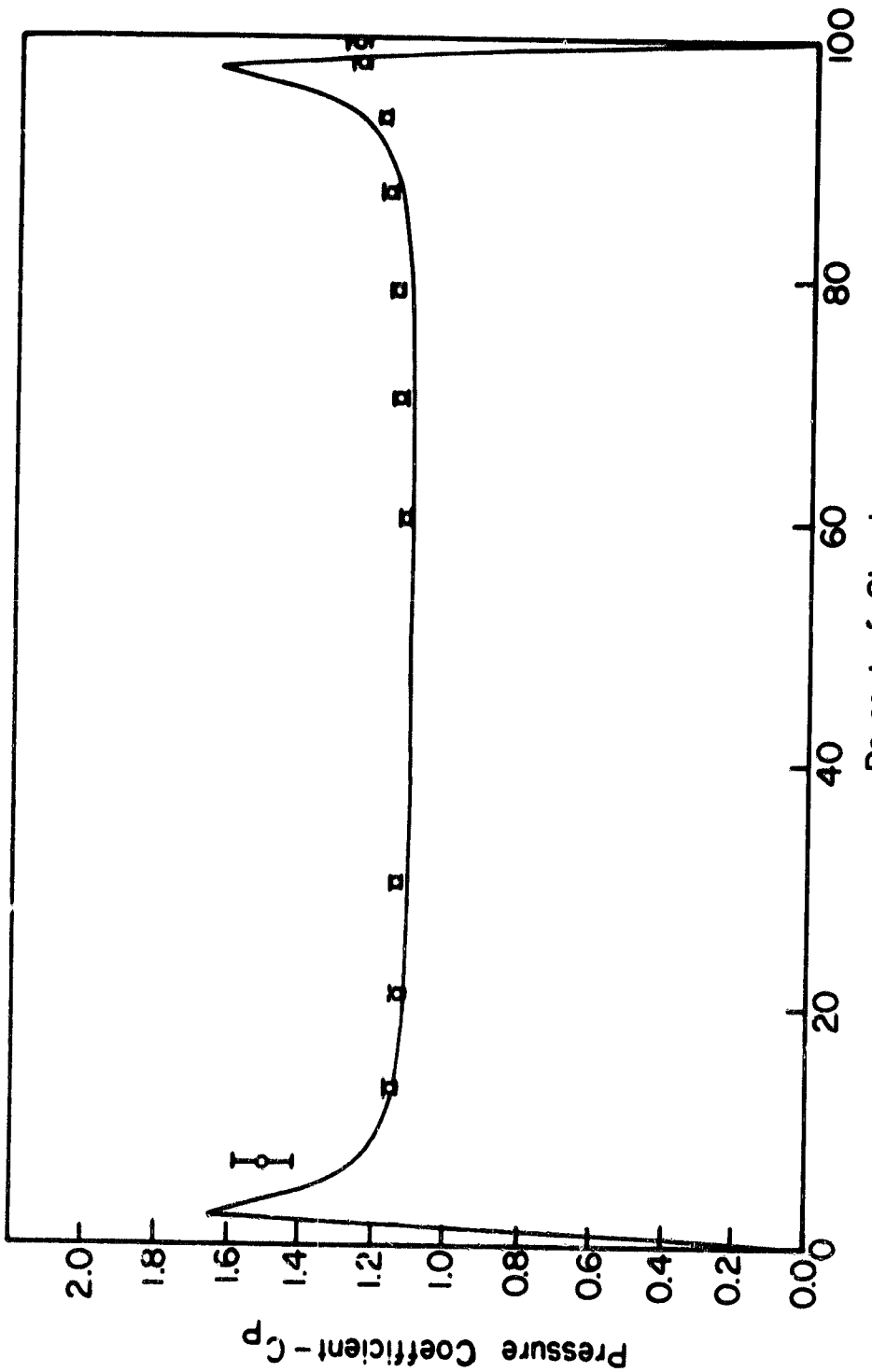

Figure C6. Pressure Coefficient Data, Experiment 4, Tip Data, Surface 2.

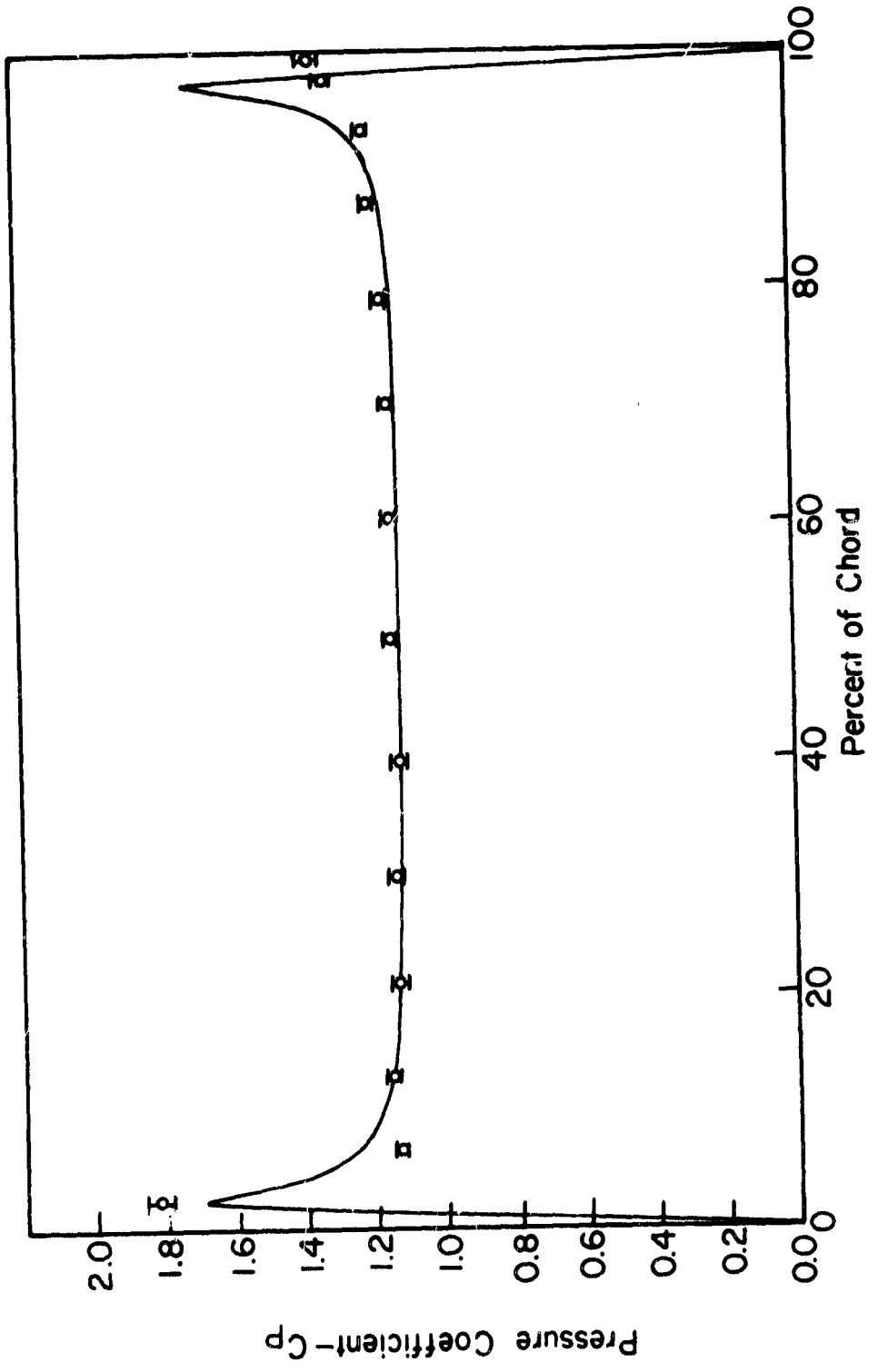

Figure C7. Pressure Coefficient Data, Experiment 2, Midspan Data, Surface 1.

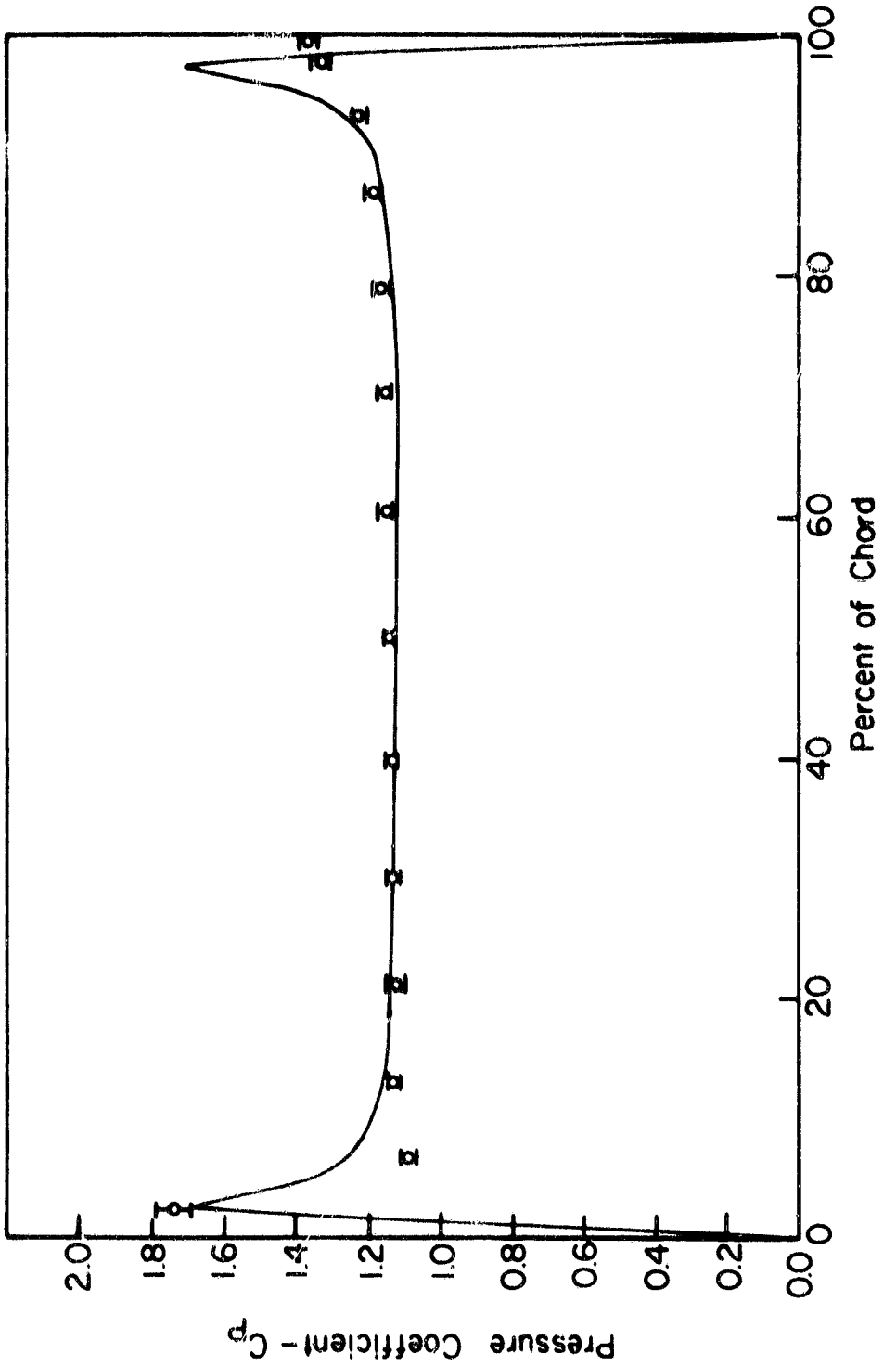

Figure C8. Pressure Coefficient Data, Experiment 2, Midspan Data, Surface 2.

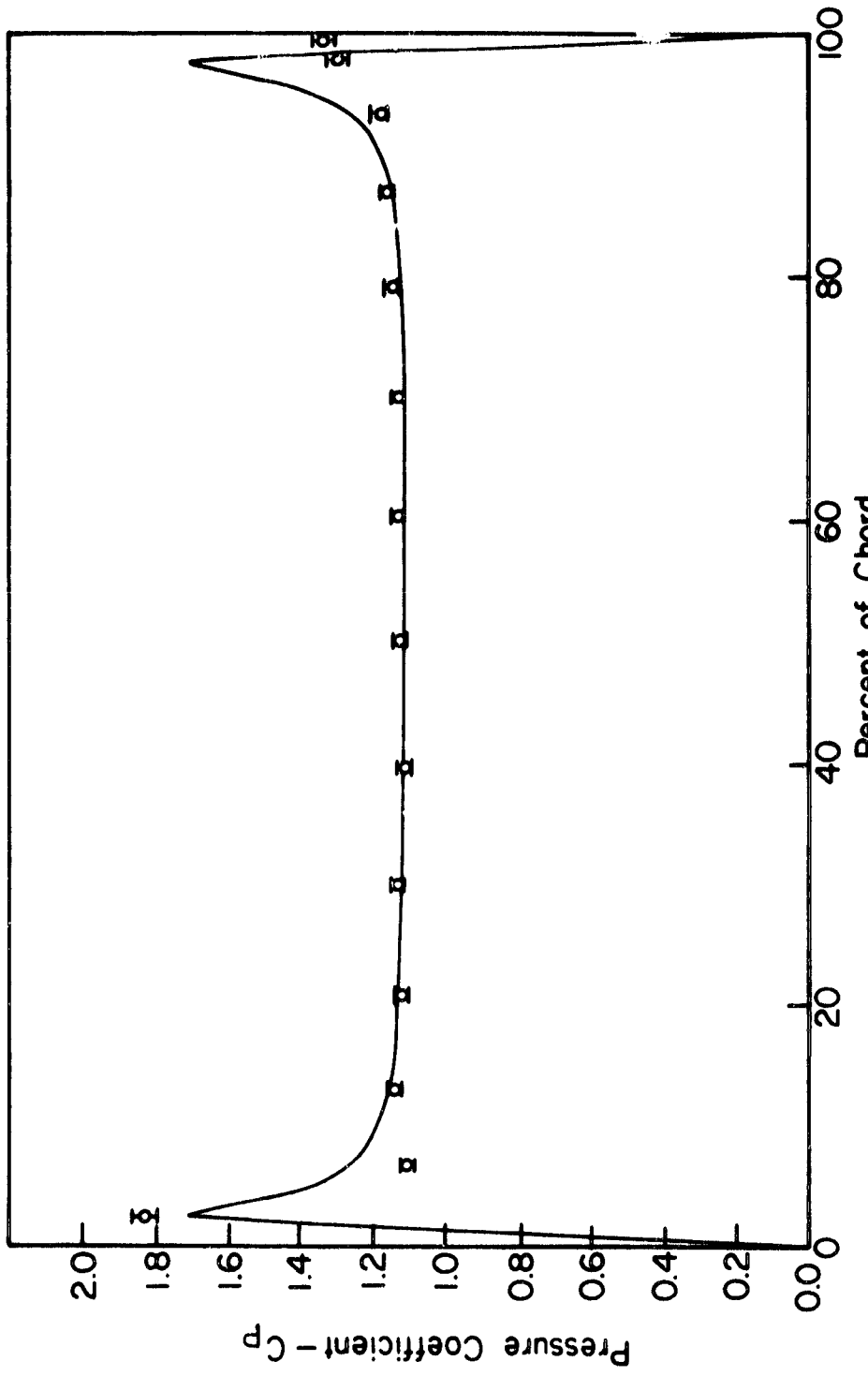

Figure C9. Pressure Coefficient Data, Experiment 3, Midspan Data, Surface 1.

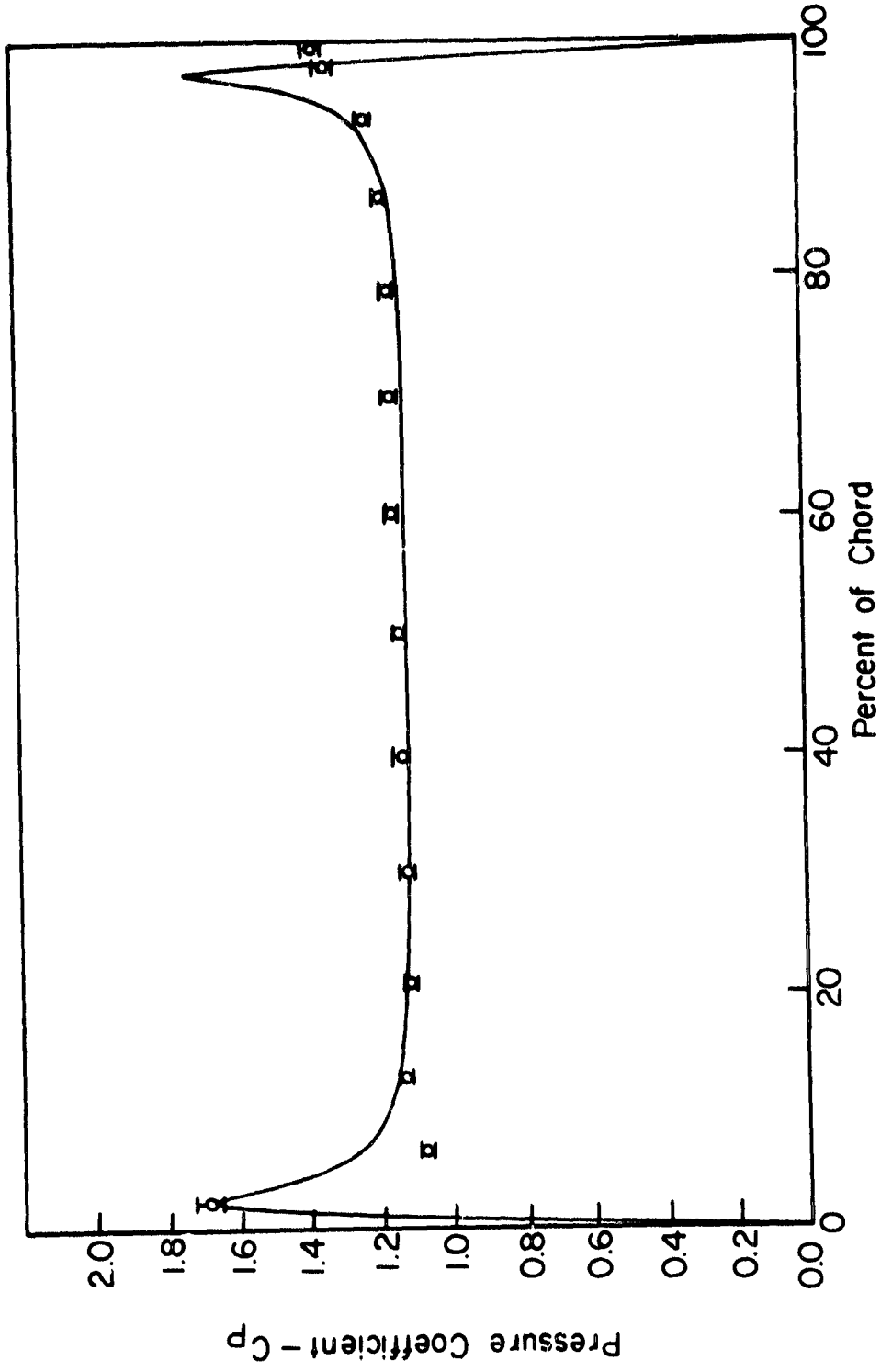

Figure C10. Pressure Coefficient Data, Experiment 3, Midspan Data, Surface 2.

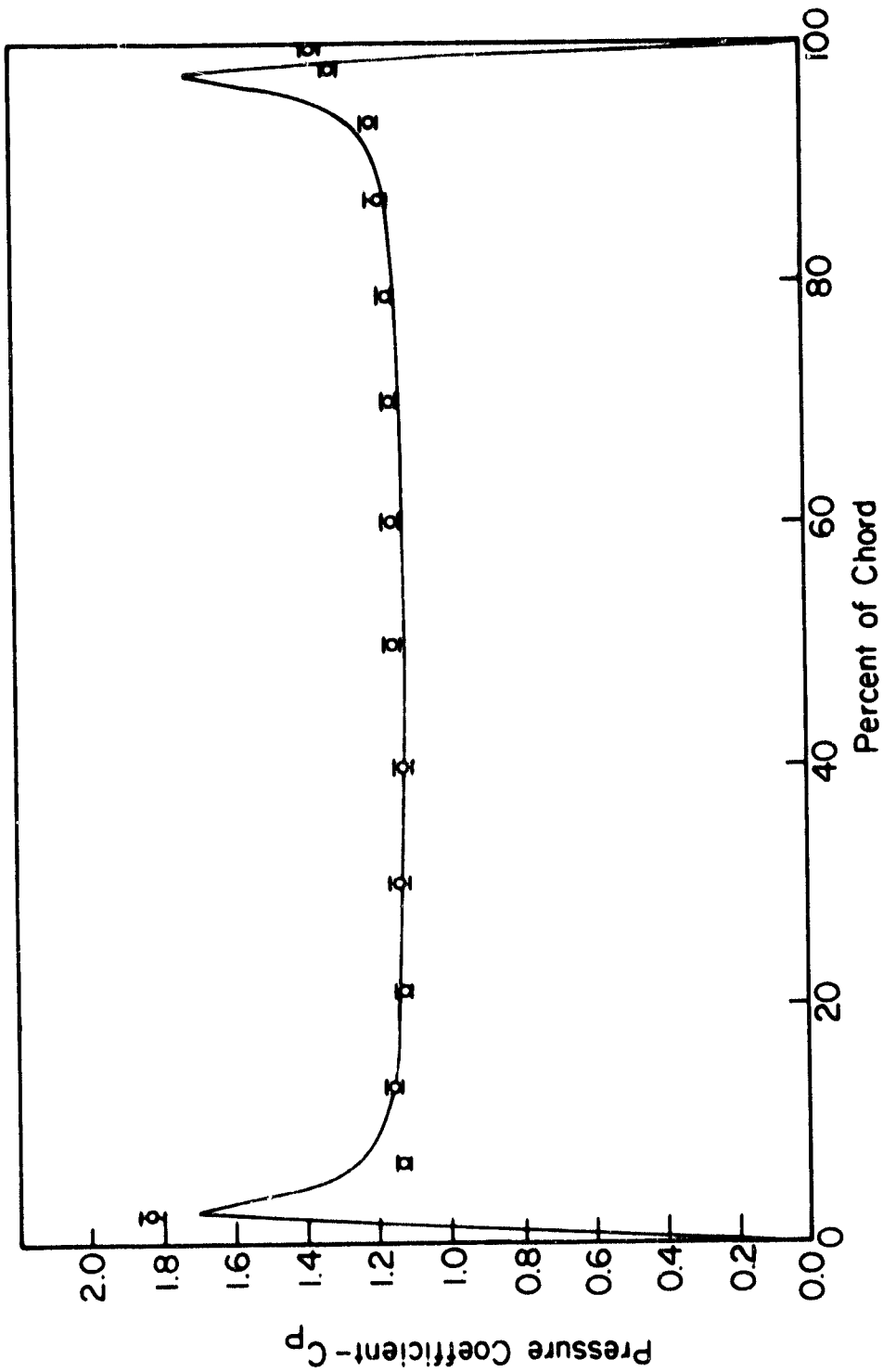

Figure C11. Pressure Coefficient Data, Experiment 4, Midspan Data, Surface 1.

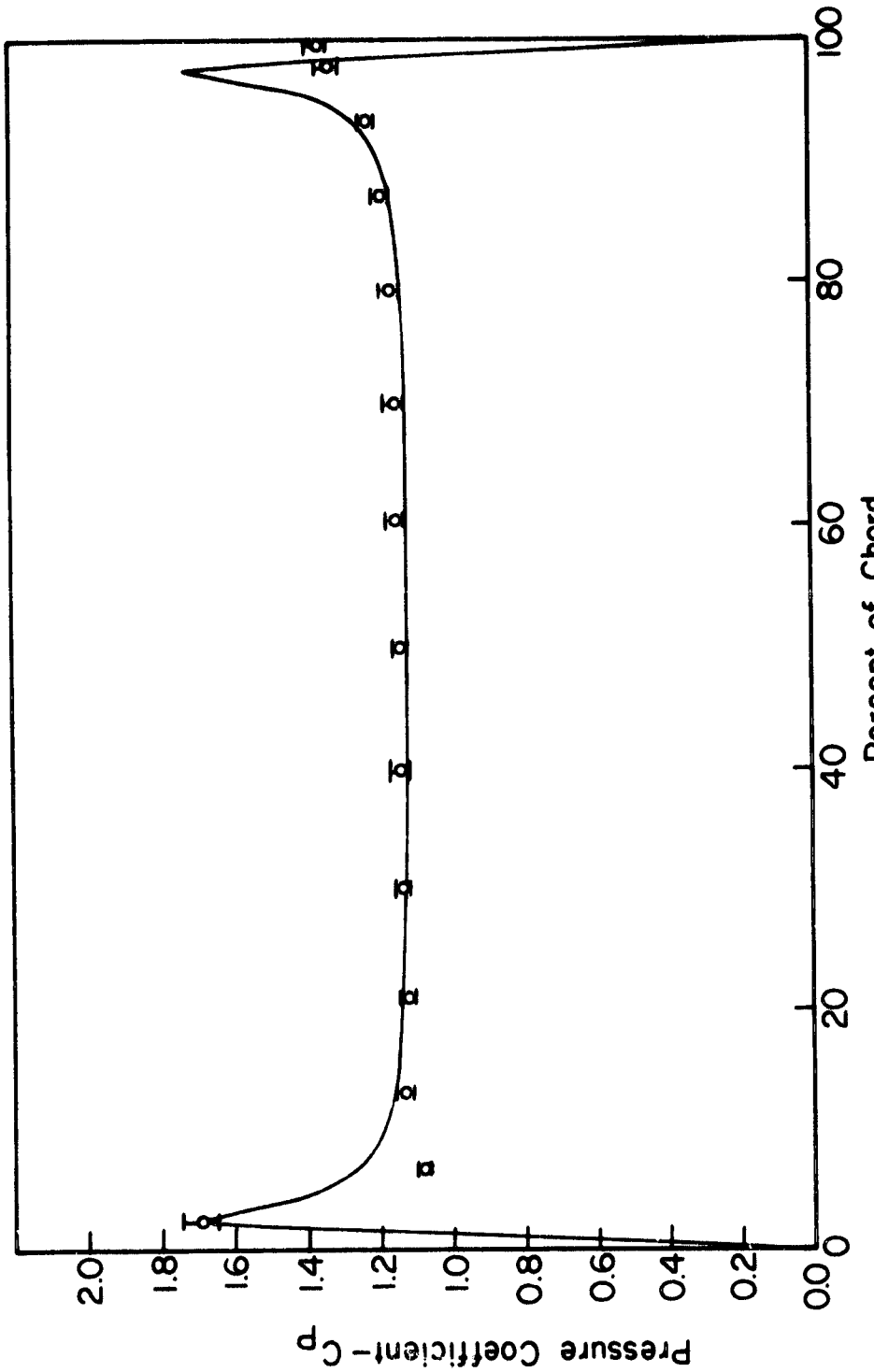

Figure C12. Pressure Coefficient Data, Experiment 4, Midspan Data, Surface 2.

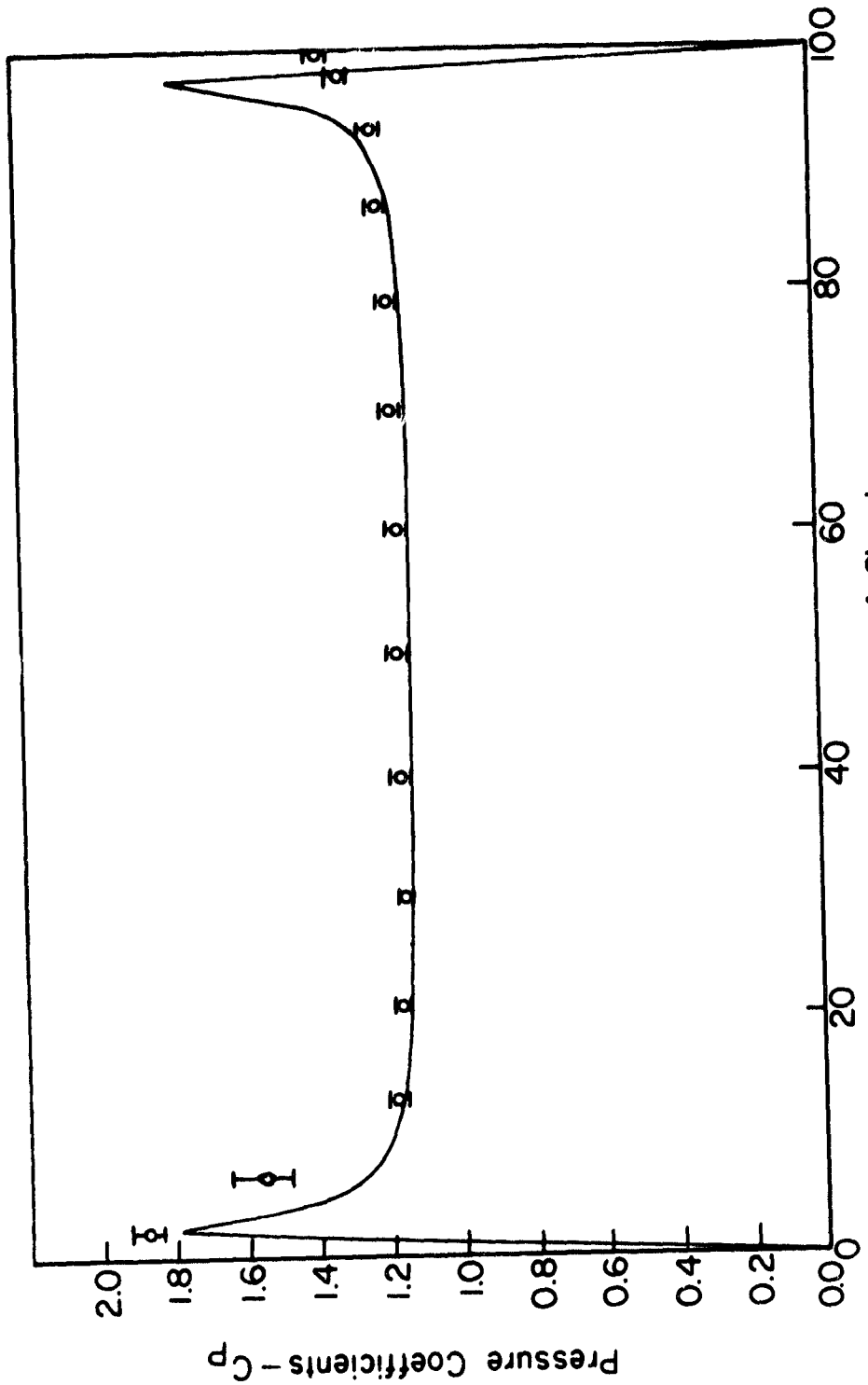

Figure C13. Pressure Coefficient Data, Experiment 2, Hub Data, Surface 1.

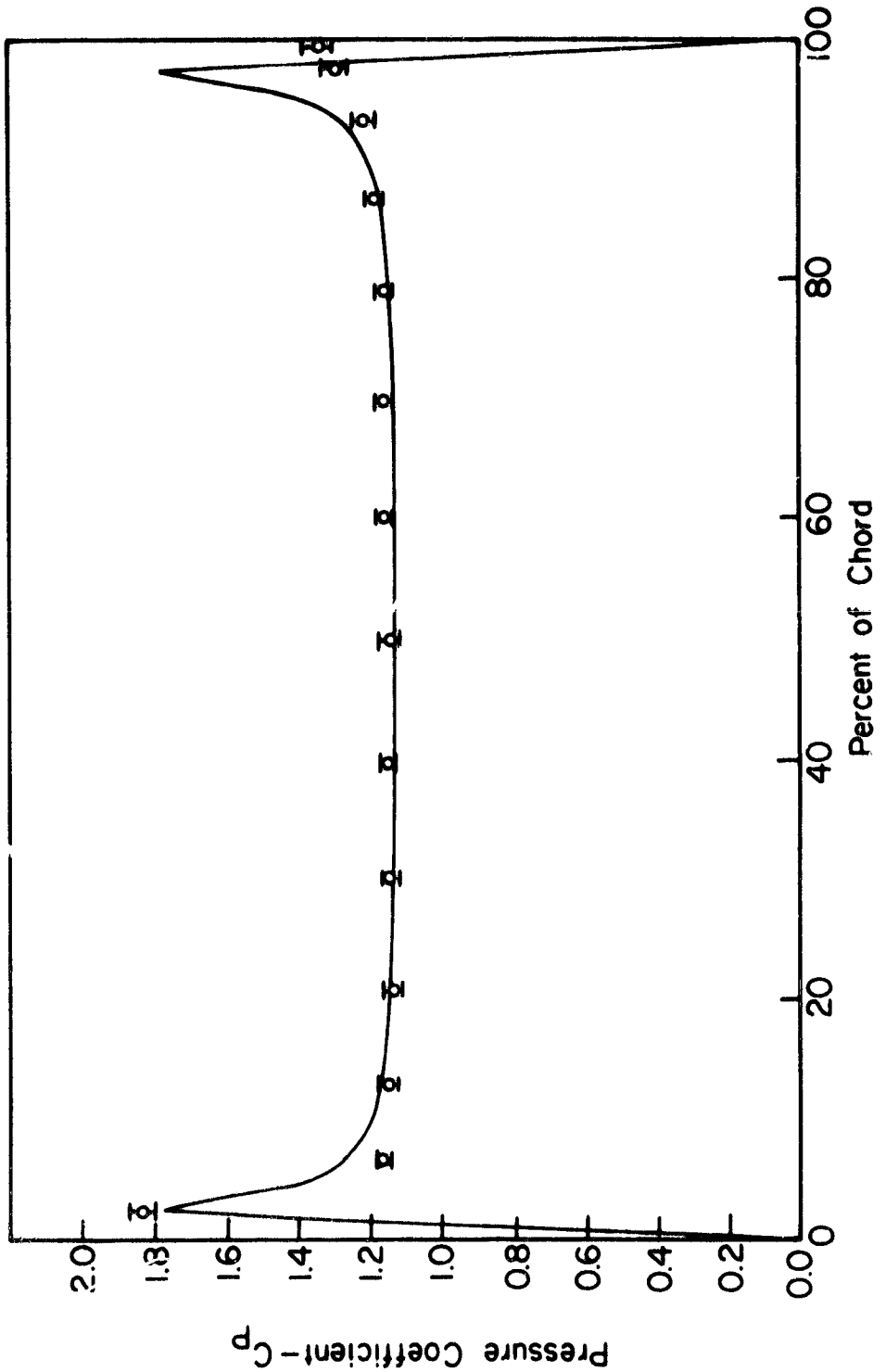

Figure C14. Pressure Coefficient Data, Experiment 2, Hub Data, Surface 2.

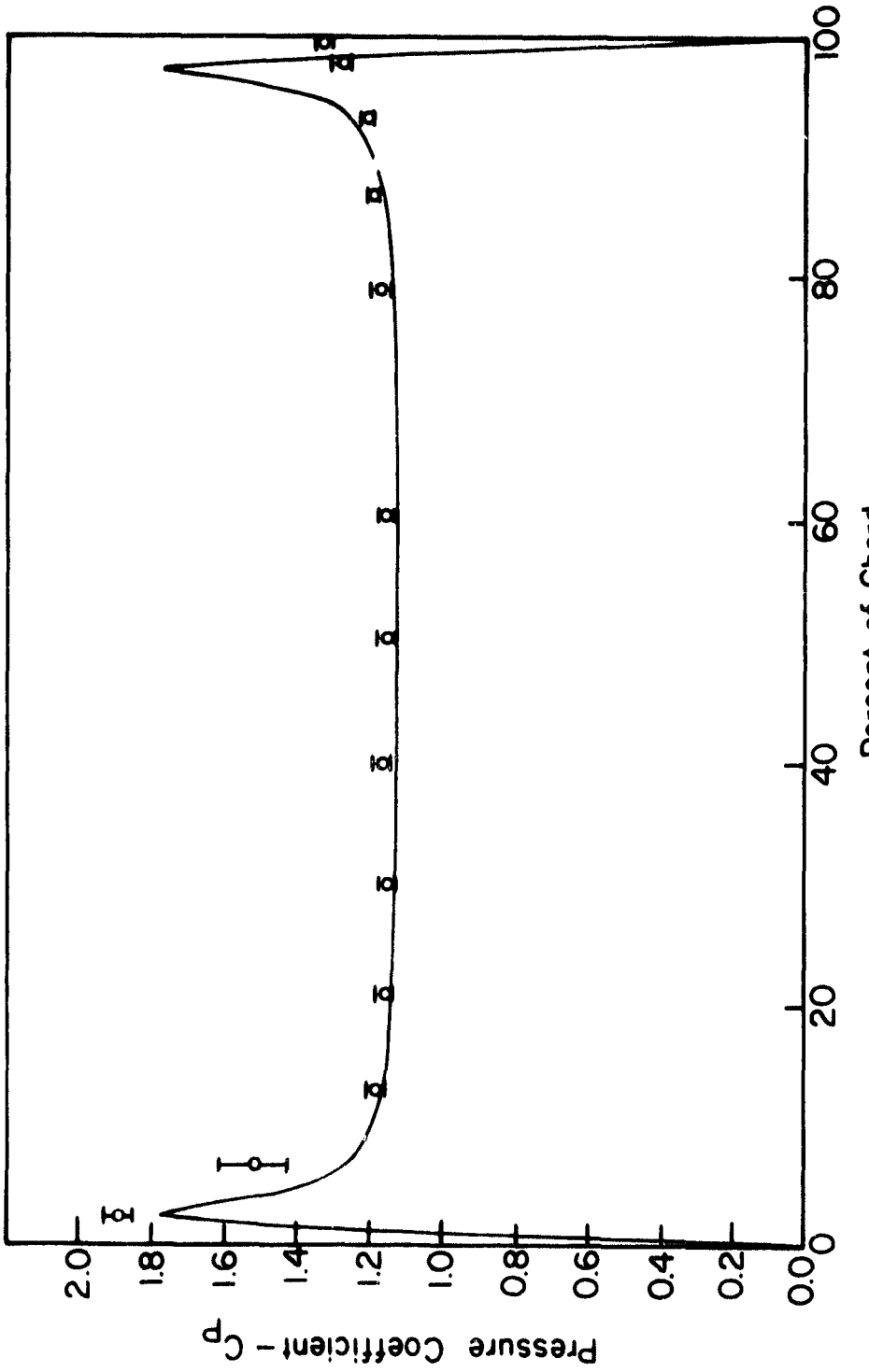

Figure C15. Pressure Coefficient Data, Experiment 3, Hub Data, Surface 1.

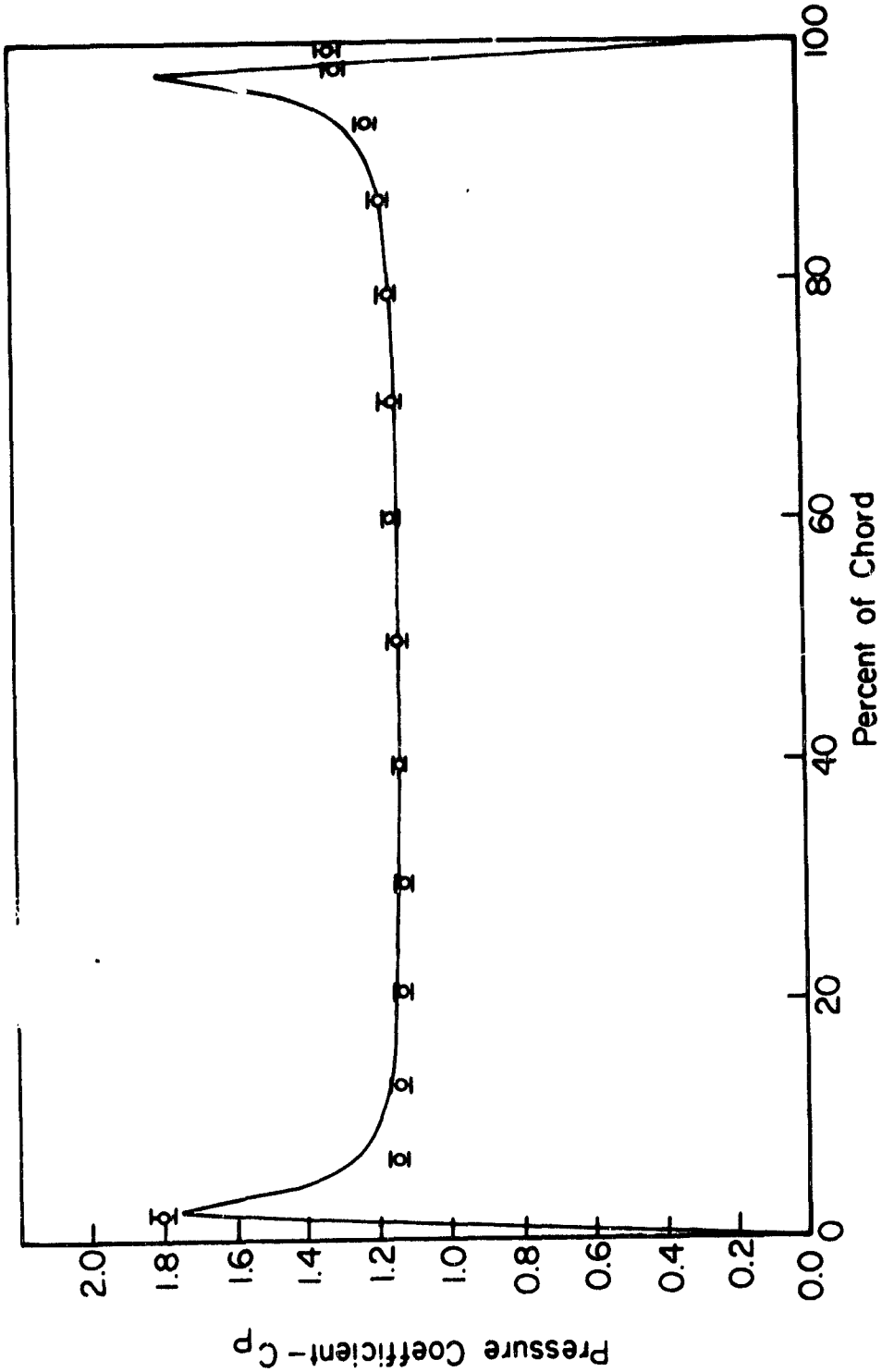

Figure C16. Pressure Coefficient Data, Experiment 3, Hub Data, Surface 2.

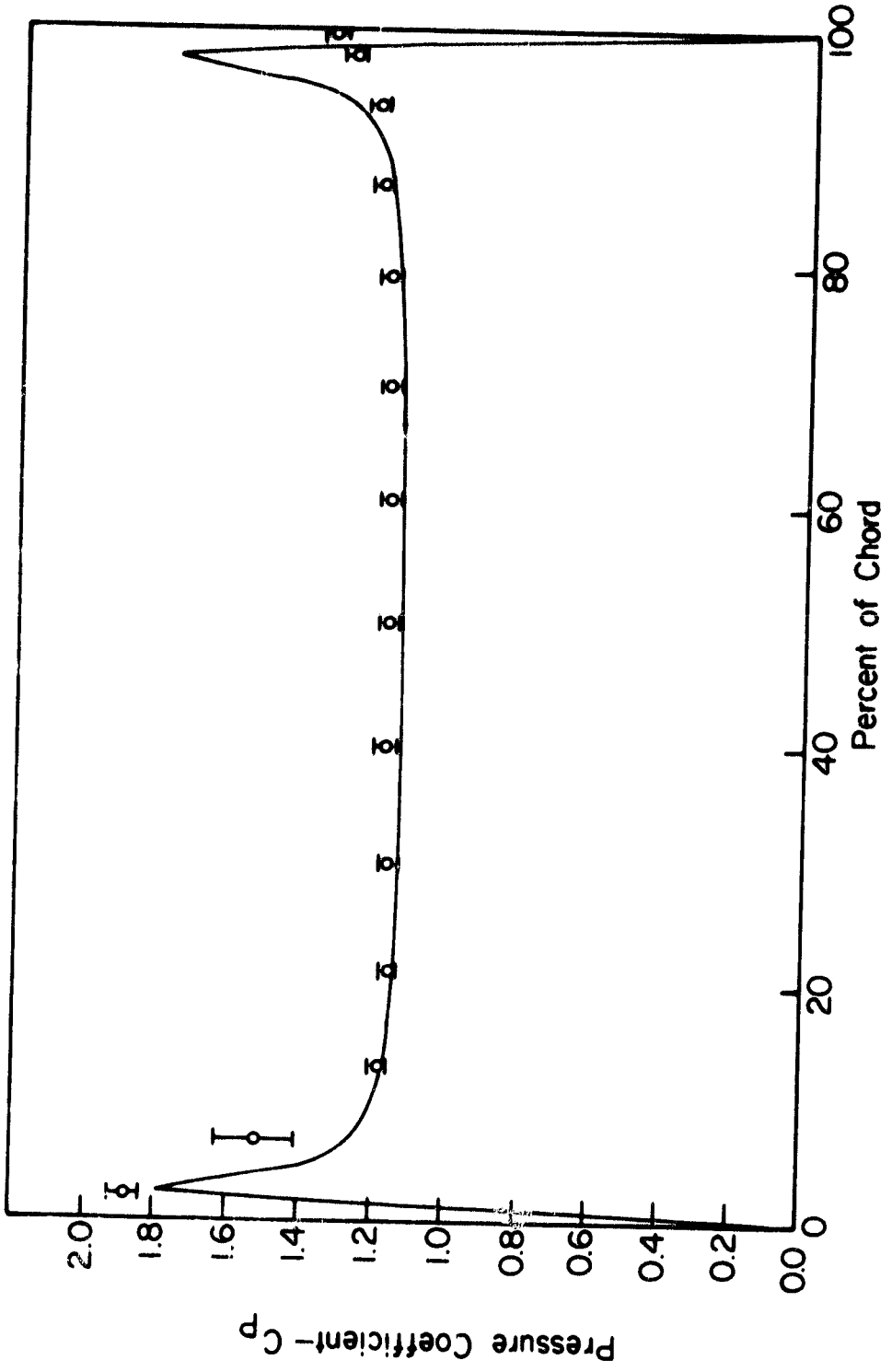

Figure C17. Pressure Coefficient Data, Experiment 4, Hub Data, Surface 1.

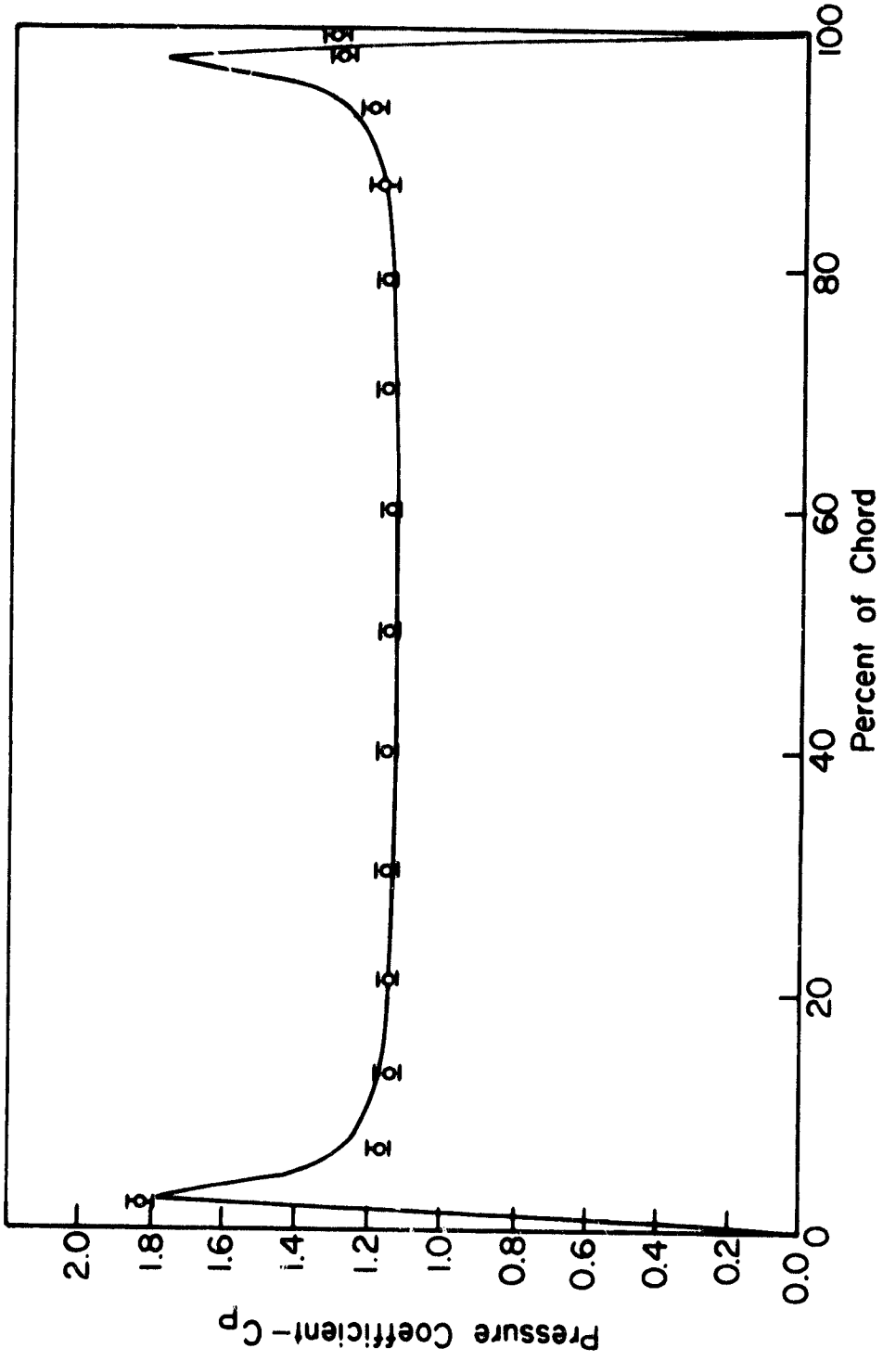

Figure C18. Pressure Coefficient Data, Experiment 4, Hub Data, Surface 2.

Appendix D

Tabular Presentation of Data

This appendix presents the airfoil surface pressure coefficient data in tabular form in Tables D1 through D24. Only the mean values are given. The confidence intervals are graphically indicated in Chapter 5 and in Appendix C.

Associated with each set of data is a mass-averaged velocity used to compute the pressure coefficients. The actual cascade inlet velocity profiles are presented in Table D25.

Table D1. Pressure Coefficient Data, Experiment 1, Tip Data, Surface 1

Mass-Averaged Velocity = 29.97 m/s	
Percent Chord	Pressure Coefficient
2.25	1.793
6.78	1.191
13.08	1.163
20.90	1.161
29.92	1.152
39.75	-.--
50.00	-.--
60.25	1.161
70.08	1.189
79.10	1.205
86.92	1.226
93.32	1.248
97.75	1.343
99.30	1.379

Table D2. Pressure Coefficient Data, Experiment 1, Tip Data, Surface 2

Mass-Averaged Velocity = 29.97 m/s	
Percent Chord	Pressure Coefficient
2.25	-.--
6.78	1.535
13.08	1.193
20.90	1.171
29.92	1.178
39.75	-.--
50.00	-.--
60.25	1.162
70.08	1.188
79.10	1.193
86.92	1.225
93.32	1.233
97.75	1.318
99.30	1.363

Table D3. Pressure Coefficient Data, Experiment 2, Tip Data, Surface 1

Mass-Averaged Velocity = 30.96 m/s	
Percent Chord	Pressure Coefficient
2.25	1.721
6.78	1.128
13.08	1.116
20.90	1.101
29.92	1.106
39.75	-.--
50.00	-.--
60.25	1.118
70.08	1.140
79.10	1.154
86.92	1.172
93.32	1.196
97.75	1.278
99.30	1.319

Table D4. Pressure Coefficient Data, Experiment 2, Tip Data, Surface 2

Mass-Averaged Velocity = 30.96 m/s	
Percent Chord	Pressure Coefficient
2.25	-.--
6.78	1.470
13.08	1.170
20.90	1.150
29.92	1.140
39.75	-.--
50.00	-.--
60.25	1.125
70.08	1.147
79.10	1.153
86.92	1.181
93.32	1.208
97.75	1.283
99.30	1.336

Table D5. Pressure Coefficient Data, Experiment 3, Tip Data, Surface 1

Mass-Averaged Velocity = 29.83 m/s	
Percent Chord	Pressure Coefficient
2.25	1.717
6.78	1.130
13.08	1.109
20.90	1.095
29.92	1.094
39.75	-.--
50.00	-.--
60.25	1.098
70.08	1.132
79.10	1.137
86.92	1.162
93.32	1.182
97.75	1.262
99.30	1.288

Table D6. Pressure Coefficient Data, Experiment 3, Tip Data, Surface 2

Mass-Averaged Velocity = 29.83 m/s	
Percent Chord	Pressure Coefficient
2.25	-.--
6.78	1.487
13.08	1.167
20.90	1.149
29.92	1.148
39.75	-.--
50.00	-.--
60.25	1.134
70.08	1.148
79.10	1.155
86.92	1.173
93.32	1.191
97.75	1.269
99.30	1.289

Table D7. Pressure Coefficient Data, Experiment 4, Tip Data, Surface 1

Mass-Averaged Velocity = 30.08 m/s	
Percent Chord	Pressure Coefficient
2.25	1.752
6.78	1.148
13.08	1.116
20.90	1.111
29.92	1.108
39.75	-.--
50.00	-.--
60.25	1.111
70.08	1.144
79.10	1.150
86.92	1.169
93.32	1.185
97.75	1.271
99.30	1.292

Table D8. Pressure Coefficient Data, Experiment 4, Tip Data, Surface 2

Mass-Averaged Velocity = 30.08 m/s	
Percent Chord	Pressure Coefficient
2.25	-.--
6.78	1.508
13.08	1.159
20.90	1.144
29.92	1.146
39.75	-.--
50.00	-.--
60.25	1.132
70.08	1.145
79.10	1.158
86.92	1.182
93.32	1.199
97.75	1.268
99.30	1.292

Table D9. Pressure Coefficient Data, Experiment 1, Midspan Data, Surface 1

Mass-Averaged Velocity = 29.97 m/s	
Percent Chord	Pressure Coefficient
2.25	1.834
6.78	1.140
13.08	1.165
20.90	1.143
29.92	1.152
39.75	1.138
50.00	1.159
60.25	1.162
70.08	1.171
79.10	1.186
86.92	1.207
93.32	1.227
97.75	1.334
99.30	1.383

Table D10. Pressure Coefficient Data, Experiment 1, Midspan Data, Surface 2

Mass-Averaged Velocity = 29.97 m/s	
Percent Chord	Pressure Coefficient
2.25	1.760
6.78	1.119
13.08	1.162
20.90	1.149
29.92	1.168
39.75	1.175
50.00	1.181
60.25	1.194
70.08	1.201
79.10	1.207
86.92	1.229
93.32	1.268
97.75	1.383
99.30	1.425

Table D11. Pressure Coefficient Data, Experiment 2, Midspan Data, Surface 1

Mass-Averaged Velocity = 30.96 m/s	
Percent Chord	Pressure Coefficient
2.25	1.832
6.78	1.142
13.08	1.165
20.90	1.141
29.92	1.146
39.75	1.129
50.00	1.152
60.25	1.154
70.08	1.153
79.10	1.172
86.92	1.197
93.32	1.212
97.75	1.322
99.30	1.363

Table D12. Pressure Coefficient Data, Experiment 2, Midspan Data, Surface 2

Mass-Averaged Velocity = 30.96 m/s	
Percent Chord	Pressure Coefficient
2.25	1.750
6.78	1.099
13.08	1.146
20.90	1.132
29.92	1.140
39.75	1.144
50.00	1.150
60.25	1.162
70.08	1.166
79.10	1.174
86.92	1.195
93.32	1.229
97.75	1.337
99.30	1.372

Table D13. Pressure Coefficient Data, Experiment 3, Midspan Data, Surface 1

Mass-Averaged Velocity = 29.83 m/s	
Percent Chord	Pressure Coefficient
2.25	1.843
6.78	1.127
13.08	1.159
20.90	1.138
29.92	1.150
39.75	1.130
50.00	1.145
60.25	1.155
70.08	1.154
79.10	1.174
86.92	1.184
93.32	1.206
97.75	1.314
99.30	1.356

Table D14. Pressure Coefficient Data, Experiment 3, Midspan Data, Surface 2

Mass-Averaged Velocity = 29.83 m/s	
Percent Chord	Pressure Coefficient
2.25	1.705
6.78	1.092
13.08	1.149
20.90	1.131
29.92	1.137
39.75	1.148
50.00	1.150
60.25	1.164
70.08	1.165
79.10	1.173
86.92	1.187
93.32	1.229
97.75	1.332
99.30	1.364

Table D15. Pressure Coefficient Data, Experiment 4, Midspan Data, Surface 1

Mass-Averaged Velocity = 30.08 m/s	
Percent Chord	Pressure Coefficient
2.25	1.839
6.78	1.141
13.08	1.164
20.90	1.136
29.92	1.147
39.75	1.131
50.00	1.153
60.25	1.155
70.08	1.157
79.10	1.174
86.92	1.189
93.32	1.204
97.75	1.311
99.30	1.362

Table D16. Pressure Coefficient Data, Experiment 4, Midspan Data, Surface 2

Mass-Averaged Velocity = 30.08 m/s	
Percent Chord	Pressure Coefficient
2.25	1.714
6.78	1.095
13.08	1.145
20.90	1.129
29.92	1.144
39.75	1.151
50.00	1.150
60.25	1.168
70.08	1.159
79.10	1.176
86.92	1.197
93.32	1.228
97.75	1.338
99.30	1.372

Table D17. Pressure Coefficient Data, Experiment 1, Hub Data, Surface 1

Mass-Averaged Velocity = 29.97 m/s	
Percent Chord	Pressure Coefficient
2.25	1.886
6.78	1.503
13.08	1.188
20.90	1.169
29.92	1.161
39.75	1.175
50.00	1.176
60.25	1.175
70.08	1.190
79.10	1.198
86.92	1.217
93.32	1.235
97.75	1.315
99.30	1.393

Table D18. Pressure Coefficient Data, Experiment 1, Hub Data, Surface 2

Mass-Averaged Velocity = 29.97 m/s	
Percent Chord	Pressure Coefficient
2.25	1.885
6.78	1.210
13.08	1.193
20.90	1.194
29.92	1.192
39.75	1.203
50.00	1.196
60.25	1.210
70.08	1.207
79.10	1.222
86.92	1.242
93.32	1.275
97.75	1.364
99.30	1.399

Table D19. Pressure Coefficient Data, Experiment 2, Hub Data, Surface 1

Mass-Averaged Velocity = 30.96 m/s	
Percent Chord	Pressure Coefficient
2.25	1.889
6.78	1.565
13.08	1.183
20.90	1.163
29.92	1.152
39.75	1.162
50.00	1.163
60.25	1.161
70.08	1.171
79.10	1.178
86.92	1.204
93.32	1.217
97.75	1.296
99.30	1.359

Table D20. Pressure Coefficient Data, Experiment 2, Hub Data, Surface 2

Mass-Averaged Velocity = 30.96 m/s	
Percent Chord	Pressure Coefficient
2.25	1.834
6.78	1.170
13.08	1.158
20.90	1.146
29.92	1.148
39.75	1.155
50.00	1.150
60.25	1.168
70.08	1.170
79.10	1.170
86.92	1.189
93.32	1.223
97.75	1.301
99.30	1.347

Table D21. Pressure Coefficient Data, Experiment 3, Hub Data, Surface 1

Mass-Averaged Velocity = 29.83 m/s	
Percent Chord	Pressure Coefficient
2.25	1.894
6.78	1.521
13.08	1.184
20.90	1.163
29.92	1.154
39.75	1.171
50.00	1.159
60.25	1.161
70.08	--.--
79.10	1.179
86.92	1.197
93.32	1.212
97.75	1.287
99.30	1.329

Table D22. Pressure Coefficient Data, Experiment 3, Hub Data, Surface 2

Mass-Averaged Velocity = 29.83 m/s	
Percent Chord	Pressure Coefficient
2.25	1.808
6.78	1.152
13.08	1.144
20.90	1.134
29.92	1.129
39.75	1.139
50.00	1.139
60.25	1.147
70.08	1.150
79.10	1.155
86.92	1.175
93.32	1.204
97.75	1.286
99.30	1.299

Table D23. Pressure Coefficient Data, Experiment 4, Hub Data, Surface 1

Mass-Averaged Velocity = 30.08 m/s	
Percent Chord	Pressure Coefficient
2.25	1.876
6.78	1.515
13.08	1.179
20.90	1.159
29.92	1.153
39.75	1.170
50.00	1.165
60.25	1.162
70.08	1.171
79.10	1.176
86.92	1.201
93.32	1.210
97.75	1.283
99.30	1.339

Table D24. Pressure Coefficient Data, Experiment 4, Hub Data, Surface 2

Mass-Averaged Velocity = 30.08 m/s	
Percent Chord	Pressure Coefficient
2.25	1.829
6.78	1.172
13.08	1.153
20.90	1.145
29.92	1.147
39.75	1.156
50.00	1.151
60.25	1.157
70.08	1.163
79.10	1.166
86.92	1.178
93.32	1.207
97.75	1.291
99.30	1.309

Table D25. Inlet-Velocity Profile Data

% of Annulus Span from Hub to Tip	Velocity in m/s Exp.1	Exp.2	Exp.3	Exp.4
5.7	30.11	31.16	30.00	30.24
17.5	30.02	31.05	29.93	30.18
27.9	29.94	30.95	29.82	30.07
38.0	30.06	31.08	29.92	30.16
48.7	30.08	31.07	29.92	30.16
59.4	30.10	31.08	29.94	30.20
69.0	30.07	31.06	29.92	30.15
78.9	30.05	31.03	29.87	30.14
87.8	30.01	30.98	29.81	30.08
96.1	29.25	30.14	29.16	29.43

Appendix E

NASA Computer Codes

Two NASA-developed computer codes were used to predict the chordwise distribution of the airfoil surface pressure coefficient. The two programs, MERIDL [8] and TSONIC [9] are based on inviscid analyses and are intended for computing turbomachine flow fields.

The governing flow equations are the continuity equation, the momentum equation (the inviscid form of the Navier-Stokes equations), and the thermodynamic equations. For steady subsonic flows, these equations form a system of elliptic partial differential equations. Solving an elliptic system requires that the flow conditions be completely specified on all boundaries of the solution region. Specifying the flow conditions downstream of an airfoil cascade requires either knowledge of or assumptions about how much the cascade turns the flow. For the case at hand, this is an almost trivial assumption as the airfoils are flat plates set at 0 incidence. Both programs generate two-dimensional grids upon which the governing equations are solved as finite difference equations using successive-over-relaxation.

The MERIDL program generates its grid along the hub-to-tip mean stream-sheet in the center of the airfoil passage. This stream-sheet is assumed to have the same shape as the airfoil camber line with flow-matching corrections at the leading and trailing edges. One of the primary purposes of the MERIDL program is to compute the radial shift of the streamlines in the solution region (airfoil passage). Part of MERIDL's output is the input, in its required format, for the TSONIC program. It was to be expected for the facility geometry (constant radius annulus walls and flat-plate airfoils at 0 incidence) that there would be very little radial shift of the streamlines. MERIDL was primarily used for completeness and to generate the extensive input required for TSONIC.

The TSONIC program generates its numerical grid and solves the governing equations along an airfoil-to-airfoil stream-sheet. The program assumes that this stream-sheet is a surface of revolution. Any arbitrary stream-sheet from hub to tip can be specified provided that MERIDL had been instructed to generate the appropriate input to TSONIC. Part of the output from TSONIC is the airfoil surface velocities. These can easily be converted to the corresponding pressure coefficients by dividing them by the mass-averaged velocity through the facility and squaring the results.